New Ruthenium Pincer Catalysts for (De)hydrogenation Reactions

Cumulative dissertation

for the acquisition of the academic degree

doctor rerum naturalium (Dr. rer. nat.)

of the Faculty of Mathematics and Natural Sciences

at the University of Rostock

Submitted in Rostock on the 14.01.2025
by Hendrik Andreas Kempf, born on 26th November 1996 in Aschaffenburg, Germany

https://doi.org/10.18453/rosdok_id00005177

The presented work was accomplished at the Leibniz-Institut für Katalyse e.V. in the research group Angewandte Homogenkatalyse of Prof. Dr. Matthias Beller between April 2021 and January 2025.

Reviewer 1: Prof. Matthias Beller, Leibniz-Institut für Katalyse e.V.
Reviewer 2: Prof. Martin Nielsen, Technical University of Denmark

Date of submission: 14.01.2025
Date of defence: 17.06.2025

I STATEMENT OF AUTHORSHIP

Hiermit versichere ich, Hendrik Kempf, an Eides Statt die vorliegende Arbeit

„New Ruthenium Pincer Catalysts for (De)hydrogenation Reactions"

selbstständig und ohne Benutzung anderer als der angegebenen Hilfsmittel angefertigt habe. Alle Stellen, die wörtlich oder sinngemäß aus veröffentlichten oder nicht veröffentlichten Schriften entnommen wurden, sind als solche kenntlich gemacht.

Rostock, den

……

Hendrik Kempf

II ACKNOWLEDGEMENTS

Firstly, I would like to thank Matthias Beller for giving me the opportunity to do my doctoral thesis in his working group. I am thankful, that despite his busy schedule, he always managed to find time and discuss my research progress. During our meetings he always gave great insights and had a positive outlook into the future.

Next, I would like to thank Henrik Junge. As the leader of the subgroup “catalysis for energy” and my immediate supervisor he always supported me with his great knowledge about the practical and theoretical aspects of dehydrogenation reactions, as well as in the preparation of manuscripts. I would further like to thank him for his support and valuable discussions outside of our academic work.

I would further like to thank all collaborators within the MEGA project. Through our meetings I always learned a lot about the constructing and running a demonstration plant. I am also thankful to Alexander Heidenreich, Florian Kohler, and the OxFA GmbH for their funding and valuable scientific discussions.

Furthermore, I would like to thank my collaborators within Likat Carolin Stein, Niklas Both, Germán López Robledo, Anke Spannenberg, Kathrin Junge, and Haijun Jiao for their contributions to the manuscripts.

I would also like to thank my colleagues of the “catalysis for energy group” for the great and productive working atmosphere. I would like to especially thank Anja Kammer for all her help with our equipment and support in analytical questions; Duo Wei for all his help in the beginning of my PhD; Lorenz Dittrich and Carolin Stein for our discussions about chemistry and life; Elisabetta Alberico for her vast knowledge and support in complex synthesis; and lastly Hilario Diego Huerta Zeron for always brightening the mood and providing a great working atmosphere.

Next, I would like to thank all my friends for all their support throughout the last years. Weather I already know you for all my life, or only got to meet you in the last few months, you all made my time in Rostock enjoyable and helped making this thesis possible.

Lastly, I thank my family for their ongoing support throughout my life and especially during my PhD. Whenever I had a question or problem you were always there.

Thank you all.

III KURZZUSAMMENFASSUNG

Im Rahmen der vorliegenden Arbeit wurden mehrere neue Ruthenium-Pincer-Komplexe hergestellt und deren Eignung für verschiedene Modellreaktionen evaluiert.

Durch die Reaktion von [Ru(CO)(Cl)H(PPh_3)$_3$] mit *N*,*N*'-Bis(diisopropylphosphino)-benzoguanamin wurden Benzoguanamin-basierte PNP-Pincer-Komplexe synthetisiert. Hierbei entstand eine monomere und eine dimere Spezies. In Letzterer agiert der Pincer-Ligand überbrückend, wodurch er mit einem Phosphor- und einem Stickstoffatom an das erste und mit einem weiteren Phosphoratom an das zweite Metallzentrum koordiniert. Beide Komplexe konnten durch SC-XRD und NMR charakterisiert und in Modellreaktionen, namentlich der Ameisensäuredehydrierung, der CO_2 Hydrierung, sowie der Reduktion ungesättigter organischer Moleküle, eingesetzt werden. Weiterhin wurde die Umwandlung zwischen der monomeren und dimeren Spezies untersucht.

Durch die Reaktion von *N*,*N*-Bis(2-(diisopropylphosphanyl)ethyl)prop-2-yn-1-amin mit [Ru(CO)(Cl)H(PPh_3)$_3$] wurde eine neue Klasse der Pincer-Komplexe eingeführt, nämlich PNPC-Pincer-Komplexe. Mehrere Repräsentanten dieser Unterkategorie wurden synthetisiert und durch eine Kombination aus NMR und SC-XRD charakterisiert. Das katalytische Potential der Komplexe wurde in der Ameisensäuredehydrierung und in Transfer(de)hydrierungen untersucht. Mechanistische Untersuchungen zeigten zwei konkurrierende Reaktionsmechanismen auf. Im Ru-C Mechanismus wird Ameisensäure durch den Bruch der Ru-C Bindung aktiviert, während diese Bindung im Ru-H Mechanismus intakt bleibt.

Schließlich wurden die im Rahmen dieser Arbeit synthetisierten Katalysatoren in der wässrigen Niedertemperatur-Methanolreformierung eingesetzt. Hierzu wurden standardisierte Reaktionsbedingungen definiert, welche eine industrielle Anwendbarkeit zum Ziel haben. Unter diesen Reaktionsbedingungen wurden die neu synthetisierten Katalysatoren getestet und mit etablierten Katalysatoren verglichen. Abschließend wurde die generelle industrielle Anwendbarkeit der Methanolreformierung vor dem Hintergrund der standardisierten Reaktionsbedingungen kritisch diskutiert.

IV ABSTRACT

Several new ruthenium pincer complexes were prepared and their suitability for various model reactions was evaluated.

Benzoguanamine based PNP-pincer complexes were synthesized by the reaction of $[Ru(CO)(Cl)H(PPh_3)_3]$ with ligand *N*,*N*'-bis(diisopropylphosphino)-benzoguanamine. A monomeric and a dimeric species were formed. In the latter, the pincer ligand acts as a bridging ligand, coordinating with one phosphorous and one nitrogen atom to the first metal center and with the second phosphorous atom to the second metal center. Both complexes were characterized by SC-XRD and NMR investigations. They were employed in different model reactions, namely the dehydrogenation of formic acid, the hydrogenation of CO_2 and the dehydrogenation of unsaturated organic compounds. Furthermore, the interconversion between the monomeric and dimeric species was investigated.

A new class of cyclometallated pincer complexes, namely PNPC ones, were synthesized by the reaction of *N*,*N*-bis(2-(diisopropylphosphaneyl)ethyl)prop-2-yn-1-amine with $[Ru(CO)(Cl)H(PPh_3)_3]$. Multiple representatives of this subclass were synthesized and characterized by a combination of NMR and SC-XRD. Their catalytic potential was investigated in formic acid dehydrogenation and transfer (de)hydrogenation reactions. Mechanistic investigations of the formic acid dehydrogenation reaction revealed two competing reaction mechanisms. In the Ru-C pathway, reaction proceeds via the Ru-C bond cleavage, while this bond stays intact in the Ru-H mechanism.

These complexes were investigated in the low temperature methanol aqueous phase reforming (APR). For this purpose, standardized reaction conditions, focusing on the practical application of methanol APR, were defined. Herein synthesized as well as state-of-the-art complexes were tested under the proposed standard conditions. Having established practical reaction conditions, the general economic feasibility of methanol APR was discussed.

V TABLE OF CONTENTS

VI ABBREVIATIONS

The following abbreviations are used throughout the text:

ΔG	change in Gibbs free energy
APR	aqueous phase reforming
cp*	pentamethylcyclopentadienyl
DBN	1,5-diazabicyclo[4.3.0]non-5-ene
DBU	1,8-diazabicyclo[5.4.0]undec-7-ene
DFT	density functional theory
DMF	dimethylformamide
DMSO	dimethyl sulfoxide
FA	formic acid
GC-FID	gas chromatograph equipped with a flame ionization detector
HRMS	high resolution mass spectrometry
KIE	kinetic isotope effect
LD_{50}	lethal dose, 50%
LT-PEMFC	low temperature polymer electrolyte membrane fuel cell
M	molar
NHC	N-heterocyclic carbene
NMR	nuclear magnetic resonance (spectroscopy)
ppm	parts per million
SC-XRD	single crystal x-ray diffraction
T_{set}	set temperature
TBAF	tetra-*n*-butylammonium fluoride
tetraphos	tris-[2-(diphenylphosphin)ethyl]phosphine
THF	tetrahydrofuran
TOCSY	total correlation spectroscopy
TOF	turnover frequency
TOF_{max}	maximum observed turnover frequency
TON	turnover number

1 INTRODUCTION

1.1 Catalysis

In the last century, there has been a large increase in our standard of living.[1, 2] This can be seen – among others – in the continuously increasing population on earth and the rising life expectancy at birth.[3, 4] One key factor enabling these improvements is the constant development of new and optimization of existing catalytic methods.[5, 6] For example, the invention of the Haber-Bosch process allowed the production of fertilizers applying nitrogen from air.[6, 7] This, in turn greatly increased the available food supply and allowed for the growth of our population.[8] Additionally, the development of appropriate catalysts, like Ziegler-Natta catalysts, enabled the synthesis of polymers, heavily impacting the materials used nowadays in daily life.[6, 9] Furthermore, the evolution of catalytic methods paved the way for the synthesis of pharmaceuticals, enabling the treatment of illnesses and increasing the life expectancy.[10-13] Those methods include cross-coupling reactions,[12] metathesis[14-16] and (de)hydrogenation[17-20] reactions. In the past two decades so-called pincer complexes gained a lot of interest for the latter reactions.[20-24]

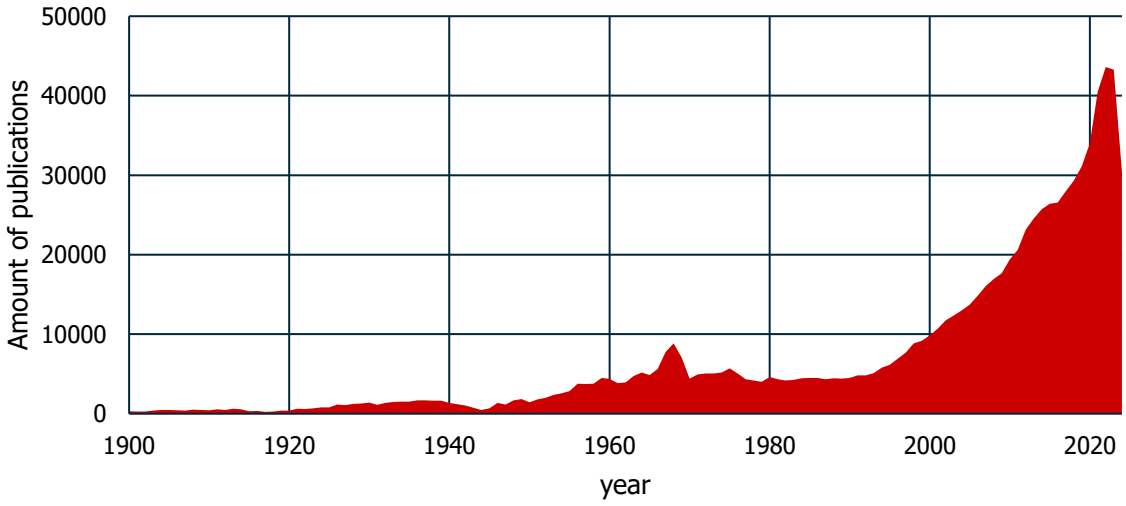

Figure 1. Publications about „catalysis“ per year found by SciFinder.

As highlighted in Figure 1, research in catalysis is strongly growing since 1990, culminating in the incorporation of at least one catalytic step during the synthesis of over 80% of all products nowadays.[25, 26] However, most of the chemical processes are based on fossil fuels, and with the increasing severity of climate change, new solutions for a green chemical industry based on renewables must be found.[27, 28] In this transformation of the chemical industry, catalysis is expected to play a major role in enabling new and efficient reaction pathways and in turn may lead to the development of new and the improvement of existing chemical processes.[26, 28] To achieve this goal, new catalysts must be developed.[27]

1.2 Hydrogen economy

In this regard, one field of research is the transformation of our electrical power supply from fossil towards renewable energy sources.[29-31] Currently, more than 50% of Germanys electricity is produced from renewable resources with wind and photovoltaic energy being the largest contributors (Figure 2).[32] However, their production capacities heavily depend on weather conditions and therefore do not always coincide with demand.[30, 31, 33] To solve this issue, energy storage solutions must be developed and implemented.[30, 31, 33] One possibility is the transformation of electrical into chemical energy.[30, 33, 34] This can, for example, be achieved by water electrolysis to hydrogen and oxygen gas.[30, 33, 34] The reverse process, the energy release from these gases, can easily be achieved in a fuel cell.[30, 35, 36] The energy carrier utilized in this example, hydrogen gas, is widely regarded as very promising due to its high gravimetric energy content of 120 MJ/kg.[29, 34]

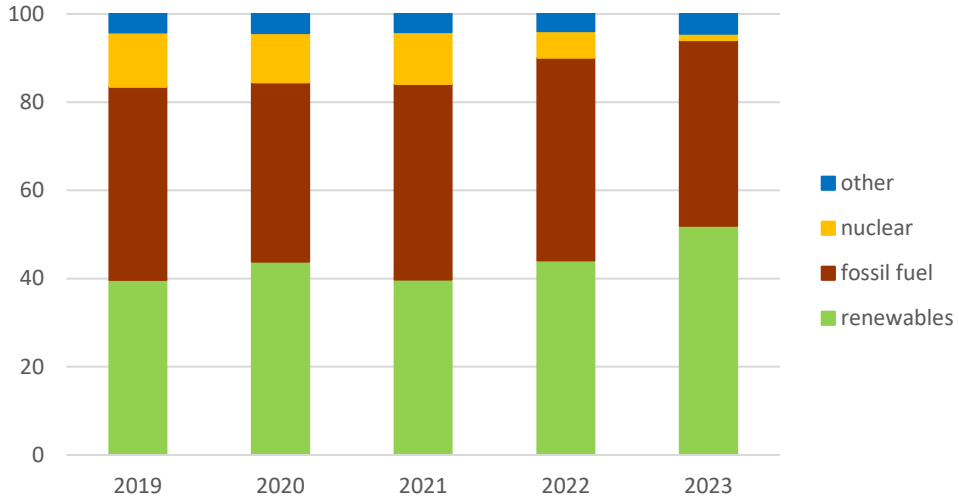

Figure 2. Percentual contribution to electricity production in Germany between 2019 and 2023.[32]

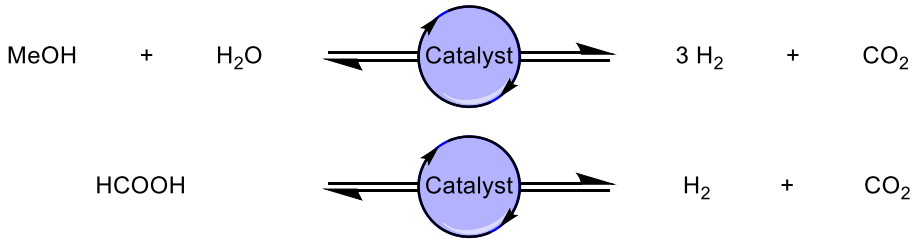

Scheme 1. Schematic representation of formic acid and methanol (de)hydrogenation.

However, the storage of energy in form of hydrogen gas poses significant challenges. Due to its low volumetric energy density, its efficient storage requires high pressure or cryogenic equipment.[29, 33, 37, 38] Additionally, hydrogen gas forms explosive mixtures with oxygen thus posing significant safety risks.[29, 33, 37, 38] Therefore, the transformation of hydrogen gas into and its release from energy storage materials is being investigated (Scheme 1).[27, 35-38] Some examples of such storage materials include, among others, ammonia, ammonia-boranes, decalin, methylcyclohexane, and perhydro-dibenzyltoluene.[38-42] However, one of the most promising storage materials is methanol.[40] With a hydrogen content of 12.6 wt% it shows

excellent storage capacity. Though, its synthesis and the release of hydrogen usually requires harsher conditions compared to another promising hydrogen storage material formic acid.[27, 33, 36] The potential of both those hydrogen storage materials will be highlighted in the following chapters.

1.2.1 Methanol dehydrogenation

Similar to the hydrogen economy, a methanol economy was proposed already in 1986 by Asinger and later on further developed by Olah, Prakash and Goeppert.[43, 44] It encompasses the synthesis of methanol from renewable resources and its use as a feedstock in the chemical industry to replace oil and gas. Overlapping with the hydrogen economy, the use of methanol as an energy carrier is also proposed.

For a successful application of methanol as an energy storage material, some prerequisites must be fulfilled in the methanol reformation process. Firstly, the produced gas must contain <10 ppm CO impurities, as they are vital for the efficient use of a low temperature polymer electrolyte membrane fuel cell (LT-PEMFC). [45] Furthermore, hydrogen production rate, catalyst and ligand price, as well as stability must be taken into account for an economically feasible process. The best chance to fulfill these requirements, lies in the low temperature (<100 °C) reformation, as higher reaction temperatures enable the increasing formation of CO. It can either be formed from the product gas mixture *via* reverse water gas shift reaction or by the decomposition of intermediately produced formic acid. The latter is less prevalent at low temperatures. Especially the requirements of low CO content and low reaction temperature are hard to achieve using heterogeneous catalysts.[24, 37, 40] However, two publications stand out utilizing heterogeneous catalysts:

In 2002, the first examples of aqueous phase reforming (APR) of methanol were shown by Dumesic and co-workers.[46] Utilizing a Pt@γ-Al catalyst, a TOF of 420 h^{-1} could be achieved at 230 °C and 29 bar. However, the produced gas contained comparably high CO impurities (300 ppm). Secondly, Hu, Qu and co-workers used platinum on porous CeO_2 nanorods for the steam reforming of methanol and could achieve a hydrogen production rate of 199 $\mathrm{mol_{H_2}\,mol_{Pt}^{-1}}$ at 135 °C with CO impurities of 320 ppm.[47] Even at 100 °C they could produce hydrogen gas with similar activities to homogeneous systems.

Switching to homogeneous catalysts, methanol dehydrogenation was first independently described by the groups of Beller and co-workers,[48] as well as Trincado, Grützmacher, and co-workers[49] in 2013 (Figure 3). The former utilized a ruthenium pincer complex **A**. In a strong basic reaction solution (8 M KOH), a TOF of 4,700 h^{-1} with low CO concentration (<10 ppm) was achieved. The latter utilized a tetradentate ruthenium complex **B** and reached a TOF of 54 h^{-1} with triethylamine as base. CO impurities were not detected; however, the detection limit of the used analytical method was not specified. In 2014 Beller and co-workers reported a

bicatalytic, additive free system for methanol APR (Figure 3).[50] One catalyst – Ru-MACHO-BH **E** – showed excellent activity in the dehydrogenation of methanol to formic acid. A second catalyst – $[Ru(dppe)_2(H)_2]$ (**F**) – was added for the efficient dehydrogenation of formic acid to CO_2 resulting in a synergistic effect and a TOF of 94 h^{-1} with a high gas purity (<8 ppm CO). The same concept was used in 2019 for methanol APR in presence of base to improve Beller's work from 2013 (Figure 3).[51] By the addition of triglyme as a solvent, it was possible to lower the base concentration from 8 M to 0.33 M KOH. Due to the lower base concentration, a "working phase" could be observed with a TOF of 194 h^{-1}. This state is characterized by the stable evolution of a 3:1 H_2 to CO_2 gas mixture. Similar to their earlier work, CO impurities were below 10 ppm.

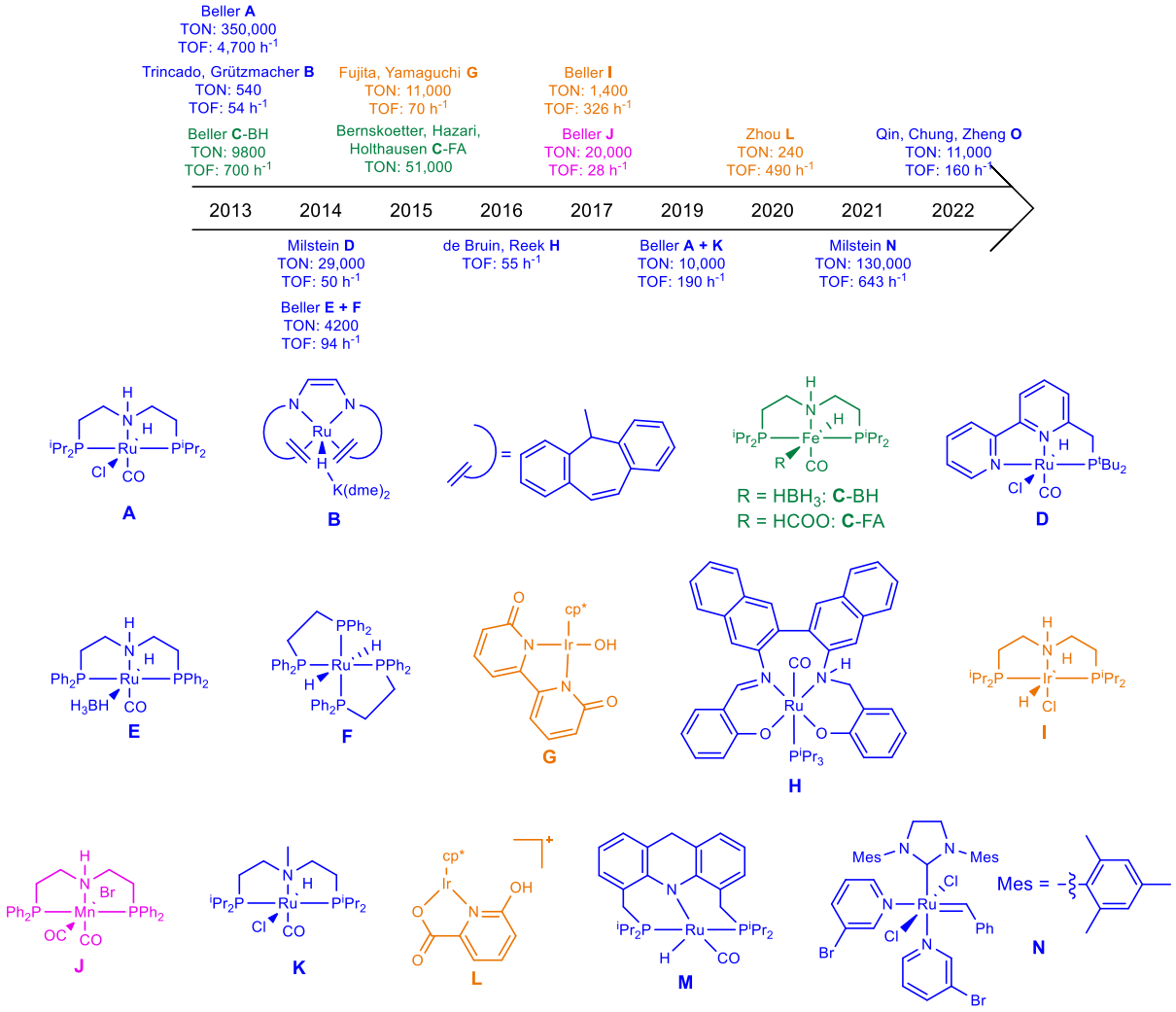

Figure 3. Important ruthenium (blue), iron (green), iridium (orange), and manganese (purple) catalysts for methanol APR. For experimental details see appendix. Figure adapted from ref[52].

Moreover, Milstein and co-workers utilized a ruthenium PNN-pincer **D** complex achieving a TOF of 50 h^{-1} at 100 °C reaction temperature in 2014 (Figure 3).[53] It was possible to recycle the reaction solution three times without loss of activity. The CO content was not reported. Further increase of the nitrogen content in the ligand let to the RuNNN catalyst described by Kumar and co-workers in 2023.[29] However, this change only allowed incomplete reformation

of methanol. Formic acid was formed as a product with a yield of 81%. Similarly, methanol APR with a ruthenium NHC-complex yielded potassium formate.[54]

Other ruthenium-based methanol APR systems include a salen complex **H** by de Bruin, Reek and co-workers (Figure 3).[55] Here, a TOF of 55 h^{-1} was reached, while CO content remained below an unspecified detection limit. A different tetradentate ligand was employed by Qin, Zhu, Zheng and co-workers in 2023.[56] At 120 °C reaction temperature, a TOF of 158 h^{-1} with low CO impurities (<10 ppm) was achieved. Milstein and co-workers also showed methanol APR at elevated temperatures (150 °C).[57] The addition of 1-hexanethiol as an additive enabled the high TOF (643 h^{-1}) with CO impurities below 20 ppm. Lastly, Qin, Chung, Zheng, and co-workers demonstrated the ability of Grubbs-catalysts (**N**) to perform methanol APR (Figure 3).[58] They reached a TOF of 158 h^{-1} with <10 ppm CO impurities.

Besides these ruthenium systems, iridium-based complexes showed good results in methanol APR. Already in 2015, Fujita, Yamaguchi and co-workers reached a TOF of 70 h^{-1} with a bipyridyl based complex **G** (Figure 3).[59] Notably, a TON of 10,500 could be reached. Two years later, Beller and co-workers improved the TOF to 326 h^{-1} by employing an iridium pincer complex **I** (Figure 3).[60] By careful optimization of the ligand sphere **L**, Zhou and co-workers could reach a TOF of almost 500 h^{-1} (Figure 3).[61] However, CO values were either not reported or below an unspecified detection limit for all these three publications.

As highlighted previously, noble metal complexes show good activities in methanol dehydrogenation. Additionally to these systems, non-noble metal based complexes are known for methanol APR. In 2017, Beller and co-workers demonstrated the ability of manganese pincer complexes **J** to perform this reaction (Figure 3).[62] A TON of 20,000 showed impressive stability of the complex, however CO impurities were not analyzed. Already in 2013, iron catalyzed methanol APR was reported for the first time (Figure 3).[63] A TOF of 702 h^{-1} and TON of almost 10,000 could be reached with low CO impurities (<10 ppm). Further improvement of the reaction conditions by Bernskoetter, Hazari, Holthausen and co-workers led to an increase in stability to yield a TON of 51,000 (Figure 3).[64] However, CO values increased to <0.1%. In this reaction system, a Lewis acid was employed to enhance the decarboxylation of the iron formate complex **C**-FA.

To summarize, many molecularly defined complexes for methanol APR were developed. Catalysts mostly operated below 100 °C, fulfilling one prerequisite for successful application of the resulting hydrogen in a LT-PEMFC. However, in literature often the CO content was either not reported or found to be below an unspecified detection limit. Due to missing this critical information, the evaluation of those reaction systems towards application is severely hindered.

1.2.2 Formic acid dehydrogenation

Another hydrogen storage medium considered for a hydrogen economy is formic acid.[65-69] Compared to methanol it possesses a lower energy density with a hydrogen content of 4.4 wt% (12.6 wt% for methanol, Table 1). However, its dehydrogenation is more exothermic (ΔG = -32.9 kJ/mol) and can therefore be achieved at milder reaction conditions compared to methanol (ΔG = 8.9 kJ/mol).[66, 70] Consequently, significantly more catalytic systems have been developed for the dehydrogenation of formic acid, than for methanol. In Figure 4 the most important systems are highlighted, with a focus on pincer complexes.

Table 1. Properties of formic acid and methanol.[66]

	Methanol	Formic acid
Molecular formula	CH_3OH	HCO_2H
Molecular mass	32.042 g/mol	46.026 g/mol
Gravimetric hydrogen density	126 g/kg	44 g/kg
Volumetric hydrogen density	99 g/L	52 g/L
Density	0.79 g/m^3	1.22 g/m^3
Boiling point	65 °C	101 °C
Vapor pressure (20 °C)	130.3 hPa	42.0 hPa
Explosion limits (upper – lower)	6 – 36 vol%	18 – 57 vol%
Flash point	11 °C	48 °C
Workplace exposure limit	200 mL/m^3	5 mL/m^3
LD_{50} (oral, rat)	5.628 g/kg	1.100 g/kg

First reports of formic acid decomposition date back by more than 100 years.[71, 72] These early investigations utilized reaction temperatures well above 100 °C and various metals and metal oxides, as well as glass as catalyst. Starting from 1967, research mainly focused on catalysts based on noble metals, such as iridium,[73, 74] palladium,[75] platinum,[76, 77] rhodium[73, 78] and ruthenium.[66, 79] Ligands consisted primarily of simple monodentate phosphines. During this time, best productivity and selectivity was achieved with iridium- and ruthenium-based catalysts. However, high reaction temperatures were generally required, and low stability was observed in most cases.

In 1998, Puddephatt and co-workers laid the foundation for the dehydrogenation of formic acid with diphosphine-based ligands (Figure 4).[80, 81] Their binuclear ruthenium complex achieved a TOF of 500 h^{-1} at room temperature, the highest activity up to that point. This catalytic system was further developed by Beller and co-workers (Figure 4).[82-84] More specifically, the active catalyst was formed *in situ* from $[Ru(Cl)_2(benzene)]_2$ as the metal precursor and a phosphine ligand. Triphenylphosphine was found to yield the highest activity among the investigated monodentate phosphine ligands. 1,2-Bis(diphenylphosphino)ethane gave the best activity

overall, however a long induction period was observed. Investigations into the employed amine bases revealed that structurally similar bases typically yielded comparable activities. Among the investigated bases DBN (1,5-diazabicyclo(4.3.0)non-5-ene) gave the most promising results. Overall, a TOF of 459 h^{-1} over the first three hours of the reaction was reached at 40 °C reaction temperature. This reaction system was further optimized towards continuous flow.[85, 86] Here, a TON of 1,000,000 was achieved with stable gas evolution over 45 days.

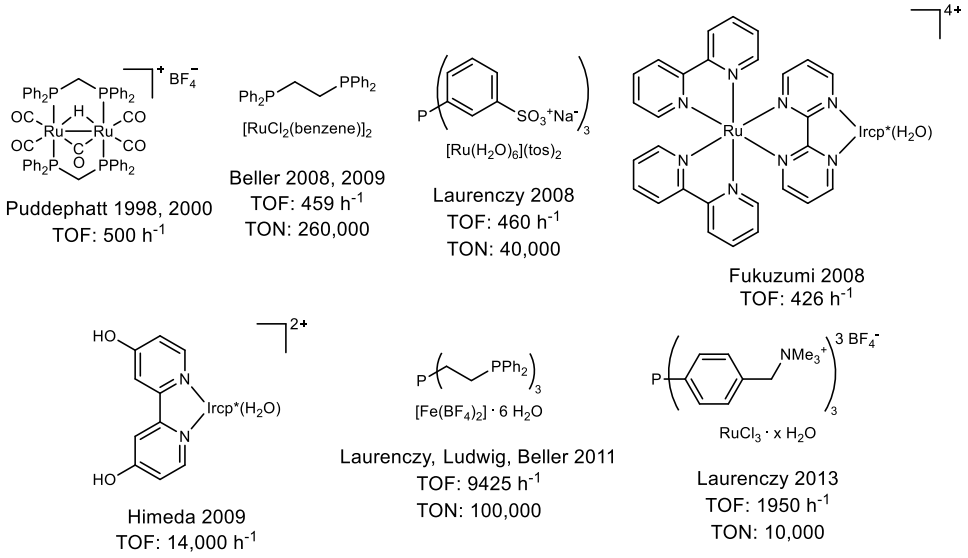

Figure 4. Selected examples of early works on formic acid dehydrogenation.

At the same time, Laurenczy and co-workers took a different approach towards formic acid dehydrogenation.[87-89] They utilized a water-soluble complex prepared in situ from $RuBr_3 \cdot xH_2O$ or $[Ru(H_2O)_6]^{2+}$ and meta-trisulfonated triphenylphosphine (Figure 4). Already at room temperature formic acid dehydrogenation was observed. At 120 °C reaction temperature, a TOF of 460 h^{-1} was reached. Furthermore, a continuous flow system was developed with H_2 production rate of 290 mL/min. Besides the anionic phosphine ligand, cationic ones were employed by the same group (Figure 4).[90] They achieved a TOF of 1950 h^{-1} at 120 °C and a TON of 10,000 over 30 catalytic cycles.

Another important formic acid dehydrogenation system was developed by Fukuzumi and co-workers between 2008 and 2010.[91-93] Their best catalytic system consisted of a bimetallic ruthenium-iridium complex and achieved a TOF of 426 h^{-1} at room temperature in an aqueous solution (Figure 4). Investigations of the pH-influence revealed a high impact on the activity with a maximum at pH 3.8. A similar monometallic complex was developed by Himeda and co-workers (Figure 4).[94, 95] They utilized functionalized bipyridyl ligands with iridium, ruthenium and rhodium as metal centers. Especially iridium complexes showed high activity (TOF: 14,000 h^{-1}) at 90 °C. Besides the generation of H_2-gas, the synthesis of HD and D_2 was demonstrated in high purity (98%).[96] Based on this research, a multitude of different diamino-ligands were synthesized and applied later on by various research groups.[67, 68]

In 2011, Laurenczy, Ludwig, Beller and co-workers demonstrated the base-free dehydrogenation of formic acid amine mixtures utilizing an iron-based tetraphos catalyst (Figure 4).[97] They reached a TOF of up to 9425 h^{-1} at 80 °C reaction temperature. Furthermore, in a continuous flow setup, a gas evolution rate of 326 mL/min could be reached without deactivation over 14 h and a total TON of almost 100,000. The tetraphos ligand was further employed in formic acid dehydrogenation with other metal centers, like ruthenium[98] or platinum.[99] Gonsalvi and co-workers synthesized linear versions of the tetraphos ligand.[100] However, they observed lower catalytic activity compared to the tripodal tetraphos ligand.

Pincer complexes were employed in formic acid dehydrogenation for the first time in 2011 by Morokuma, Nozaki, and co-workers (Figure 5).[101] Utilizing iridium as the metal center, a TOF of 120,000 h^{-1} was reached. However, TON remained low (200). The first ruthenium catalyzed system utilizing pincer ligands was developed by Pidko and co-workers in 2014 (Figure 5).[102] A system was developed for the reversible hydrogen storage and release in/from formic acid. They achieved a TON of 706,500 with a TOF of 256,000 h^{-1} in the dehydrogenation step. Overall, 10 hydrogen storage-release cycles were performed without loss of activity. At the same time, Plietker and co-workers investigated a PNNP-ruthenium complex in the reversible storage and release of hydrogen (Figure 5).[103] In the dehydrogenation reaction, gas evolution rates around 1.5 L/h were achieved over 5 storage and release cycles. One year later, the Ru-MACHO complex and its N-methylated version were investigated by Czaun, Prakash, Olah, and co-workers for sodium formate dehydrogenation (Figure 5).[104] The methylated complex was shown to be more active. The same trend was observed by Beller and co-workers.[105] Mechanistic investigations revealed an inner sphere reaction mechanism.[70, 104] Czaun, Prakash, Olah, and co-workers could reach TON of 5,000 with an initial TOF of 735 h^{-1}.[104]

In 2016, a ruthenium pincer complex with aminophosphine moieties was utilized by Zheng, Huang and co-workers (Figure 5).[106] Overall, a TON of 1,100,000 was achieved with a TOF of 7,333 h^{-1}. By the variation of the reaction solvent from DMSO to DMF, TOF could be raised to 31,000 h^{-1}, however a lower TON was reached. Das, Nielsen, and co-workers developed another reaction system for reversible hydrogen storage and release (Figure 5).[107] They utilized ionic liquids as solvents and base. In the dehydrogenation of formic acid, the reaction system stayed active for 4 months, reaching a TON of $1.8 \cdot 10^7$ with an average TOF of 11,000 h^{-1}. Additionally, 12 hydrogen storage and release cycles were performed.

Iron pincer complexes were utilized for the first time in formic acid dehydrogenation by Milstein and co-workers in 2013 (Figure 5).[108] At 40 °C reaction temperature, an activity of 836 h^{-1} was achieved. In a long-term experiment, a TON of 100,000 could be reached over the course of 10 days. One year later, significant improvements were achieved by Hazari, Schneider, and co-workers (Figure 5).[109] The addition of a Lewis acid significantly improved activity (TOF: 197,000 h^{-1}) and stability (TON: 1,000,000 in 9.5 h) by assisting in the decarboxylation of the iron formate intermediate. Aminophosphine-based iron pincer

complexes were employed in formic acid dehydrogenation by Kirchner, Gonsalvi, and co-workers (Figure 5).[110] In this case, a TOF of 2,600 h^{-1} was reached. Additionally, it was reported, that the use of Lewis acids instead of base let to no conversion.

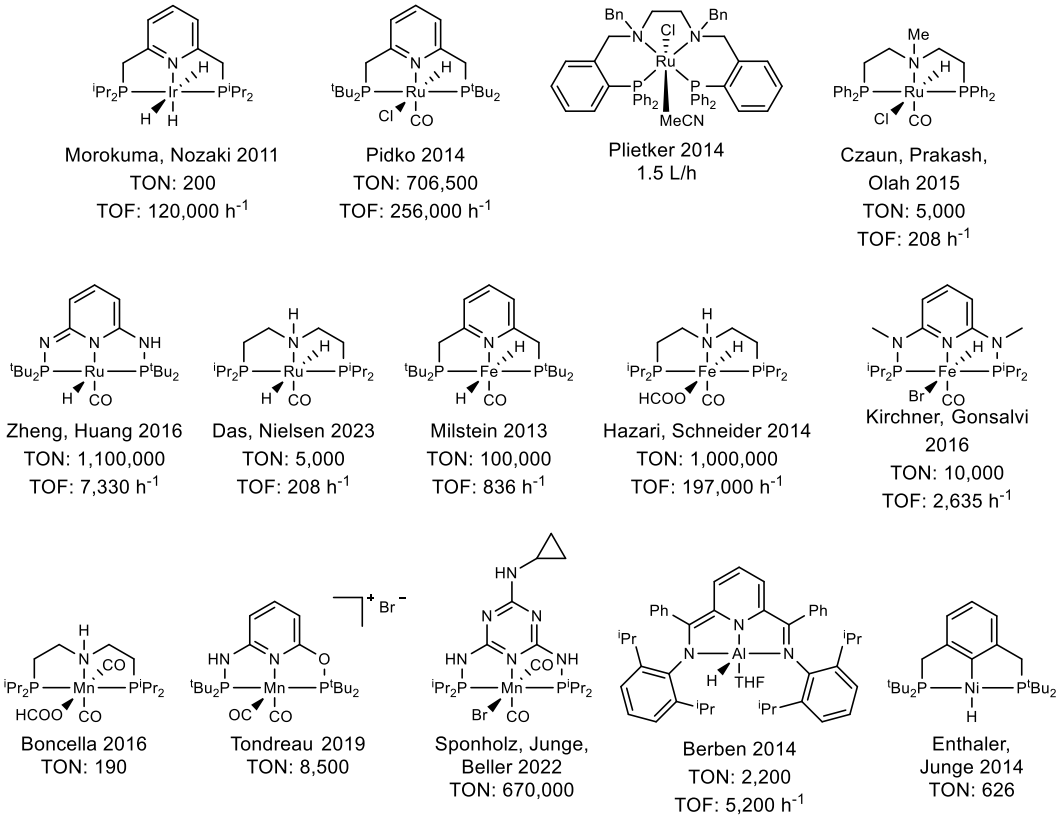

Figure 5. Selected examples of pincer complexes utilized in formic acid dehydrogenation.

Pioneering work on manganese pincer complexes for formic acid dehydrogenation was performed in 2016 by Boncella and Tondreau (Figure 5).[111] They achieved a TON of 190. The reaction conditions were slightly improved by Beller and co-workers in 2017 (TON 283).[62] By further optimization of the ligand, Tondreau and co-workers could improve the activity to 8,500 h^{-1} (Figure 5).[112] Notably, 50% conversion was reached in 2.5 min. In 2022, Sponholz, Junge, Beller, and co-workers developed a reversible hydrogen storage and release system on the basis of lysine and a manganese pincer complex (Figure 5).[113] In the dehydrogenation reaction, a total TON of 670,000 was achieved over 10 catalytic cycles.

Besides these common metals for dehydrogenation reactions, some exotic systems were developed. For example, in 2014 Berben and Myers developed an aluminium pincer complex for formic acid dehydrogenation (Figure 5).[114] Initial activity was reported to be 5,200 h^{-1}. However, TON remained comparatively low (2,200). In the same year, nickel pincer complexes were reported for formic acid dehydrogenation by Enthaler, Junge, and co-workers (Figure 5).[115] A productivity of 626 turnovers could be realized.

1.3 Pincer complexes

As evident from the examples presented in chapter 1.2, pincer complexes generally show high activities in various (de)hydrogenation reactions. Typically, pincer ligands are tridentate chelating ligands (Figure 6).[21-24, 116] The three sites coordinating to the metal center can consist of atoms like N, C, P, S, Si, B, Se, As, or Si. Pincer-based ligands and complexes are usually named after the donor atoms, i.e. PNP-ligand stands for a ligand containing two phosphorous and one nitrogen atom in the indicated order. They are separated by a spacer typically comprising of an alkylic chain. However, it can contain functionalities like NR, O, CO, or CS groups. Additionally, pincer ligands can contain a (hetero)aromatic group in their backbone.

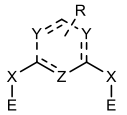

Z = N, C, S, Si, P, B, ...
X = CH_2, NR, O, CO, CS, ...
Y = CH, N, ...
E = PR_2, NR_2, NHC, $P(OR)_2$, OR, OPR_2, $OP(OR)_2$, SR, SeR, AsR, SiR, ...
R = H, alkyl, aryl, electron donating or withdrawing groups

Figure 6. General structure of pincer ligands.

Among all these possible combinations, PNP-pincer complexes are one of the most commonly used ones, especially in dehydrogenation reactions (chapter 1.2).[21-24, 116] Their first catalytic application was demonstrated 2001 by Hartwig and Kawatsura in the addition of amines to acrylic acid derivatives (Figure 7).[117] In this case, the active species was formed in situ from the ligand and a palladium precursor. One year later Rieger and co-workers utilized the first cobalt pincer complex in ethylene polymerization (Figure 7).[118] The complexes were more active by three orders of magnitude, than the corresponding NNN-pincer complexes. Further, iron pincer complexes were synthesized, however they were not applied in catalysis. McGuinness, Wasserscheid, and co-workers demonstrated the activity of chromium pincer complexes with an aliphatic backbone in the ethylene trimerization (Figure 7).[119] Similarly to the polymerization of ethylene, NNN complexes were previously applied in the trimerization of α-olefins.[120]

In 2004, ruthenium and iridium PNP-pincer complexes were first applied (Figure 7).[121, 122] Abdur-Rashid and Goussev patented the use of iridium and ruthenium pincer complex in transfer hydrogenation reactions.[121] At the same time, Milstein and co-workers investigated ruthenium pincer complexes in the dehydrogenation of alcohols.[122] Interestingly, their investigations revealed the presence of an equilibrium between a monomeric and a nitrogen bridged dimeric species. One year later, Milstein and co-workers applied this dehydrogenation in the synthesis of esters from alcohols.[123] This publication marks the first application of a ruthenium carbonyl PNP-pincer complex.

Kirchner and co-workers synthesized and characterized a multitude of new molybdenum, iron, ruthenium, nickel, and palladium PNP-pincer complexes with diaminopyridine- and benzoguanamine-based ligand backbones (Figure 7).[124] The synthesized palladium complexes

were employed in Suzuki-Miyaura cross coupling reactions[124] and iron complexes in the synthesis of 3-hydroxyacrylates.[125] Similar iron complexes with pyridine backbones were synthesized in 2011 by Milstein and co-workers (Figure 7).[126] They were applied in the hydrogenation of ketones. In the same year, the famous Ru-MACHO complex was firstly reported by Kuriyama and co-workers (Figure 7).[127] Applications include the hydrogenation of esters to alcohols. Notably, 2.2 t of methyl (*R*)-lactate could be reduced with this complex.

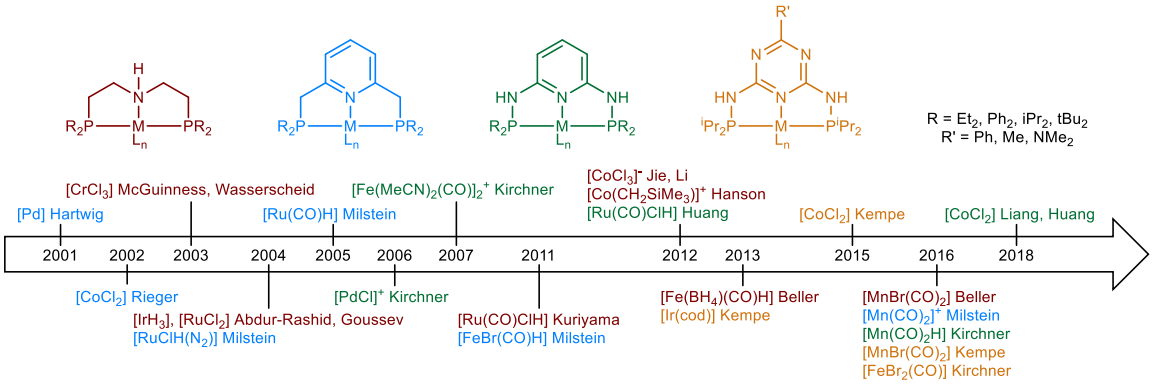

Figure 7. Application of PNP-pincer complexes in catalysis. Colors symbolize the different ligand backbone structures. Figure adapted from ref[128].

In 2012 Jie, Li, and co-workers, as well as Hanson and co-workers reported cobalt PNP-pincer complexes for the polymerization of 1,3-butadiene, as well as the hydrogenation of C=C, C=O, and C=N double bonds respectively (Figure 7).[129, 130] At the same time Huang and co-workers utilized diaminopyridine-based PNP-pincer complexes in the transfer hydrogenation of different ketones.[131] In the next year, an iron pincer complex was utilized for the first time in the dehydrogenation of methanol (see chapter 1.2.1).[63] Simultaneously, Kempe and Michlik applied the benzoguanamine ligand backbone for the first time in catalysis.[132] Their iridium complex showed high activity in the synthesis of pyrroles from secondary alcohols and amino alcohols. Shortly after, the same group demonstrated the activity of the related cobalt complexes in the hydrogenation of C=O double bonds.[133]

2016 marks the start of the investigation of manganese-based PNP-pincer complexes (Figure 7). First works were performed by the working groups of Beller,[13] Milstein,[134] Kirchner,[135] and Kempe[136] within the same year. They all reported manganese pincer complexes with different ligand backbones. Applications include the hydrogenation of ketones,[13, 136] aldehydes,[13, 136] nitriles,[13] as well as the synthesis of secondary amines[135] and aldimines[134, 135] from alcohols and imines. The triazine-based ligand backbone was further investigated by Kirchner and co-workers.[137] They demonstrated the ability of iron complexes to alkylate amines with alcohols. This type of ligand backbone can easily be modified at the triazine ring (Figure 7, R'). This allows for easy fine-tuning of electronic properties and thereby optimization of the catalyst for a given reaction. Lastly, Liang, Huang, and co-workers reported cobalt pincer complexes based on the diaminopyridine scaffold (Figure 7).[138] They were employed in the hydrogenation of nitriles.

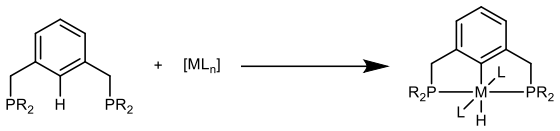

Figure 8. General synthesis of PCP-pincer complexes.

Another interesting subclass are PCP-pincer ligands and their complexes. Typically, PCP-pincer complexes are synthesized as highlighted in Figure 8. Coordination of the ligand proceeds *via* activation of the C-H bond of the ligand. Consequently, additional reactivity can be expected at this position. Indeed, Jia and co-workers observed the incorporation of phenylacetylene into the Ru-C bond back in 1996 (Figure 9).[139, 140]

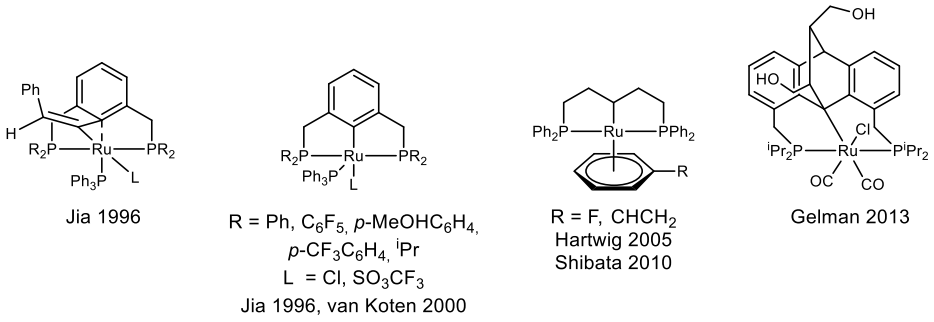

Figure 9. Ruthenium PCP-pincer complexes. Figure adapted from ref[141].

As highlighted in chapter 1.2.2, nickel PCP-complexes have been employed in the dehydrogenation of formic acid.[115] Focusing on ruthenium PCP-complexes, Jia and co-workers first synthesized arylic PCP-pincer complexes (Figure 9).[139, 140] They were later on employed by van Koten and co-workers in the transfer hydrogenation of ketones.[142-144] In 2005, Hartwig and co-workers synthesized and characterized alkylic PCP-pincer complexes (Figure 9).[145] Applications include the hydroamination of vinylarenes[145] and catalytic nucleophilic substitution reactions.[146] Gelman and co-workers investigated PCP-pincer complexes based on the anthracene scaffold (Figure 9). They were applied in dehydrogenative coupling reactions and transfer hydrogenations.[147-149]

2 OBJECTIVES

As highlighted in chapter 1, new catalysts are needed for the transformation of the chemical industry from fossil fuel-based feedstocks to renewable resources. Therefore, we set out to synthesize new catalysts and to evaluate those in various hydrogenation and dehydrogenation reactions. In this regard, especially methanol APR became of interest for its high potential as an energy carrier in the hydrogen economy. Consequently, one goal of this work is the evaluation of methanol APR in context of its industrial applicability.

The first approach towards the synthesizing new catalysts is based on the guanamine backbone. As evident from chapter 1.3, ruthenium complexes bearing this ligand were previously not prepared. Based on their structural similarity to other ruthenium pincer complexes, a highly active catalyst should be formed. Therefore, these new complexes will be evaluated in various dehydrogenation and hydrogenation reactions.

In the second approach, it is planned to immobilize ruthenium pincer complexes. In this way, the advantages of homogeneous (e.g. high activity) and heterogeneous (e.g. easy catalyst recovery) catalysts can be combined. To enable the immobilization, the introduction of an anchoring group to the ligand backbone is necessary. In this regard, it is planned to investigate the catalytic activity of these newly synthesized complexes.

3 RESULTS AND DISCUSSION

3.1 Guanamine-Based Ruthenium Pincer Complexes

As highlighted in the introduction, the evolution of the chemical industry towards progressively applying renewable resources necessitates new catalysts. As pincer complexes show great potential in various dehydrogenation and hydrogenation reactions, they became of interest for further evaluation. To the best of our knowledge ruthenium PNP-pincer complexes with a guanamine-based ligand backbone have not been synthesized before (see chapter 1.3 and Figure 7). Therefore, we set out to synthesize this subclass of PNP-pincer complexes and evaluate it in (de)hydrogenation reactions.

3.1.1 Complex synthesis and characterization

Ligand **1** was synthesized in a straightforward manner from benzoguanamine and chlorodiisopropylphosphine.[132, 133] The complexation was performed with $[Ru(CO)(Cl)H(PPh_3)_3]$ according to reported methods for similar complexes (Scheme 2).[131] However, the reaction was unselective and multiple products were formed. Separation by column chromatography yielded two products. Structural determination by NMR was difficult, however high-resolution mass spectrometry suggested the formation of a monomeric (**2m**) and dimeric (**2d**) species. Indeed, SC-XRD led to the assigned structures of **2m** and **2d** (Figure 10).

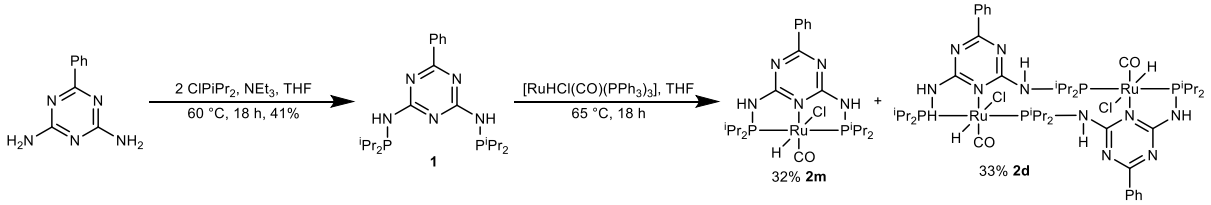

Scheme 2. Synthesis of ligand **1** and its complexation with $[Ru(CO)(Cl)H(PPh_3)_3]$ to yield monomeric **2m** and dimeric complex **2d**. Scheme adapted from ref[128].

Crystals suitable for x-ray diffraction were grown from vapor diffusion of pentane into a saturated solution of the complexes in THF. In both complexes, the metal centers are coordinated by two phosphorous and one nitrogen atom of ligand **1**, as well as a hydrido, chloro and carbonyl ligand. A distorted octahedral coordination environment is formed. In **2m**, pincer ligand **1** coordinates meridionally to the metal center, as commonly observed for PNP-pincer complexes (Figure 10, left).[123, 131-133, 136, 137, 150] In **2d**, the pincer ligand acts as a bridging ligand, coordinating with one phosphorous and one nitrogen atom to the first metal center and with the second phosphorous atom to another metal center (Figure 10, right). To the best of our knowledge, this coordination of guanamine-based PNP-pincer ligands was not reported previously.

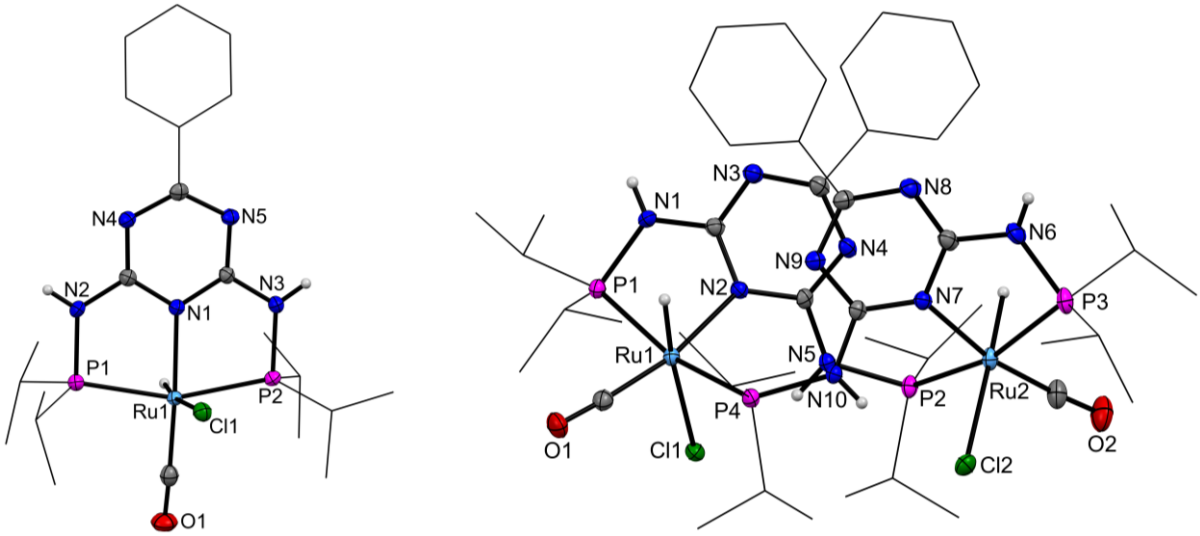

Figure 10. Molecular structure of **2m** (left) and **2d** (right). Displacement ellipsoids are drawn at 30% (**2d**) and 50% (**2m**) probability at 110 K. Hydrogen atoms are omitted for clarity, except those on Ru and N. Phenyl and isopropyl groups are displayed as wire frames for better graphical representation. Disordered parts of **2d** are shown only in one position. Figure adapted from ref[128].

In both complexes, the distortion of the octahedral coordination environment is most pronounced in the P-Ru-P angles (**2m**: P1-Ru1-P2: 160.03(3)°; 2d: P1-Ru1-P4: 162.867(19)°, P2-Ru2-P3: 162.76(2)°; expected: 180°). Furthermore, the triazine plane in **2d** (mean deviation of the best plane: 0.06 and 0.07 Å) deviates significantly from the planarity observed in **2m** (mean deviation of the best plane: 0.006 Å). Additionally, Ru and N atoms neighboring this plane deviate more strongly from it in **2d** (distance to the plane: Ru1: 0.75, N1: 0.21, N5: 0.35, Ru2: 0.84, N6: 0.22, N10: 0.33 Å), than **2m** (largest deviation for C4 (phenyl ring) from the plane: 0.06 Å).

3.1.2 Dehydrogenation of formic acid

Having both complexes in hand, their potential as catalysts was examined in several benchmark reactions. First, the dehydrogenation of formic acid was investigated. As highlighted in chapter 1.2.2, several metal PNP-pincer complexes showed good activity in formic acid dehydrogenation. Therefore, the new complexes **2m** and **2d** were compared to these reaction systems for an initial evaluation (Table 2). For comparison especially the reaction systems published by Pidko and co-workers (2014),[102] Zheng, Huang, and co-workers (2016),[106] and Beller and co-workers (2019)[105] are of interest due to their structural similarities but also differences to **2m** and **2d**.

First, two sets of reaction conditions based on a strong base (KOH) published by Beller and co-workers were investigated. Reaction conditions A are strongly basic. Here, dimeric complex **2d** showed similar activities as complexes **3**. Both were outperformed by complex **4**. In the more acidic variation - conditions B - complexes **2d**, **3** and **4** showed activites within the same order of magnitude. To our delight new complex **2m** was significantly more active. Switching to

reaction conditions with an amine-base, the new complexes **2m** and **2d** were not able to reach the activities achieved with complex **5** in conditions C. However, with a different solvent and base (conditions D), complexes **2m** and **2d** showed the most promising results so far. Hence, these reaction conditions were further investigated.

Table 2. Initial screening of reaction conditions published in literature. Table adapted from ref[128].

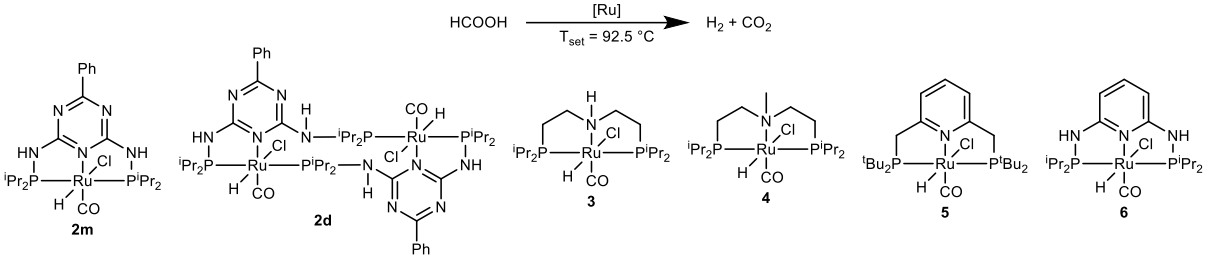

Reaction conditions	Literature		New Complexes	
	Catalyst	TOF [h^{-1}]	Catalyst	TOF [h^{-1}]
Conditions A[105]	**3**	2,100[105]	**2d**	2,700
	4	4,200[105]		
Conditions B[105]	**3**	5,300[105]	**2m**	67,000
	4	9,000[105]	**2d**	3,600
Conditinos C[102]	**5**	256,000[102]	**2m**	98,000
			2d	42,000
Conditinos D[106]	**6**	7,300[106]	**2m**	354,000
			2d	128,000

Reaction conditions: T_{set} = 92.5 °C, Conditions A: formic acid (1.2 mL), KOH (40 mmol), H_2O (8.8 mL), triglyme (4 mL), catalyst (4.4 µmol); Conditions B: formic acid (1.9 mL), KOH (40 mmol), H_2O (8.1 mL), triglyme (4 mL), catalyst (4.4 µmol); Conditions C: formic acid (2.22 to 15 mL/h), $NHex_3$ (11.4 mL), DMF (23.6 mL), catalyst (1.42 µmol); Conditions D: formic acid (0.30 to 4.6 mL/h), NEt_3 (1.5 mL), DMSO (5 mL), catalyst (1.00 µmol).

First, the maximum activity was determined in batch reactions. It was calculated from the gas evolution during set time intervals. Monomeric complex **2m** reached a maximum activity of 470,000 h^{-1} (Table 3, entry 1). Lower catalytic activity was observed for dimeric complex **2d** (TOF_{max}: 54,000 h^{-1}, Table 3, entry 2). Notably, activity could be improved when the reaction was continued by addition of more formic acid (TOF_{max}: 112,000 h^{-1}). This is attributed to the poor solubility of **2d** in DMSO during the first run. Pincer complex **3** showed the lowest activity among all tested complexes (TOF_{max}: 38,500 h^{-1}, Table 3, entry 3). As expected, its methylated variant **4** is significantly more active with a TOF_{max} of 280,000 h^{-1} (Table 3, entry 4).[105] Furthermore it shows the highest activity among the tested known complexes (TOF_{max}: 155,000 h^{-1} for **5** and 200,000 h^{-1} for **6**, Table 3, entries 5 and 6). It is worth noting, that the activity of **6** was significantly improved in comparison to literature (200,000 h^{-1} to 7,333 h^{-1}) due to changing from P^tBu_2 to P^iPr_2 groups. Overall, complex **2m** showed the highest activity and consequently the shortest reaction time for full conversion among all tested complexes.

Table 3. Comparison of ruthenium PNP-pincer complexes in formic acid dehydrogenation. Table adapted from ref[128].

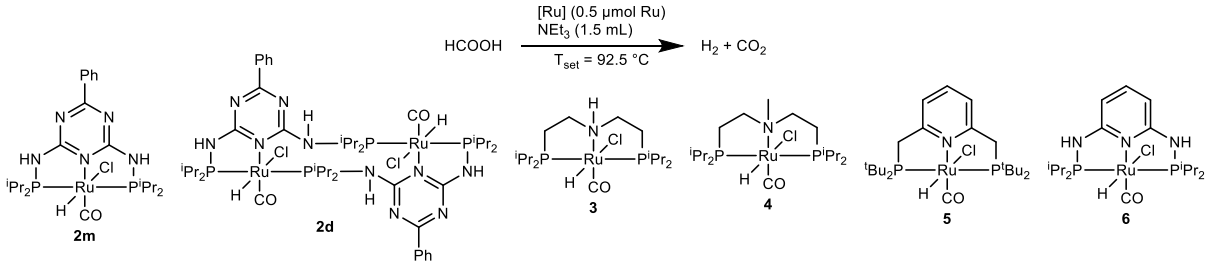

Entry	Catalyst	Reaction time until full conversion [min]	TOF_{max} [h^{-1}]	TON
1	**2m**	3	470,000	23,000
2	**2d**	40	54,000	23,000
		16[a)]	112,000	23,000
3	**3**	50	38,500	23,000
4	**4**	6	280,000	23,000
5	**5**	13	155,000	23,000
6	**6**	9	200,000	23,000

Reaction conditions: Formic acid (0.41 mL, 10.8 mmol), NEt_3 (1.5 mL), DMSO (5 mL), catalyst (0.50 µmol Ru), T_{set} = 92.5 °C. Reactions were started by catalyst addition and repeated at least twice with a standard deviation of <10%. a) Data after continuation of the experiment by addition of formic acid (0.41 mL, 10.8 mmol).

Table 4. Continuous addition reactions. Table adapted from ref[128].

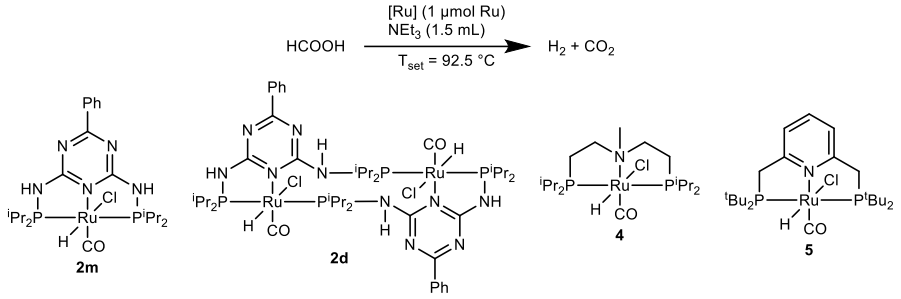

Entry	Catalyst	Reaction time [min]	TOF_{max} [h^{-1}]	TON
1	**2m**	62	350,000	240,000
2	**2d**	150	130,000	250,000
3	**4**	60	230,000	125,000
4	**5**	80	185,000	175,000

Reaction conditions: formic acid (4.6 - 13 mL/h), NEt_3 (1.5 mL), DMSO (5 mL), catalyst (1.0 µmol Ru), T_{set} = 92.5 °C. TOF_{max} was determined by variation of formic acid dosage rate.

The most active complexes were examined more closely in reactions with continuous addition of formic acid. By a slow increase of the formic acid addition speed, the maximum activity was determined. Typically, a sharp drop of activity was observed, when the amount of formic acid inside the reactor surpassed the amount of base, i.e. the addition of new formic acid surpassed its consumption. Similar to the batch reactions, **2m** was the most active complex with a TOF_{max}

of 350,000 h^{-1} (Table 4, entry 1) followed by **4** (TOF_{max}: 230,000 h^{-1}, Table 4, entry 3). Dimeric complex **2d** reached a maximum activity of 130,000 h^{-1} and **5** of 185,000 h^{-1} (Table 4, entries 2 and 4).

3.1.3 Hydrogenation of CO_2

Based on the promising results for formic acid dehydrogenation, we became interested in the reverse reaction, the hydrogenation of CO_2. Combining both reactions would allow the reversible storage and release of hydrogen gas in the form of formic acid and demonstrate its applicability as an energy carrier.

Table 5. Ruthenium pincer complex catalyzed CO_2 hydrogenation. Table adapted from ref[128].

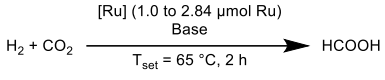

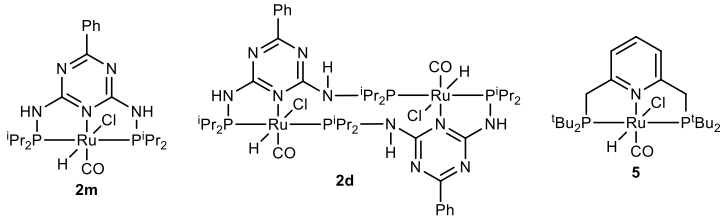

Entry	Catalyst	Amount of Ru metal [µmol]	TOF [h^{-1}]	Yield [mmol]
1	**2d**[a)]	2.00	0	0
2	**2d**[a)]	1.00	0	0
3	**2m**[a)]	1.00	6,300	13
4	**5**[a)]	1.00	4,600	9
5	**2d**[b)]	2.84	20,900	59
6	**2d**[b)]	1.40	27,200	38
7	**2m**[b)]	1.42	7,300	21
8	**5**[b)]	1.42	36,000[102]	102

Reaction conditions: a) All reactions were done in a 300 mL stainless steel autoclave with 12 mL glass vials. NEt_3 (1.5 mL), DMSO (5 mL), H_2 (20 bar), CO_2 (20 bar), T_{set} = 65 °C, 2 h. Yields were determined by ^1H NMR with DMF as internal standard. b) conditions analogous to ref[102]. All reactions were done in a 100 mL stainless steel autoclave. DBU (5.0 mL), DMF (30.0 mL), catalysts (1.42 µmol Ru unless noted otherwise), H_2 (20 bar), CO_2 (20 bar), T_{set} = 65 °C, 2 h. Yields were determined by ^1H NMR with toluene as internal standard. All experiments were repeated at least once.

First, the same reaction conditions as for formic acid dehydrogenation were employed. However, **2d** was inactive and the activity of **2m** and **5** remained comparatively low (TOF: 6,300 h^{-1} for **2m** and 4,600 h^{-1} for **5**, Table 5, entries 1 to 4). Therefore, the optimized reaction conditions from Pidko and co-workers were further investigated.[102] Interestingly, dimeric complex **2d** outperformed its monomeric counterpart significantly (27,200 h^{-1} for **2d** to 7,300 h^{-1} for **2m**, Table 5, entries 6 and 7). Additionally, it was shown, that an increase in metal

loading leads to the expected lower activity and higher yield (Table 5, entry 5). However, established catalyst **5** proved to be the most active for this reaction (TOF: 36,000 h^{-1}, Table 5, entry 8).

3.1.4 Hydrogenation of unsaturated organic compounds

As **2m** and **2d** proved to be active hydrogenation catalysts, the reduction of different functional groups became of interest, too. More specifically, acetophenone, 4-phenylbenzonitrile, methyl benzoate and quinoline were chosen as benchmark substrates for ketones, nitriles, esters and heteroaromatic compounds. In the presence of base (KO^{t}Bu) all substrates could be reduced in good to excellent yields under reaction conditions typically found used for homogeneous ruthenium hydrogenation catalysis (64% to 98% yield, Scheme 3).[116, 127, 151-153] In most cases monomeric catalyst **2m** gave higher yields than the dimeric complex **2d** (94% to 98% vs. 66% to 77%). Notably, hydrogenation of methyl benzoate yielded the same yield (64%) for both complexes.

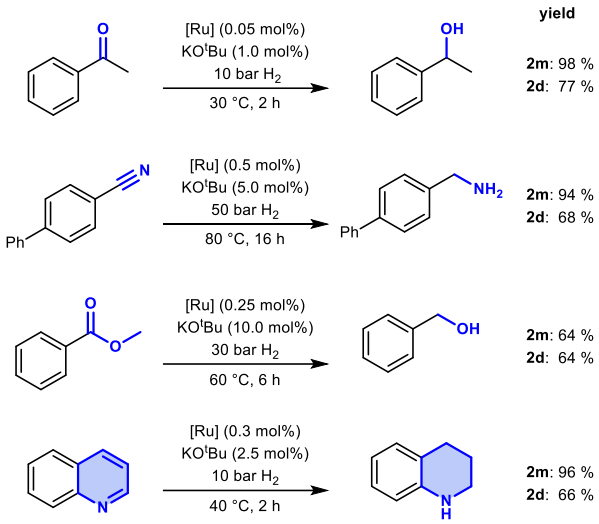

Scheme 3. Hydrogenation of functional groups utilizing guanamine-based ruthenium PNP-pincer complexes **2m** and **2d**. Scheme adapted from ref[128].

3.1.5 Catalyst integrity under catalytic conditions

As both complexes **2m** and **2d** typically exhibit different catalytic activity in the tested reactions, it can be assumed, that there is no interconversion between both species. To further prove the integrity of both species during catalysis, a solution of each complex was heated to 115 °C for 18 h. Only 8% of **2d** converted into **2m**, whereas no interconversion was observed for the latter. In the presence of base (NEt_3, 2 h, 90 °C), with both complexes no reaction took place. Consequently, both complexes can be assumed to be stable under the employed reaction conditions with the conversion of **2d** to **2m** only taking place at elevated reaction temperatures.

3.2 Ruthenium PNPC-Pincer Complexes – A New Class of Metal Pincer Complexes

Based on our research groups long interest in the application of different pincer complexes in catalytic reactions,[13, 48, 60, 63, 113, 153, 154] we envisioned their immobilization to improve reusability and economic viability (for an economic evaluation of pincer complexes in methanol dehydrogenation see chapter 3.3). Therefore, the introduction of suitable substituents on the nitrogen atom of the pincer ligand was investigated. This led to the serendipitous discovery of a new class of metal pincer complexes, namely Ru-PNPC-ones.

3.2.1 Complex synthesis and characterization

For the immobilization of pincer complexes, it was planned to connect the complex to an anchoring group on the support *via* a Sharpless-type click reaction. This concept was successfully applied by Lo and Copéret for NHC-based pincer complexes in 2019.[155] Consequently, an alkyne group had to be introduced in the ligand backbone. Hence, ligand **7** was synthesized starting with the alkylation of bis-(2-chloroethyl)-ammonium chloride with 3-(trimethylsilyl)-propargylbromide (Scheme 4). Subsequent phosphination yielded the protected ligand **7'** in 75%. After its deprotection, ligand **7** was synthesized in 78% yield.

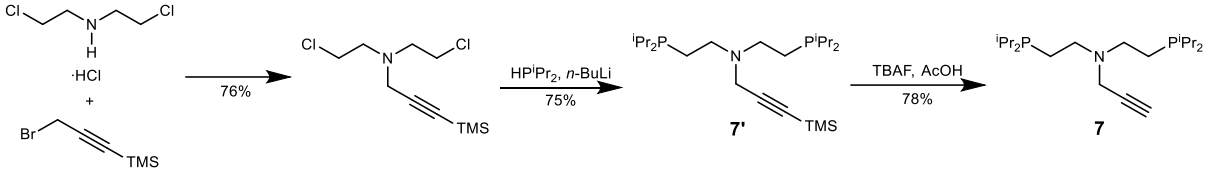

Scheme 4. Synthesis of ligand **7** and its protected variant **7'**. Scheme adapted from ref[141].

Afterwards, the reaction of **7** with [Ru(CO)(Cl)H(PPh_3)$_3$] was investigated (Scheme 5). At 60 °C reaction temperature, 6 d were needed to reach full conversion of the ligand. However, a product mixture was formed. With an increased reaction temperature (120 °C), full conversion could be achieved in 3 h. Additionally, better selectivity could be observed in ^{1}H and ^{31}P NMR leading to the isolation of a mixture of **8** and **10** in 15% yield via column chromatography. To improve selectivity and yield of the complex synthesis, n-butyl ammonium acetate was added. Further, the reaction time could be decreased to 36 h at 60 °C. Finally, yield could be increased to 66% in the reaction at 120 °C leading to the isolation of complexes **8** and **9** with a ratio of 41:59. Computationally, a difference in Gibbs free energy of 0.96 kcal/mol was calculated, corresponding to a ratio of 17:83. It is worth noting, that the original target complex **11** could not be obtained *via* this route, as the synthesis led to the serendipitous discovery of PNPC-pincer complexes.

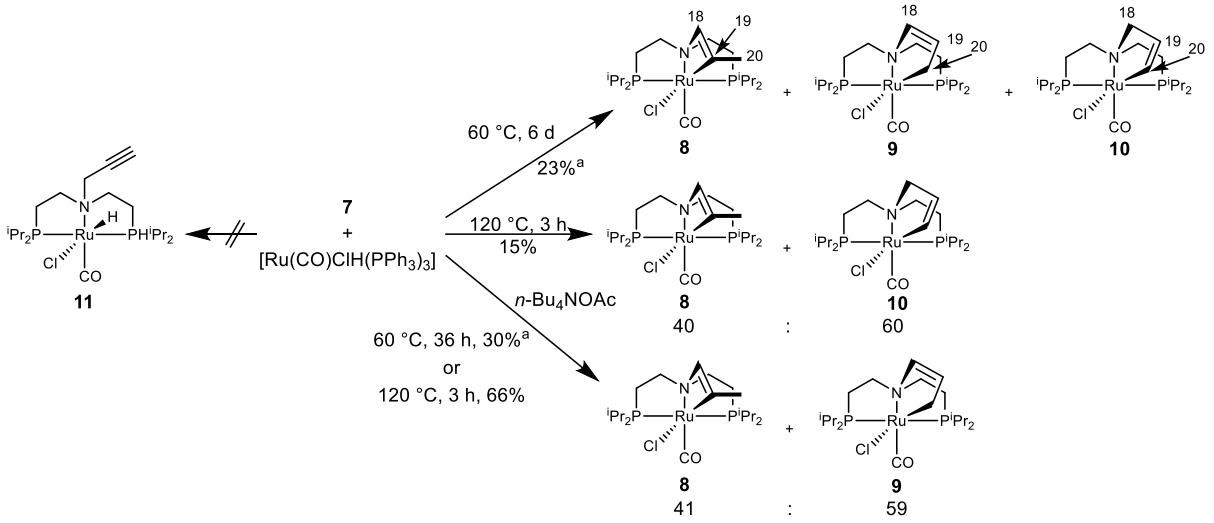

Scheme 5. Synthesis of PNPC-complexes **8** to **10**. Scheme adapted from ref[141].

Complexes **8** and **9** were characterized by a combination of NMR and SC-XRD. Crystals suitable for SC-XRD were obtained from a concentrated solution of the complex mixture in ethyl acetate yielding mixed crystals of both species. In both **8** and **9**, a distorted octahedral coordination environment is formed around the metal center by two phosphorous, one carbon and one nitrogen atom of ligand **7**, as well as a carbonyl and chlorido ligand.

In complex **8** (Figure 11, left), the coordination of C19B to the metal center is indicated by its chemical shift (^{13}C NMR: 160.0 ppm). Furthermore, the position of the double bond between C18B and C19B is evident from the characteristic shift of the adjacent atoms (^{1}H NMR: 4.98 (H18B) ppm; ^{13}C NMR: 160.0 (C19B), 120.3 (C18B) ppm). The positioning of the double bond is in further agreement with the observed bond length between C18B and C19B (1.336(10) Å) as it is within range of a typical C(sp^2)-C(sp^2) double bond.[156, 157] The assigned structure is further supported by the splitting pattern, as it indicates the presence of a CH and a CH_3 group with a coupling constant of 2.0 Hz, being in line with a ^{4}J coupling.

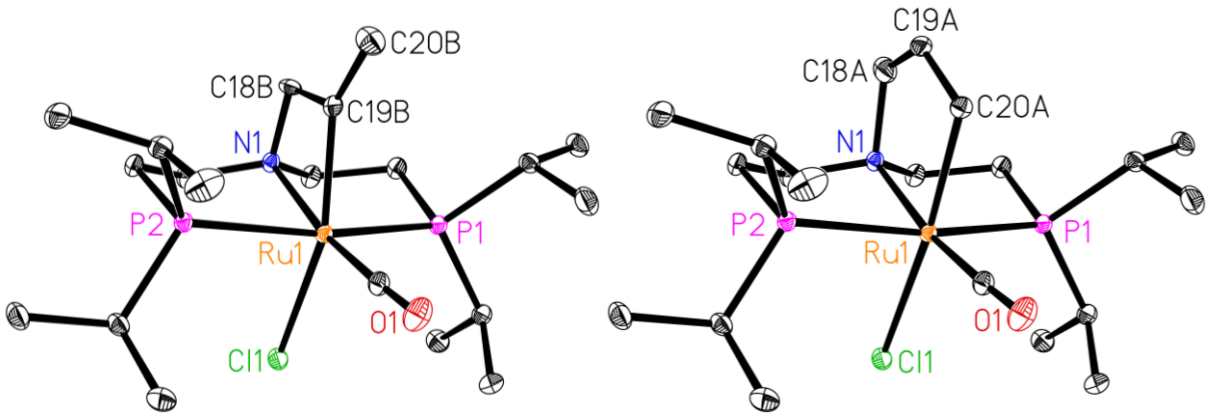

Figure 11. Crystal structure of the mixed crystal of **8** (left, atoms with the suffix A are omitted) and **9** (right, atoms with the suffix B are omitted) Displacement ellipsoids are drawn at 30% probability at 110 K. Hydrogen atoms are omitted for clarity. Figure adapted from ref[141].

In complex **9** (Figure 11, right), a double bond can be located between C18A and C19A due to the chemical shift of the adjacent atoms (^{1}H NMR: 5.70 (H18A), 4.45 (H19A) ppm; ^{13}C NMR: 141.2 (C18A), 137.1 (C19A) ppm). Additional evidence can be found in the bond length of 1.352(7) Å at this position. Based on these results in combination with the splitting pattern and DEPT measurements, a N–CH=CH–CH_2 fragment was assigned. Subsequently, the coordination of C20A to the metal center can be found in the crystal structure.

Complex **10** could only be characterized by NMR, as it was not possible to obtain crystals suitable for x-ray structural analysis. Opposite to complexes **8** and **9**, the double bond was assigned between C19 and C20 by chemical shift of the corresponding atoms (^{1}H NMR: 7.27 (H20), 5.45 (H19) ppm; ^{13}C NMR: 157.1 (C20), 124.5 (C19) ppm; For numbering of atoms see Scheme 5). Based on these data, coordination of C20 to the metal center is likely. Furthermore, the chemical shift of C18 (^{13}C NMR: 64.5 ppm) and H18 (^{1}H NMR: 2.69 ppm) suggests the presence of a NCH_2 fragment. Based on these findings in combination with splitting patterns and coupling constants, structural elucidation could be realized.

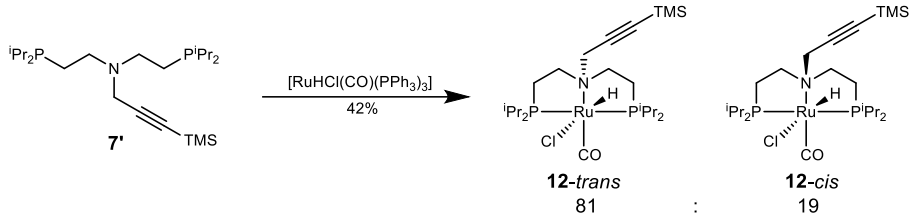

Scheme 6. Complexation of ligand **7'** to yield complexes **12**-*cis* and **12**-*trans* with a ratio of 19:81. The ratio of both isomers was determined by ^{1}H NMR and assigned by NOESY measurements. Scheme adapted from ref[141].

In addition to these results, the complexation of ligand **7'** with [Ru(CO)(Cl)H(PPh_3)$_3$] was carried out (Scheme 6). Pincer complex **12** could be synthesized in 42% yield. Notably, the presence of the *cis*- and *trans*-isomers in an 19:81 ratio could be observed. Computationally, a similar ratio of 11:89 was determined (**12**-*trans* was computed to be more stable by 1.25 kcal/mol than **12**-*cis*). Moreover, the deprotection of **12** yielded an unknown main product, whose structural elucidation was not possible.

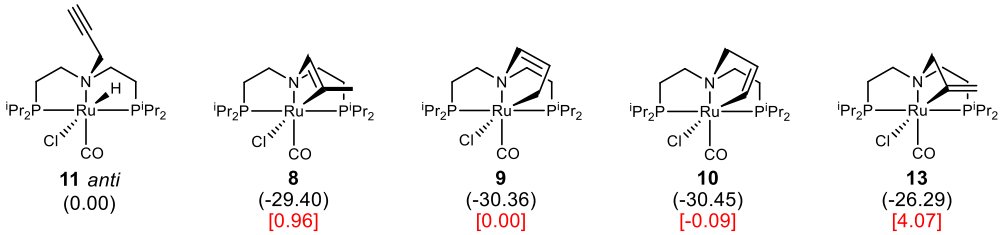

Figure 12. Calculated Gibbs free energies of (ΔG, kcal/mol) of Ru-PNPC pincer complexes **8** to **11** and **13**. Figure adapted from ref[141].

For further investigation of the stability of the complexes, DFT calculations were performed using B3PW91/TZVP for full structural optimization and energy calculations (Figure 12). It could be shown that coordination of the propylene arm by its partial reduction with the hydrido

ligand of the metal precursor is strongly exergonic by roughly -30 kcal/mol (Figure 12, difference between **11** and **10**, **13**). Successive isomerization of the formed double bond leads to complexes **8** and **9**. It is worth noting, that exocyclic isomer **13** is significantly less stable, than its endocyclic counterparts and could therefore not be observed experimentally.

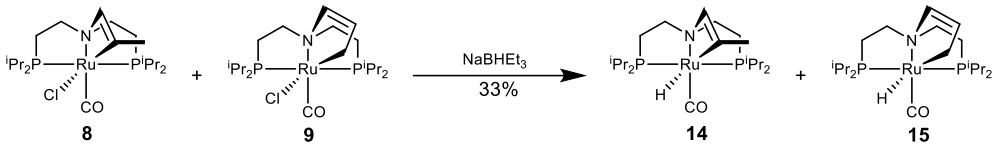

Scheme 7. Synthesis of hydrido PNPC-complexes **14** and **15**. Scheme adapted from ref[141].

To enable the use of the complexes in base free reactions, complexes **8** and **9** were transformed into the hydrido PNPC-complexes **14** and **15** utilizing $NaBHEt_3$ (Scheme 7). The desired product was isolated in 33% yield while retaining the isomeric ratio of the educt complexes.

3.2.2 Dehydrogenation of formic acid

Having synthesized several new Ru-PNPC-pincer complexes, first their potential in formic acid dehydrogenation was investigated, as this reaction is of high interest for hydrogen storage technologies, as highlighted in chapter 1.2.2. More specifically, a mixture of complexes **14** and **15** was employed, as they (i.e. complexes **8** and **9**) could be synthesized in high yield. As it was not possible to purify the isomeric mixture and obtain the pure complex, the mixture of both isomers was used as catalyst. Previously, Beller and co-workers showed, that formic acid dehydrogenation is unaffected by the concentration of base below a concentration of 0.7 M.[105] Indeed, this effect could also be observed for the new PNPC-complexes, where similar activity was observed between complexes **14** + **15** and the base-activated complexes **8** + **9** (Table 6, entry 1 and 2, **14** + **15**: TOF: 598 h^{-1}, TON: 1610; **8** + **9**: TOF: 540 h^{-1}, TON: 1500).

Furthermore, the new PNPC-pincer complexes **14** and **15** were compared to state-of-the-art metal PNP-pincer complexes. As base-free formic acid dehydrogenation was examined, the activated complexes **3**-H and **4**-H necessary for the reaction were prepared. As expected from literature, complex **4**-H proved to be the most active among the PNP-pincer complexes (Table 6, entries 3-5; **3**-H: TOF: 378 ,**4**-H: TOF: 584, **16**-BH: 415 h^{-1}).[105] To our delight, PNPC-pincer complexes **14** and **15** gave similar activity compared to the PNP-pincer complexes. Furthermore, it is worth noting, that activity was observed in additive free methanol dehydrogenation for PNPC-complexes **14** and **15**. However, in this latter case reproducibility remained poor.

Table 6. Additive free formic acid dehydrogenation utilizing ruthenium pincer complexes. Table adapted from ref[141].

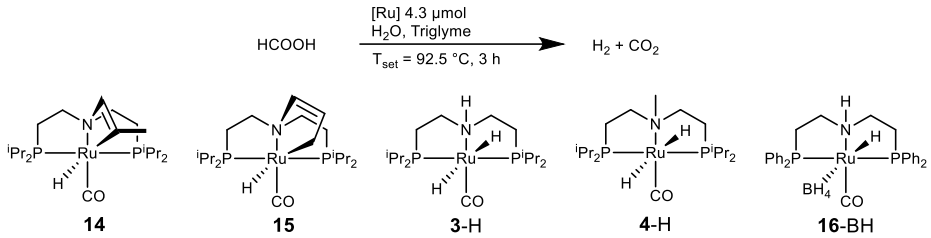

Entry	Catalyst	TOF_{1h} [h^{-1}]	TON_{3h}	CO content [ppm]
1[b)]	**8** + **9**	540	1500	3
2	**14** + **15**	598	1610	<1
3	**3**-H	378	1040	4
4	**4**-H	584	1730	2
5	**16**-BH	415	1280	3

Reaction conditions: a) formic acid (32 mmol, 1.2 mL), H_2O (8.8 mL), triglyme (4 mL), catalyst (4.3 µmol), 92.5 °C. Reactions were performed at least twice with a standard deviation <15%, except entry for 3. b) The complex was activated with 1.6 eq. of KOH prior to the reaction.

3.2.3 Transfer (de)hydrogenation of organic compounds

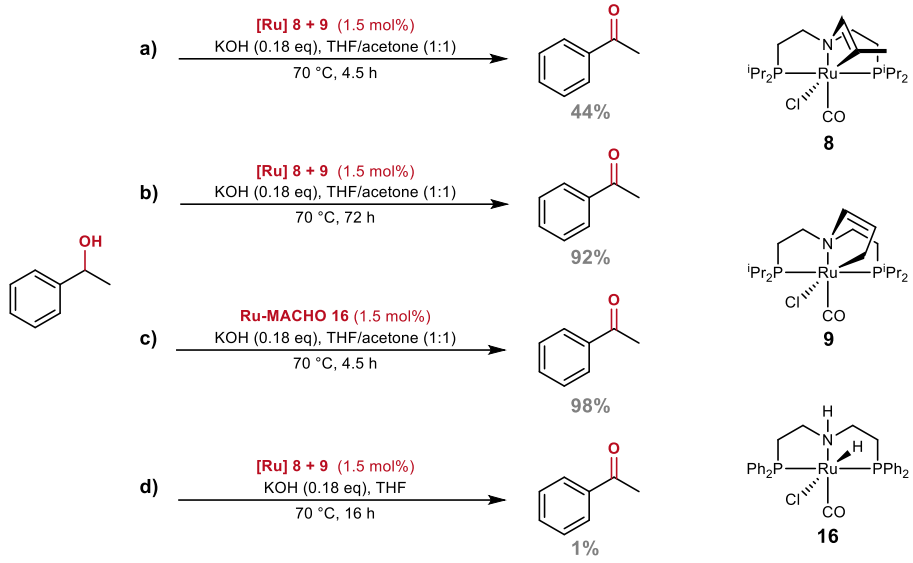

Scheme 8. Transfer dehydrogenation of 1-phenylethanol utilizing complexes **8** + **9** and **16**. Scheme adapted from ref[141].

Reaction conditions: Substrate: 0.25 mmol; a, b, c: THF/acetone 1:1 (10 mL); d: THF (10 mL). Yields were determined by GC-FID analysis using hexadecane as internal standard. Catalyst concentration is reported as the amount of complex mixture employed. Equivalents refer to the substrate.

Having observed good activity in dehydrogenation reactions, the potential of the new Ru-PNPC-complexes in transfer dehydrogenation and transfer hydrogenation reactions was investigated. Starting with the dehydrogenation of 1-phenylethanol, 44% yield was reached

after 4.5 h (Scheme 8a). Comparing the PNPC-complexes **8** + **9** to the established Ru-MACHO complex (**16**), 98% yield was reached with the latter under the same reaction conditions (Scheme 8c). It was possible to increase yield with PNPC complexes **8** + **9** to 92% by raising the reaction time to 72 h (Scheme 8b). Finally, the necessity of a hydrogen acceptor was demonstrated, as a reaction without acetone in an open system led to low yield (Scheme 8d). It is worth noting, that aldol addition and condensation of acetone was the main source of side product formation (4-hydroxypentan-2-one and pent-3-en-2-one).

Having demonstrated good catalytic activity in the transfer dehydrogenation, the transfer hydrogenation of unsaturated organic compounds was investigated. More specifically ketones, alkanes and alkynes were examined utilizing reaction conditions established in literature (Scheme 9).[142-144, 158, 159] In the transfer hydrogenation of ketones (acetophenone and cyclohexanone) both substrates could be reduced in quantitative yield within 4 h utilizing **16** or PNPC-pincer complexes **8** + **9** (Scheme 9a, 9b). When comparing both complexes at shorter reaction times (15 min), PNPC-complexes **8** + **9** were outperformed by **16**.

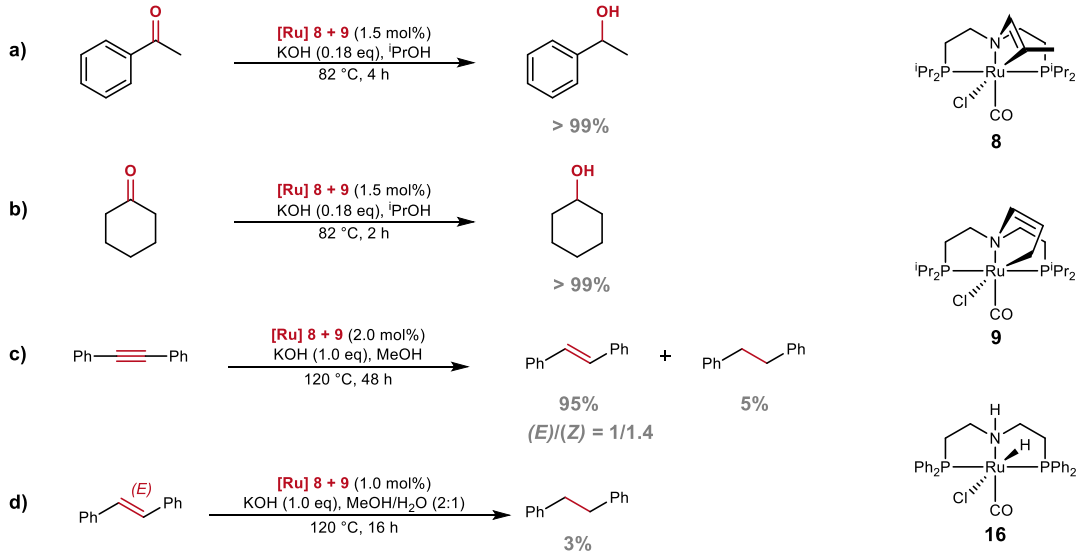

Scheme 9. Transfer hydrogenation of unsaturated organic compounds utilizing complexes **8** + **9**. Scheme adapted from ref[141].

Reaction conditions: a, b: Substrate: 0.25 mmol, ^{i}PrOH (10 mL); c: Substrate: 0.25 mmol, MeOH (2 mL); d: Substrate: 0.25 mmol, MeOH/H_2O 2:1 (2 mL). Yields were determined by GC-FID analysis using hexadecane as internal standard. Catalyst concentration is reported as the amount of complex mixture employed. Equivalents refer to the substrate.

Having observed activity in the dehydrogenation of methanol (see chapter 3.2.2) its use as the hydrogen source was investigated in the transfer hydrogenation of alkenes and alkynes. In the transfer hydrogenation of diphenylacetylene semi-hydrogenation of the triple bond to stilbene was observed in 95 % yield within 48 h (Scheme 9c). The remaining 5% were attributed to the fully reduced product. The catalyst slightly favored the formation of the (*Z*) isomer over the (*E*) isomer (*E*/*Z* = 1/1.4). Jagadeesh, Balaraman, and co-workers utilized Ru-MACHO **16** for the same reaction and observed invers selectivity with an *E*/*Z* ratio of 100/1.[158] Additionally, higher side-product formation i.e. over reduction was observed in their case (10% compared to 5%).

To further highlight the improved chemoselectivity, the reduction of stilbene was attempted utilizing the optimized reaction conditions by Jagadeesh, Balaraman, and co-workers.[158] Here, only 3% of the fully reduced product was found with complex **8** + **9** (Scheme 9d). Furthermore, the transfer hydrogenation of diazobenzene and methyl benzoate were attempted unsuccessfully.

3.2.4 Mechanistic investigations

As the complexes **14** and **15** (and complexes **8** and **9**) proved to be active catalysts in various transfer hydrogenation and dehydrogenation reactions, the elucidation of the reaction mechanism came to our attention. Especially the stability of the characteristic Ru-C bond is of interest. Focusing on formic acid dehydrogenation, a reaction *via* an inner sphere mechanism can be expected, as it was postulated for related Ru-PNP complexes.[70] Based on this mechanism, two reaction pathways are possible, which were investigated by DFT calculations for complexes **14** and **15** (Figure 13 and 14): First, coordination of formic acid proceeds via Ru-C bond cleavage, a formal metathesis between the Ru-C bond of the complex and the O-H bond of formic acid, resulting in the formation of complexes **14A** and **15A** (Ru-C route, cleavage of Ru-C bond). Subsequent CO_2 release leads to the formation of dihydrido complexes **14B** and **15B**. In the second route, a formal acid base reaction between the metal hydride and formic acid leads to the release of hydrogen gas and the formation of formate complexes **14C** and **15C** whilst keeping the Ru-C bond intact (Ru-H route, Ru-C bond stays intact). Reaction is followed by the release of CO_2 to reform complexes **14** and **15**. It is worth noting that complexes **14** and **15** are isoenergetic thereby enabling direct comparison of their activity.

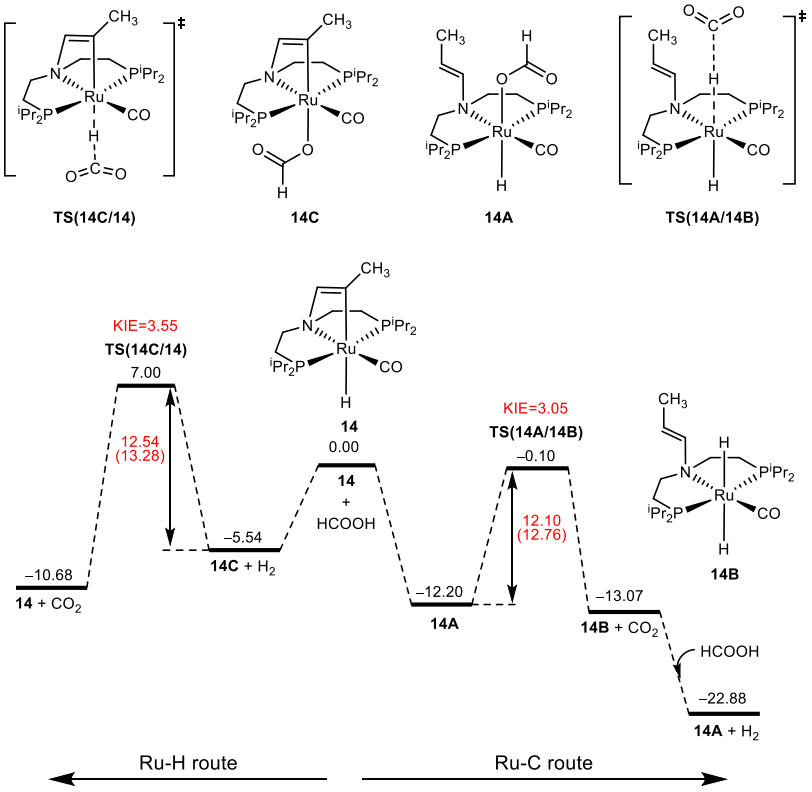

Figure 13. Formic acid dehydrogenation with complex **14** showing Ru-H (left) and Ru-C (right) route. Gibbs free energies are given in kcal/mol. Figure adapted from ref[141].

For complex **14**, initial reaction with formic acid is energetically more favoured via the Ru-C route (-12.20 kcal/mol) than the Ru-H route (-5.54 kcal/mol, Figure 13). Consequently, breaking of the Ru-C bond is thermodynamically more favored than of the Ru-H bond by 6.66 kcal/mol. In the Ru-C route, CO_2 elimination proceeds via CH-activation and **TS(14A/14B)** with a Gibbs free energy barrier of 12.10 kcal/mol. It is exergonic by 0.87 kcal/mol. Subsequent hydrogen release by a reaction of **14B** with one equivalent formic acid and regeneration of **14A** is exergonic by 9.81 kcal/mol. In the Ru-H route CO_2 elimination proceeds via C-H activation and **TS(14C/14)**. It has a Gibbs free energy barrier of 12.54 kcal/mol and is exergonic by 5.14 kcal/mol. Additionally, complex **14** is regenerated.

Comparing both routes, they have close Gibbs free energy barriers (12.10 and 12.54 kcal/mol). However, due to the higher stability of **14A** compared to **14C**, Ru-C route should be more favored based on the Curtin-Hammett principle.

Similar to complex **14**, for complex **15** the initial reaction with formic acid is thermodynamically more favored via Ru-C route, than Ru-H route (-7.65 kcal/mol vs. -4.52 kcal/mol). CO_2 release and C-H activation via **TS(15A/15B)** is slightly exergonic by 1.01 kcal/mol in the Ru-C pathway with a Gibbs free energy barrier of 11.63 kcal/mol. Subsequent reaction with one equivalent of formic acid and H_2 release is exergonic by 9.67 kcal/mol, leading to the reformation of **15A**. In the Ru-H route CH-activation and CO_2 release is thermodynamically favorable by 6.16 kcal/mol. The energy barrier of **TS(15C/15)** is with 10.70 kcal/mol smaller, than in the Ru-C route (**TS(15A/15B)**: 11.63 kcal/mol).

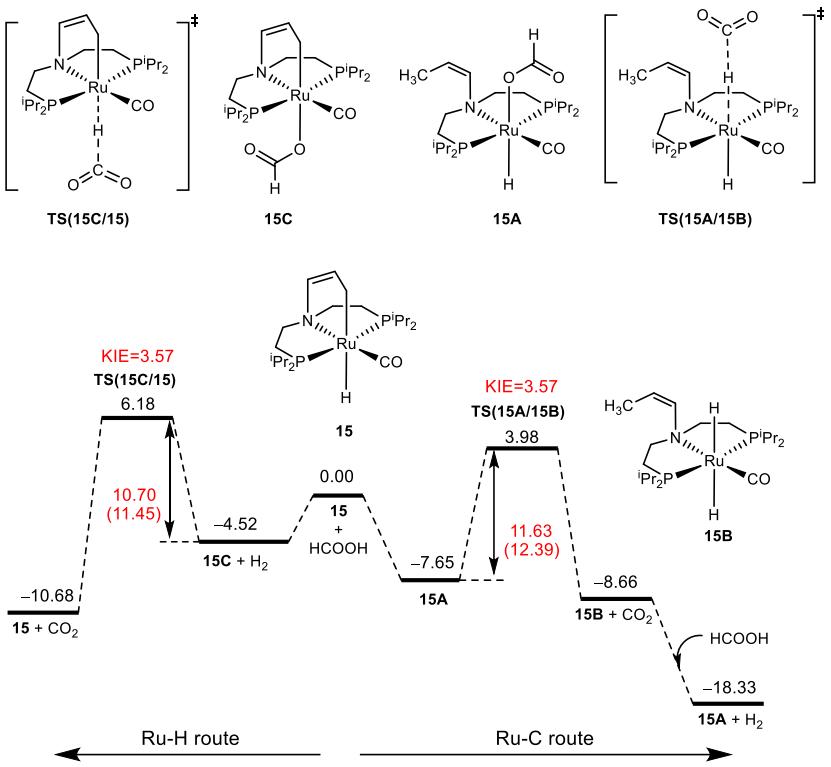

Figure 14. Formic acid dehydrogenation with complex **15** showing Ru-H (left) and Ru-C (right) route. Gibbs free energies are given in kcal/mol. Figure adapted from ref[141].

To summarize, in both complexes **14** and **15**, Gibbs free energy barriers of the transition states of both routes remain close (12.10 vs. 12.54 kcal/mol and 11.63 vs. 10.70 kcal/mol). However, considering the stability of the formate complexes **14A**, **14C**, **15A**, and **15C** reaction via the Ru-C route should be thermodynamically more favorable. In addition, the kinetic isotope effect (KIE) for deuterated formic acid (DCOOD) was determined to be 3.05 for **14** and 3.57 for **15** in the Ru-C route.

Experimental investigations were carried out to prove, weather formic acid dehydrogenation proceeds *via* Ru-C or Ru-H route. In a first reaction, the mixture of complexes **14** and **15** was reacted with stoichiometric amounts of formic acid and monitored at different reaction times by NMR. Overall, 5 main products were observed, whose concentration changed with ongoing reaction time. After 6 h, mainly one product was formed, which was assigned to **15C** due to the presence of one formate signal (^{1}H NMR: 9.02 (s) ppm), the absence of a hydride signal and the chemical shift of the phosphorous atoms, as well as the propene-arm (^{1}H NMR: 5.66 (dt, J = 5.1, 3.3 Hz), 4.39 (dt, J = 4.8, 2.3 Hz) ppm; ^{31}P NMR: 60.09 ppm). Furthermore, the observed characteristic signals are similar to those of the related formate complex **4**-FA.[70]

After 5 d at RT, the amount of **15C** decreased to 44%. Furthermore, the observation of four other species became possible. Characteristic signals were assigned to hydrido formate complexes (^{1}H NMR: 9.27 (s), 9.24 (s), 9.19 (s), 9.17 (s), -16.84 (t, J = 18.6 Hz), -16.90 (t, J = 18.2 Hz), -16.99 (t, J = 18.7 Hz), -17.17 (t, J = 18.8 Hz) ppm; ^{31}P NMR: 71.84, 71.14, 69.61, 69.37 ppm), showing similarities to **4**-FA. Consequently, the structures of **14A**, **15A** and their

corresponding *cis* isomers were assigned (referring to the orientation of the propylic arm and the hydrido ligand).

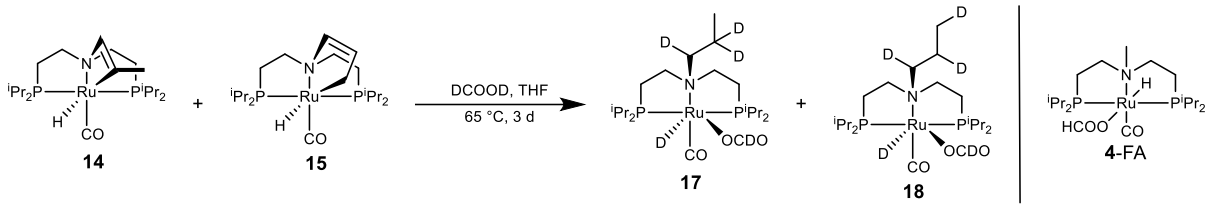

Scheme 10. Transfer hydrogenation of unsaturated organic compounds utilizing complexes **8** + **9**. Scheme adapted from ref[141].

In a second experiment, catalysis was performed in the presence of deuterated formic acid (DCOOD, Scheme 10). As the PNPC-ligand stays intact in the Ru-H pathway, no incorporation of deuterium into the ligand backbone is expected. Further, the formation of a Ru-D or Ru-OOCD complex is likely. In the Ru-C pathway, the Ru-C bond is broken and consequently, the incorporation of deuterium into the ligand backbone is expected. Furthermore, a [Ru(D)$_2$(CO)(PNP)] or [RuD(OOCD)(CO)(PNP)] species should be formed. After reaction at 65 °C for 3 d in a pressure tube, the reaction solution was analyzed by NMR. Similar to the reaction with stoichiometric amounts of formic acid, formate and hydride signals were found (^{2}H NMR: 8.43 (s, br), -17.19 (s, br) ppm). In combination with the ^{31}P NMR spectrum (^{31}P NMR: 71.59, 69.69 ppm), the formation of hydrido formate complexes is indicated. Furthermore, signals in the alkylic region were observed (^{2}H NMR: 3.60 (s, br), 2.79 (s, br), 1.76 (s, br), 1.55 (s, br), 1.28 (s, br), 0.75 (s, br) ppm) and in combination with TOCSY and 2D-measurements assigned to propylic groups. Consequently, the formation of **17** and **18** is likely.

Based on these results, the initial formation of **14C** and **15C** upon addition of formic acid should be kinetically controlled and the subsequent formation of other products (Ru-H vs. Ru-C route) thermodynamically controlled. Thus, in the beginning of the reaction, catalysis mainly proceeds *via* Ru-H route. With ongoing reaction time, the concentration of **14A** and **15A** increases and the Ru-C pathway should become dominating.

3.3 A Critical Evaluation of Methanol APR

3.3.1 Development of standardized reaction conditions

As methanol is a promising energy carrier, we became interested in investigating its reformation to hydrogen gas as part of the hydrogen economy. Additionally, as highlighted in chapter 1.2.1, ruthenium and iron pincer complexes were among the most active ones in this reaction. Therefore, we became interested in evaluating the previously introduced Ru-PNPC- and Ru-guanamine-based PNP-pincer complexes in methanol APR. For an improved evaluation of new catalysts in this reaction, standardized reaction conditions will be developed and evaluated. Additionally, methanol reformation is critically investigated towards its potential as an energy storage medium on an industrial scale.

Scientific literature revealed a high impact of different reaction conditions, including additives, on the catalytic activity (see chapter 1.2.1). To develop standardized reaction conditions, reported examples were evaluated based on two main criteria: 1) Catalysts should show good activities under the respective reaction conditions, and 2) should allow for the generation of significant amounts of hydrogen gas in a quickly reached and stable working phase. Additionally, catalysts should operate at low temperatures (<100 °C) and with high selectivity (<10 ppm CO impurities). Based on these criteria, two different reaction conditions were chosen as a potential standard:

1.: Basic additives (Beller and co-workers): MeOH (9 mL), H_2O (1 mL), triglyme (20 mL), KOH (10 mmol), catalyst (0.015 mol%, 8.5 µmol), T_{set} = 92.5 °C.[51]

2.: Lewis acidic additives (Bernskoetter, Hazari, Holthausen, and co-workers): MeOH (160 µL), H_2O (18 µL), EtOAc (10 mL), $LiBF_4$ (0.1 mmol), catalyst (0.01 mol%, 0.1 µmol), T_{set} = 80 °C.[64]

In the work by Bernskoetter, Hazari, Holthausen, and co-workers high stability (TON: 51,000 h^{-1}) was quickly reached during a stable working phase. Basic additives on the other hand showed a high activity during a quickly reached working phase whilst retaining high stability (TON: 10,000; TOF: 190 h^{-1}). These latter reaction conditions will be highlighted first in the following chapter.

3.3.2 Basic additives

Proper evaluation of (strongly) basic additives requires a closer look on the underlying reactions. Generally, high reaction temperatures and ambient pressure are beneficial for methanol APR (most literature systems operate between 80 and 100 °C). Without additives, these reaction temperatures can't be reached, as the internal reaction temperature is limited by the boiling point of methanol (65 °C).[51] The reaction temperature can be increased by the

addition of a strong base.[48, 51, 55, 58, 63] For example, in an 8 M KOH solution, internal reaction temperature increased to 88.5 °C.[51] Another way to achieve the same result is the introduction of a high boiling solvent in addition to lower amounts of a strong base as additive.[51]

Evaluation of the effect of a strong base (for simplicity KOH in the following example) on catalysis requires a closer look at the underlying reactions. In the beginning of the reaction, KOH consumes the produced CO_2 and is thereby converted to carbonate (equation 1). Thus, a strong base is converted in a weaker one and the pH-value drops. This process is called initiation phase and ends when all base is consumed (Figure 15). It is characterized by a high reaction rate and the evolution of pure hydrogen gas. As it consumes base, the process is not sustainable.

$$CH_3OH + H_2O + KOH \rightarrow 3\,H_2 + KHCO_3 \quad (1)$$

$$CH_3OH + H_2O \rightarrow 3\,H_2 + CO_2 \quad (2)$$

After the initiation phase, the working phase starts. As there is no more strong base being consumed, a stable pH is reached and a mixture of H_2 and CO_2 is produced (equation 2). Consequently, a stable reaction with lower activity, than in the working phase is reached (Figure 15).

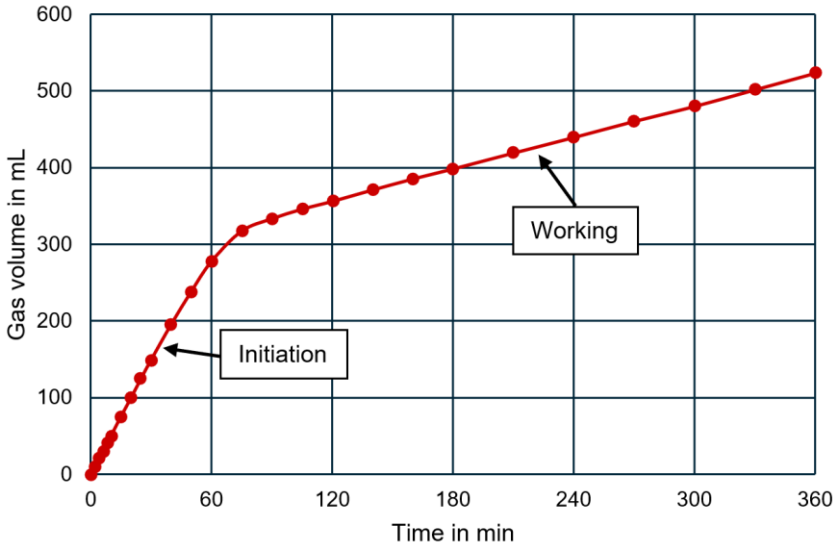

Figure 15. Exemplary ruthenium catalyzed methanol APR showing different reaction phases. Scheme adapted from ref[52].

As low base concentrations are beneficial for quickly reaching the working phase, the addition of a high boiling solvent is necessary to reach high reaction temperatures. Therefore, the reaction conditions developed by Beller and co-workers in 2019 were chosen for further evaluation as a potential standard among all other base-mediated literature examples.[51]

Having defined standardized reaction conditions, their suitability was first investigated using different ruthenium pincer complexes (Table 7). To validate our results, two literature known complexes were investigated first. Indeed, with a working phase TOF of 143 h^{-1} for **3** and 168 h^{-1} for **4**, comparable results to literature were obtained (Table 7, entries 1 and 2).[51] It is

worth noting, that an increase in CO impurities was observed (53 and 19 ppm, respectively). Similarly, with most other catalysts, a CO content between 10 and 90 ppm was detected.

Table 7. Ruthenium catalyzed methanol APR utilizing basic reaction conditions.[a] Table adapted from ref[52].

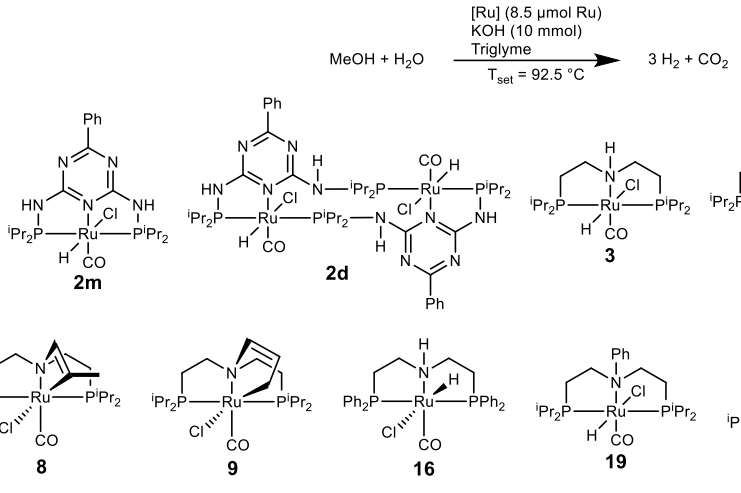

Entry	Catalyst	Initiation time [h]	Initiation phase TOF [h^{-1}]	Working phase TOF [h^{-1}]	Gas evolution rate [mL/h]	CO content [ppm]
1	**3**	1.8	917	144	42	57
2	**4**	3.0	547	168	48	24
3	**8** + **9**[b]	3.5	519	153	43	50
4	**19**[b]	4 d[c]	16	–	–	65
5	**16**	2.7	597	153	44	58
6	**20**	5.0	339	122	33	<10
7	**6**	18 h	84	0	0	563
8	**2m**[b]	8 d	9	2	0.43	86
9	**2d**[b]	31 d[c]	5	–	–	31
10	**21**	30 d[c]	4	–	–	578

Reaction conditions: a) MeOH (9.00 mL), H_2O (1.00 mL), triglyme (20.0 mL), KOH (10.0 mmol), catalyst (8.32 to 8.99 µmol), T_{set} = 92.5 °C. TOF was calculated as an average over the whole initiation or working phase. Gas evolution rate was calculated as an average over the whole working phase. Working phase started after 340 mL gas evolution. b) For these complexes, methanol APR was not extensively demonstrated prior to this work. c) Estimated initiation time.

As evident from these reproduction experiments, nitrogen substitution can have a significant effect on activity. Therefore, other substituents were investigated. Starting with the PNPC-pincer complexes **8** + **9**, similar activity to complex **4** was observed (working phase TOF: 153 h^{-1}, Table 7, entry 3). The same trend could be observed for formic acid dehydrogenation (see chapter 3.2.2). When switching to a phenyl substituent (complex **19**), low catalytic activity was observed during initiation phase (TOF: 16 h^{-1}) even though the catalyst is known to be highly active in formic acid dehydrogenation (Table 7, entry 4).[160] Due to the long estimated initiation time, no working phase was recorded.

Next, a commonly used pincer complex, namely Ru-MACHO **16**, was investigated (Table 7, entry 5). With a high working phase activity of 597 h^{-1} it is among the most active catalysts for methanol APR. Based on these promising results from complexes **3**, **4**, **8** + **9**, and **16**, next variations in the ligand backbone were investigated. With a pyridyl group in the backbone (complex **20**), an increase in initiation time to 5 h was observed (Table 7, entry 6). Catalytic activity during working phase was at 122 h^{-1}. When additionally introducing aminophosphine moieties to the ligand (complex **6**), initiation time further increased to 18 h (Table 7, entry 7). However, all activity was lost in the working phase. Furthermore, it is worth noting, that CO impurities increased over the course of the reaction (10 ppm at 6 h to 563 ppm at 7 d). This increase corresponds to the loss of the CO ligand from the catalyst, rendering it inactive. Newly introduced guanamine based pincer complexes **2m** and **2d** (see chapter 3.1) showed long initiation time (8 d and 31 d, respectively, Table 7, entries 8 and 9). **2m** further showed low activity during working phase (TOF: 2 h^{-1}). Lastly, an acridine based pincer complex **21**, recently employed by Milstein and co-workers in methanol APR, was investigated.[57] In their case reaction was carried out at 150 °C with thiol additives. However, at 90 °C catalytic activity remained low (initiation phase TOF: 4 h^{-1}), rendering the observation of the working phase impossible (Table 7, entry 10). In addition, with 578 ppm, high CO impurities were detected.

Table 8. Metal catalyzed methanol APR utilizing basic reaction conditions.[a] Table adapted from ref[52].

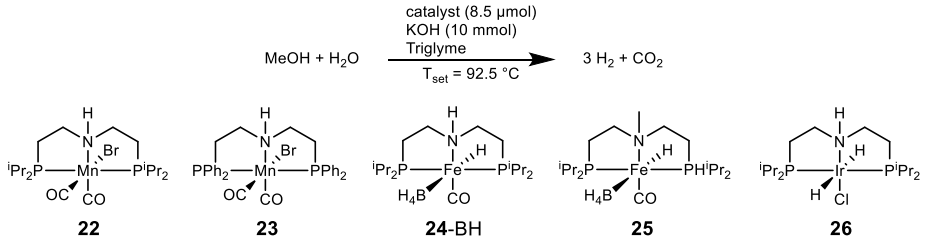

22 **23** **24**-BH **25** **26**

Entry	Catalyst	Initiation time [h]	Initiation phase TOF [h^{-1}]	Working phase TOF [h^{-1}]	Gas evolution rate [mL/h]	CO content [ppm]
1	**22**	–	–	–	–	–
2	**23**[b]	–	–	–	–	–
3	**24**-BH	8.7 h	183	44	12	48
4	**25**[b]	17 h[c]	92	–	–	112
5	**26**[d]	5.4 d	17	3	0.75	60

Reaction conditions: a) MeOH (9.00 mL), H_2O (1.00 mL), triglyme (20.0 mL), KOH (10.0 mmol), catalyst (8.41 to 8.99 µmol), T_{set} = 92.5 °C, 6 h. TOF was calculated as an average over the whole initiation or working phase. Gas evolution rate was calculated as an average over the whole working phase. Working phase started after 340 mL gas evolution. b) For these complexes, methanol APR was not investigated prior to this work. c) Estimated initiation time. d) Working phase started after 450 mL gas evolution.

As highlighted in chapter 1.2.1 other metal complexes showed promising results in methanol APR. Therefore, iridium, manganese, and iron pincer complexes were further investigated under the proposed standardized reaction conditions (Table 8). First, manganese pincer

complexes **22** and **23** were examined (Table 8, entries 1 and 2). Despite being successfully applied previously,[62] they proved to be inactive under these reaction conditions. Iron pincer complex **24**-BH yielded better results (Table 8, entry 3). During the initiation phase a TOF of 183 h^{-1} was reached. Compared to previous results with similar employed base concentrations, this marks a significant improvement (0.5 M KOH, TOF: 10.3 h^{-1}).[63] Due to this enhancement, it was possible to record the working phase for the first time in base mediated iron catalyzed methanol APR with a TOF of 44 h^{-1}. Besides this iron complex, its N-methylated variation **25** was investigated, as it is known to be active in formic acid dehydrogenation[161] despite iron pincer complexes typically following an outer sphere reaction mechanism (Table 8, entry 4).[64, 154, 162-165] In this case, initiation phase activity was recorded (TOF: 92 h^{-1}). However, it remained lower by about 50% than for complex **24**-BH.

Besides these iron and manganese complexes, iridium pincer **26** was examined under the proposed standardized conditions (Table 8, entry 5). In the initiation phase, a strong increase in activity was observed. However, this phase of high activity was not stable and reaction rate slowly decreased. Iridium catalysts are known for their pH-sensitivity. As the pH-value is changing throughout the initiation phase, this "high activity phase" can be attributed to the pH-value where catalyst **26** works optimally. As one of the main criteria for the working phase is a high stability, the start of the working phase was chosen to be after the production of 450 mL of gas. Within this phase **26** was active with a TOF of 3 h^{-1}. Furthermore, due to the formation of CO impurities (60 ppm), the formation of the inactive iridium carbonyl complex is likely.[60]

3.3.3 Lewis acidic additives

Having investigated the first proposed standard reaction conditions, we switched our focus to the second set of reaction conditions using Lewis acidic co-catalysts. Bernskoetter, Hazari, Holthausen, and co-workers established the following reaction conditions in their work about the iron-catalyzed methanol APR:[64]

MeOH (160 µL), H_2O (18 µL), EtOAc (10 mL), $LiBF_4$ (0.1 mmol), catalyst (0.01 mol%, 0.1 µmol), T_{set} = 80 °C.

Utilizing these optimized reaction conditions, they achieved a high TON of 51,000 with iron PNP-pincer complex **24**-FA (Table 9, entry 1). Switching to the related complex **24**-BH, no gas evolution was observed after 18 h (Table 9, entry 2). Furthermore, activating the complex with base prior to the reaction led to no improvement (Table 9, entry 3). Therefore, reaction conditions were altered stepwise towards the basic reaction conditions described in the previous chapter (Table 9, entries 4-6). During these reactions, gas evolution cold only be observed in presence of base. The same result was obtained for ruthenium and iridium complexes **3** and **26** (Table 9, entries 7 to 14). They also proved to be inactive when only Lewis acidic additives were employed and showed activity as soon as base was introduced to the reaction system.

Notably, in all cases productivity was higher when only base and no Lewis acid were employed (280 mL to 304 mL for iron, 429 mL to 523 mL for ruthenium and 43 mL to 82 mL for iridium). Kirchner, Gonsalvi, and co-workers observed the same result with Lewis acidic additives.[110]

Table 9. Investigation of Lewis acidic additives.[a)] Table adapted from ref[52].

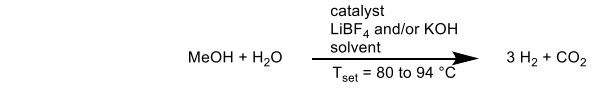

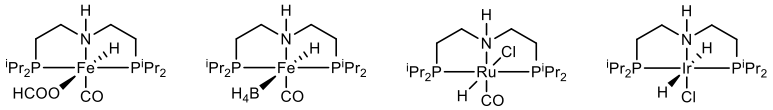

24-FA **24**-BH **3** **26**

Entry	Catalyst	Catalyst amount [µmol]	Solvent	Additives	Gas evolution [mL]
1[64]	**24**-FA	0.10	EtOAc	10 mol% $LiBF_4$	98[b)]
2	**24**-BH	0.10	EtOAc	10 mol% $LiBF_4$	0
3	**24**-BH	0.10	EtOAc	10 mol% $LiBF_4$ 0.1 mol% KOH	0
4	**24**-BH	8.39 to 8.49	Triglyme	10 mol% $LiBF_4$	0
5	**24**-BH	8.44 to 8.74	Triglyme	10 mol% $LiBF_4$, 18 mol% KOH	280
6	**24**-BH	8.52 to 8.74	Triglyme	18 mol% KOH	304
7	**3**	0.10	EtOAc	10 mol% $LiBF_4$	0
8	**3**	8.49 to 8.66	Triglyme	10 mol% $LiBF_4$	0
9	**3**	8.60 to 8.71	Triglyme	10 mol% $LiBF_4$, 18 mol% KOH	429
10	**3**	8.85 to 8.90	Triglyme	18 mol% KOH	523
11	**26**	0.10	EtOAc	10 mol% $LiBF_4$	0
12[c)]	**26**	4.25 to 4.47	Triglyme	10 mol% $LiBF_4$	0
13[c)]	**26**	4.26	Triglyme	10 mol% $LiBF_4$, 18 mol% KOH	43
14[c), 60]	**26**	4.18	Triglyme	18 mol% KOH	82

Reaction conditions: a) Reaction conditions with EtOAc as solvent: MeOH (160 µL), H_2O (18 µL), EtOAc (10.0 mL), $LiBF_4$ (10 mol%, 0.1 mmol), catalyst (0.01 mol%), T_{set} = 80 °C. The gas evolution after 18 h is recorded. Reaction conditions with triglyme as solvent: MeOH (9.00 mL), H_2O (1.00 mL), triglyme (20.0 mL), KOH (18 mol%, 10 mmol), $LiBF_4$ (10 mol%, 5.55 mmol), catalyst (8.39 to 8.90 µmol), T_{set} = 92.5 °C. The gas evolution after 6 h is recorded. Reactions without base were performed with the activated catalysts $[Ru(PN^HP^iPr)(CO)(H)_2]$ and $[Ir(PN^HP^iPr)(H)_3]$. b) The gas evolution after 52 h is recorded. c) Reaction conditions: MeOH (9.00 mL), H_2O (1.00 mL), KOH (5.00 mmol), $LiBF_4$ (5.00 mmol), catalyst (4.18 to 4.47 µmol), T_{set} = 94 °C. The gas evolution after 3 h is recorded.

To summarize, experimental results indicate a detrimental effect of Lewis acids on the catalytic activity in most cases. Therefore, low general applicability and poor suitability of the Lewis acidic reaction conditions can be determined.

3.3.4 Economic considerations

Having established and evaluated reaction conditions suitable for potential industrial applications, the viability of the best catalytic systems is economically examined. Currently, fossil fuel-based hydrogen gas is priced around 2 \$/kg. For the competitive production of hydrogen gas from methanol, a catalyst cost of 5% of the product price is assumed, a value typically found in industrial applications. Accordingly, a catalyst must be priced at less than $2.0 \cdot 10^{-4}$ \$/mol$_{H2}$ produced. With this figure, the target productivity (TON) in dependence of the catalyst price can be calculated (Figure 16).

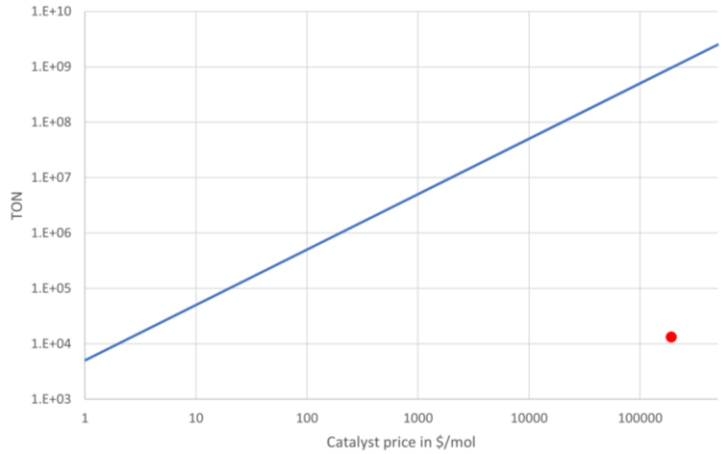

Figure 16. Catalyst productivity (TON) in dependence of its cost for methanol APR (blue). The red dot marks cost and TON for the commercially available so far best catalyst **3** under basic reaction conditions. For a catalyst to be commercially viable, it has to be above the blue line. Figure adapted from ref[52].

Examining the best commercially available catalyst **3** (priced at 405 \$/g or 190,000 \$/mol), a TON of 10^9 must be reached, for commercial viability. Considering the current activity, a lifetime of 750 years would need to be reached! As such timeframes are unrealistic, catalysts would need to be improved by at least three orders of magnitude in terms of activity and/or cost. To achieve such increases, completely new catalysts need to be developed whilst keeping these realistic requirements in mind. Furthermore, it is important to consider the cost of both metal and ligand, as they are for complexes like **3** nearly equally high. Therefore, switching from ruthenium PNP to iron PNP complexes does not significantly reduce catalyst costs.

4 CONCLUSION AND OUTLOOK

To summarize, multiple new ruthenium pincer complexes were synthesized and fully characterized by NMR spectroscopy and SC-XRD. More specifically, guanamine-based pincer complexes were synthesized. Interestingly, a monomeric **2m** and dimeric species **2d** were formed. It was only possible to convert **2d** into **2m** under harsh conditions. Thus, a good stability can be assumed during catalysis. Both complexes were examined in six different test reactions: the dehydrogenation of formic acid, hydrogenation of CO_2, and the reduction of four organic unsaturated compounds. In general, good to excellent yields and activities were obtained in all reactions with **2m** typically slightly outperforming **2d**. Notably, **2m** even outperformed established pincer complexes in the dehydrogenation of formic acid.

Besides these guanamine-based pincer complexes, a new subclass of pincer complexes, namely PNPC-pincer complexes, was introduced. They are characterized by the coordination of two phosphorous, one nitrogen and one carbon atom of the pincer ligand to the metal center. The catalytic activity of these complexes was investigated in base the free formic acid dehydrogenation and in the transfer (de)hydrogenation of organic molecules. Within these reactions, similar catalytic activity to state-of-the-art pincer complexes was observed. Mechanistic investigations revealed two competing reaction pathways. In the first, the Ru-C mechanism, the Ru-C bond is cleaved by a formal metathesis with the O-H bond of formic acid. In the second, the Ru-H mechanism, the Ru-C bond stays intact, and formic acid activation proceeds *via* an acid base reaction with the ruthenium hydride. Experimental results indicated the Ru-H mechanism to be dominant in the beginning of the reaction, while the Ru-C mechanism slowly takes over with ongoing reaction time.

These newly synthesized and state-of-the-art complexes were further employed in methanol APR. For this purpose, two sets of standardized reaction conditions were proposed whilst keeping industrial application in mind. The first reaction conditions focus on base mediated methanol APR. The most active complexes under these reaction conditions are **3**, **4**, **8** + **9**, **16**, **20**, and **24**-BH. The second standardized reaction conditions are based on Lewis acidic co-catalysts. Here, a low general applicability to other complexes was observed, rendering these reaction conditions unsuitable as a standard.

Lastly, evaluations of the economic viability of methanol APR revealed a striking need for new cheap and highly active catalysts, as state-of-the-art systems proved not to be economically viable. Within this work we demonstrated the synthesis of highly active catalysts. However, as they are based on expensive noble metals and ligands, their economic viability in methanol APR most likely remains low. Therefore, we would like to encourage all researchers working on this topic to specifically explore combinations of abundant metals and cheap ligands whilst keeping an economically viable process in mind.

5 REFERENCES

(1) Barreiro-Gen, M. Discussing Approaches to Standard of Living. In *Decent Work and Economic Growth*, Leal Filho, W., Azul, A. M., Brandli, L., Özuyar, P. G., Wall, T. Eds.; Springer, 2019; pp 1-15.

(2) Conceição, P. *Human Development Report 2023/2024*; United Nations Development Programme, New York, 2024.

(3) United Nations Department of Economic and Social Affairs Population Division *World Population Prospects 2019, Volume I: Comprehensive Tables*; 2019.

(4) Department for International Development *Growth Building Jobs and Prosperity in Developing Countries*; Department for International Development, United Kingdom, 2008.

(5) Wisniak, J. The History of Catalysis. From the Beginning to Nobel Prizes. *Educ. Quím.* **2010**, *21* (1), 60-69.

(6) van Santen, R. *Catalysis: From Principles to Applications*; Wiley-VCH, 2012.

(7) Humphreys, J.; Lan, R.; Tao, S. Development and Recent Progress on Ammonia Synthesis Catalysts for Haber–Bosch Process. *Adv. Energy Sustainability Res.* **2020**, *2* (1), 2000043.

(8) Blois, M. The Industrialization of the Haber-Bosch Process. *C&EN* **2023**, *101* (26), 20-21.

(9) Kumawat, J.; Gupta, V. K. Fundamental Aspects of Heterogeneous Ziegler–Natta Olefin Polymerization Catalysis: An Experimental and Computational Overview. *Polym. Chem.* **2020**, *11* (38), 6107-6128.

(10) Nicolaou, K. C.; Rigol, S. A Brief History of Antibiotics and Select Advances in Their Synthesis. *J Antibiot.* **2018**, *71* (2), 153-184.

(11) Nicolaou, K. C. Joys of Molecules. 1. Campaigns in Total Synthesis. *J. Org. Chem.* **2005**, *70* (18), 7007-7027.

(12) Johansson Seechurn, C. C. C.; Kitching, M. O.; Colacot, T. J.; Snieckus, V. Palladium-Catalyzed Cross-Coupling: A Historical Contextual Perspective to the 2010 Nobel Prize. *Angew. Chem. Int. Ed.* **2012**, *51* (21), 5062-5085.

(13) Elangovan, S.; Topf, C.; Fischer, S.; Jiao, H.; Spannenberg, A.; Baumann, W.; Ludwig, R.; Junge, K.; Beller, M. Selective Catalytic Hydrogenations of Nitriles, Ketones, and Aldehydes by Well-Defined Manganese Pincer Complexes. *J. Am. Chem. Soc.* **2016**, *138* (28), 8809-8814.

(14) Schrock, R. R.; Basset, J.-M.; Callens, E.; Riache, N.; Keitz, B. K.; Weinberger, D. S.; Lavallo, V.; Allen, D. P.; Solans-Monfort, X.; Copéret, C.; *et al. Handbook of Metathesis Volume 1: Catalyst Development and Mechanism*; Wiley-VCH Verlag GmbH & Co. KGaA, 2015.

(15) Hanson, P. R.; Maitra, S.; Chegondi, R.; Markley, J. L.; O'Leary, D. J.; O'Neil, G. W.; Lin, Y. A.; Davis, B. G.; Nam, Y. H.; Snapper, M. L.; *et al. Handbook of Metathesis Volume 2: Applications in Organic Synthesis*; Wiley-VCH Verlag GmbH & Co. KGaA, 2015.

(16) Slugovc, C.; Héroguez, V.; Chemtob, A.; Quemener, D.; Hanik, N.; Kilbinger, A. F. M.; Elacqua, E.; Brummelhuis, N. t.; Weck, M.; Miyake, G. M.; *et al. Handbook of Metathesis Volume 3: Polymer Synthesis*; Wiley-VCH Verlag GmbH & Co. KGaA, 2015.

(17) Kallmeier, F.; Kempe, R. Manganese Complexes for (De)Hydrogenation Catalysis: A Comparison to Cobalt and Iron Catalysts. *Angew. Chem. Int. Ed.* **2018**, *57* (1), 46-60.

(18) Das, K.; Waiba, S.; Jana, A.; Maji, B. Manganese-Catalyzed Hydrogenation, Dehydrogenation, and Hydroelementation Reactions. *Chem. Soc. Rev.* **2022**, *51* (11), 4386-4464.

(19) Wang, D.; Astruc, D. The Golden Age of Transfer Hydrogenation. *Chem. Rev.* **2015**, *115* (13), 6621-6686.

(20) Gunanathan, C.; Milstein, D. Applications of Acceptorless Dehydrogenation and Related Transformations in Chemical Synthesis. *Science* **2013**, *341* (6143), 1229712.

(21) Szabó, K. J.; Wendt, O. F. *Pincer and Pincer-Type Complexes: Applications in Organic Synthesis and Catalysis*; Wiley-VCH, 2014.

(22) van Koten, G.; Gossage, R. A. *The Privileged Pincer-Metal Platform: Coordination Chemistry & Applications*; Springer Cham, 2016.

(23) Morales-Morales, D. *Pincer Compounds: Chemistry and Applications*; Elsevier, 2018.

(24) Piccirilli, L.; Pinheiro, D. L. J.; Nielsen, M. Recent Progress with Pincer Transition Metal Catalysts for Sustainability. *Catalysts* **2020**, *10* (7), 773.

(25) *Chemical Process Catalysts*. Heraeus Holding, 2023. https://www.heraeus.com/en/hpm/hmp_products_solutions/heterogeneous_catalysts/chemical_process_catalysts/process_catalysts.html#tabs-1235788-2 (accessed 16.12.2024).

(26) Zybert, M. Applied Catalysis in Chemical Industry: Synthesis, Catalyst Design, and Evaluation. *Catalysts* **2023**, *13* (3), 607.

(27) Bai, S. T.; De Smet, G.; Liao, Y.; Sun, R.; Zhou, C.; Beller, M.; Maes, B. U. W.; Sels, B. F. Homogeneous and Heterogeneous Catalysts for Hydrogenation of CO_2 to Methanol under Mild Conditions. *Chem. Soc. Rev.* **2021**, *50* (7), 4259-4298.

(28) Klankermayer, J.; Wesselbaum, S.; Beydoun, K.; Leitner, W. Selective Catalytic Synthesis Using the Combination of Carbon Dioxide and Hydrogen: Catalytic Chess at the Interface of Energy and Chemistry. *Angew. Chem. Int. Ed.* **2016**, *55* (26), 7296-7343.

(29) Arora, V.; Yasmin, E.; Tanwar, N.; Hathwar, V. R.; Wagh, T.; Dhole, S.; Kumar, A. Pincer–Ruthenium-Catalyzed Reforming of Methanol─Selective High-Yield Production of Formic Acid and Hydrogen. *ACS Catal.* **2023**, *13* (6), 3605-3617.
(30) Ranjekar, A. M.; Yadav, G. D. Steam Reforming of Methanol for Hydrogen Production: A Critical Analysis of Catalysis, Processes, and Scope. *Ind. Eng. Chem. Res.* **2021**, *60* (1), 89-113.
(31) Moriarty, P.; Honnery, D. A Hydrogen Standard for Future Energy Accounting? *Int. J. Hydrog. Energy* **2010**, *35* (22), 12374-12380.
(32) Statistisches Bundesamt, Arbeitsgemeinschaft Energiebilanzen, Gross Electricity Production in Germany from 2019 to 2023, 2023.
(33) Mellmann, D.; Sponholz, P.; Junge, H.; Beller, M. Formic Acid as a Hydrogen Storage Material - Development of Homogeneous Catalysts for Selective Hydrogen Release. *Chem. Soc. Rev.* **2016**, *45* (14), 3954-3988.
(34) Megía, P. J.; Vizcaíno, A. J.; Calles, J. A.; Carrero, A. Hydrogen Production Technologies: From Fossil Fuels toward Renewable Sources. A Mini Review. *Energy Fuels* **2021**, *35* (20), 16403-16415.
(35) Dagle, R. A.; Holladay, J. D. Methanol Steam Reforming for Hydrogen Production. *Chem. Rev.* **2007**, *107* (10), 3992-4021.
(36) Iulianelli, A.; Ribeirinha, P.; Mendes, A.; Basile, A. Methanol Steam Reforming for Hydrogen Generation Via Conventional and Membrane Reactors: A Review. *Renew. Sust. Energ. Rev.* **2014**, *29*, 355-368.
(37) Alberico, E.; Nielsen, M. Towards a Methanol Economy Based on Homogeneous Catalysis: Methanol to H_2 and CO_2 to Methanol. *Chem. Commun.* **2015**, *51* (31), 6714-6725.
(38) Sreedhar, I.; Kamani, K. M.; Kamani, B. M.; Reddy, B. M.; Venugopal, A. A Bird's Eye View on Process and Engineering Aspects of Hydrogen Storage. *Renew. Sust. Energy Rev.* **2018**, *91*, 838-860.
(39) Zheng, J.; Zhou, H.; Wang, C.-G.; Ye, E.; Xu, J. W.; Loh, X. J.; Li, Z. Current Research Progress and Perspectives on Liquid Hydrogen Rich Molecules in Sustainable Hydrogen Storage. *Energy Stor. Mater.* **2021**, *35*, 695-722.
(40) Kumar, A.; Daw, P.; Milstein, D. Homogeneous Catalysis for Sustainable Energy: Hydrogen and Methanol Economies, Fuels from Biomass, and Related Topics. *Chem. Rev.* **2022**, *122* (1), 385-441.
(41) Abdalla, A. M.; Hossain, S.; Nisfindy, O. B.; Azad, A. T.; Dawood, M.; Azad, A. K. Hydrogen Production, Storage, Transportation and Key Challenges with Applications: A Review. *Energy Convers. Manag.* **2018**, *165*, 602-627.
(42) Chen, X.; Yang, X. Mechanistic Insights and Computational Design of Transition-Metal Catalysts for Hydrogenation and Dehydrogenation Reactions. *Chem. Rec.* **2016**, *16* (5), 2364-2378.
(43) Asinger, F. *Methanol - Chemie- Und Eneigierohstoff*; Springer Berlin, 1986.
(44) Olah, G. A.; Goeppert, A.; Prakash, G. K. S. *Beyond Oil and Gas: The Methanol Economy*; Wiley-VCH, 2006.
(45) Lopes, P. P.; Freitas, K. S.; Ticianelli, E. A. Co Tolerance of Pemfc Anodes: Mechanisms and Electrode Designs. *Electrocatal.* **2010**, *1* (4), 200-212.
(46) Cortright, R. D.; Davda, R. R.; Dumesic, J. A. Hydrogen from Catalytic Reforming of Biomass-Derived Hydrocarbons in Liquid Water. *Nature* **2002**, *418* (6901), 964-967.
(47) Zhang, S.; Liu, Y.; Zhang, M.; Ma, Y.; Hu, J.; Qu, Y. Sustainable Production of Hydrogen with High Purity from Methanol and Water at Low Temperatures. *Nat. Commun.* **2022**, *13* (1), 5527.
(48) Nielsen, M.; Alberico, E.; Baumann, W.; Drexler, H. J.; Junge, H.; Gladiali, S.; Beller, M. Low-Temperature Aqueous-Phase Methanol Dehydrogenation to Hydrogen and Carbon Dioxide. *Nature* **2013**, *495* (7439), 85-89.
(49) Rodriguez-Lugo, R. E.; Trincado, M.; Vogt, M.; Tewes, F.; Santiso-Quinones, G.; Grützmacher, H. A Homogeneous Transition Metal Complex for Clean Hydrogen Production from Methanol-Water Mixtures. *Nat. Chem.* **2013**, *5* (4), 342-347.
(50) Monney, A.; Barsch, E.; Sponholz, P.; Junge, H.; Ludwig, R.; Beller, M. Base-Free Hydrogen Generation from Methanol Using a Bi-Catalytic System. *Chem. Commun.* **2014**, *50* (6), 707-709.
(51) Agapova, A.; Junge, H.; Beller, M. Developing Bicatalytic Cascade Reactions: Ruthenium-Catalyzed Hydrogen Generation from Methanol. *Chem. Eur. J.* **2019**, *25* (40), 9345-9349.
(52) Kempf, H. A.; Junge, H.; Beller, M. Comparison of Low Temperature Methanol Aqueous Phase Reforming Catalysts─Definition of Standardized Reaction Conditions and Considerations toward Applications. *ACS Catal.* **2024**, *14*, 18116-18123.
(53) Hu, P.; Diskin-Posner, Y.; Ben-David, Y.; Milstein, D. Reusable Homogeneous Catalytic System for Hydrogen Production from Methanol and Water. *ACS Catal.* **2014**, *4* (8), 2649-2652.
(54) Qi, W.; Wang, N.; Qin, L.; Yu, P.; Zheng, Z. Panoramic Mechanistic Insights into Hydrogen Production *via* Aqueous-Phase Reforming of Methanol Catalyzed by Ruthenium Complexes of Bis-*N*-Heterocyclic Carbene Pincer Ligands. *ACS Catal.* **2024**, *14* (5), 3434-3445.
(55) van de Watering, F. F.; Lutz, M.; Dzik, W. I.; de Bruin, B.; Reek, J. N. Reactivity of a Ruthenium-Carbonyl Complex in the Methanol Dehydrogenation Reaction. *ChemCatChem* **2016**, *8* (17), 2752-2756.

(56) Chen, Z.; Xia, Y.; Ma, C.; Wang, Q.; Qin, L.; Zhu, X.; Zheng, Z. Hydrogen Production *via* the Aqueous-Phase Reforming of Methanol Catalyzed by Ru(II) Complexes of PNNP Ligands. *Inorg. Chem. Front.* **2023**, *10* (3), 756-767.
(57) Luo, J.; Kar, S.; Rauch, M.; Montag, M.; Ben-David, Y.; Milstein, D. Efficient Base-Free Aqueous Reforming of Methanol Homogeneously Catalyzed by Ruthenium Exhibiting a Remarkable Acceleration by Added Catalytic Thiol. *J. Am. Chem. Soc.* **2021**, *143* (41), 17284-17291.
(58) Wang, Q.; Lan, J.; Liang, R.; Xia, Y.; Qin, L.; Chung, L. W.; Zheng, Z. New Tricks for an Old Dog: Grubbs Catalysts Enable Efficient Hydrogen Production from Aqueous-Phase Methanol Reforming. *ACS Catal.* **2022**, *12* (4), 2212-2222.
(59) Fujita, K.; Kawahara, R.; Aikawa, T.; Yamaguchi, R. Hydrogen Production from a Methanol-Water Solution Catalyzed by an Anionic Iridium Complex Bearing a Functional Bipyridonate Ligand under Weakly Basic Conditions. *Angew. Chem. Int. Ed.* **2015**, *54* (31), 9057-9060.
(60) Prichatz, C.; Alberico, E.; Baumann, W.; Junge, H.; Beller, M. Iridium-PNP Pincer Complexes for Methanol Dehydrogenation at Low Base Concentration. *ChemCatChem* **2017**, *9* (11), 1891-1896.
(61) Bai, C.; Wang, H.; Ning, F.; Fu, J.; Wei, J.; Lu, G.; Shen, Y.; Zhou, X. Second Sphere Ligand Promoted Organoiridium Catalysts for Methanol Dehydrogenation under Mild Conditions. *ChemCatChem* **2020**, *12* (16), 4024-4028.
(62) Anderez-Fernandez, M.; Vogt, L. K.; Fischer, S.; Zhou, W.; Jiao, H.; Garbe, M.; Elangovan, S.; Junge, K.; Junge, H.; Ludwig, R.; *et al.* A Stable Manganese Pincer Catalyst for the Selective Dehydrogenation of Methanol. *Angew. Chem. Int. Ed.* **2017**, *129* (2), 574-577.
(63) Alberico, E.; Sponholz, P.; Cordes, C.; Nielsen, M.; Drexler, H. J.; Baumann, W.; Junge, H.; Beller, M. Selective Hydrogen Production from Methanol with a Defined Iron Pincer Catalyst under Mild Conditions. *Angew. Chem. Int. Ed.* **2013**, *52* (52), 14162-14166.
(64) Bielinski, E. A.; Förster, M.; Zhang, Y.; Bernskoetter, W. H.; Hazari, N.; Holthausen, M. C. Base-Free Methanol Dehydrogenation Using a Pincer-Supported Iron Compound and Lewis Acid Co-Catalyst. *ACS Catal.* **2015**, *5* (4), 2404-2415.
(65) Enthaler, S. Carbon Dioxide-the Hydrogen-Storage Material of the Future? *ChemSusChem* **2008**, *1* (10), 801-804.
(66) Loges, B.; Boddien, A.; Gärtner, F.; Junge, H.; Beller, M. Catalytic Generation of Hydrogen from Formic Acid and Its Derivatives: Useful Hydrogen Storage Materials. *Top. Catal.* **2010**, *53* (13-14), 902-914.
(67) Wang, A.; He, P.; Wu, J.; Chen, N.; Pan, C.; Shi, E.; Jia, H.; Hu, T.; He, K.; Cai, Q.; *et al.* Reviews on Homogeneous and Heterogeneous Catalysts for Dehydrogenation and Recycling of Formic Acid: Progress and Perspectives. *Energy Fuels* **2023**, *37* (22), 17075-17093.
(68) Kushwaha, S.; Parthiban, J.; Singh, S. K. Recent Developments in Reversible CO_2 Hydrogenation and Formic Acid Dehydrogenation over Molecular Catalysts. *ACS Omega* **2023**, *8* (42), 38773-38793.
(69) Guan, C.; Pan, Y.; Zhang, T.; Ajitha, M. J.; Huang, K. W. An Update on Formic Acid Dehydrogenation by Homogeneous Catalysis. *Chem. Asian J.* **2020**, *15* (7), 937-946.
(70) Alberico, E.; Lennox, A. J.; Vogt, L. K.; Jiao, H.; Baumann, W.; Drexler, H. J.; Nielsen, M.; Spannenberg, A.; Checinski, M. P.; Junge, H.; *et al.* Unravelling the Mechanism of Basic Aqueous Methanol Dehydrogenation Catalyzed by Ru-PNP Pincer Complexes. *J. Am. Chem. Soc.* **2016**, *138* (45), 14890-14904.
(71) Hinshelwood, C. N.; Topley, B. The Influence of Temperature on Two Alternative Modes of Decomposition of Formic Acid. *J. Chem. Soc. Trans.* **1923**, *123*, 1333-1338.
(72) Sabatier, P.; Mailhe, A. Catalytic Decomposition of Formic Acid. *Compt. Rend.* **1912**, *152*, 1212-1215.
(73) Forster, D.; Beck, G. R. Homogeneous Catalytic Decomposition of Formic Acid by Rhodium and Iridium Iodocarbonyls and Hydriodic Acid. *J. Chem. Soc. D* **1971**, 1072-1072.
(74) Coffey, R. S. The Decomposition of Formic Acid Catalysed by Soluble Metal Complexes. *Chem. Commun. (London)* **1967**, 923b-924.
(75) Wiener, H.; Sasson, Y.; Blum, J. Palladium-Catalyzed Decomposition of Aqueous Alkali Metal Formate Solutions. *J. Mol. Catal.* **1986**, *35* (3), 277-284.
(76) Paonessa, R. S.; Trogle, W. C. Solvent-Dependent Reactions of Carbon Dioxide with a Platinum(II) Dihydride. Reversible Formation of a Platinum(II) Formatohydride and a Cationic Platinum(II) Dimer, $[Pt_2H_3(PEt_3)_4][HCO_2]$. *J. Am. Chem. Soc.* **1982**, *104* (12), 3529-3530.
(77) Yoshida, T.; Ueda, Y.; Otsuka, S. Activation of Water Molecule. 1. Intermediates Bearing on the Water Gas Shift Reaction Catalyzed by Platinum(0) Complexes. *J. Am. Chem. Soc.* **1978**, *100* (12), 3941-3942.
(78) Strauss, S. H.; Whitmire, K. H.; Shriver, D. F. Rhodium(I) Catalyzed Decomposition of Formic Acid. *J. Organomet. Chem.* **1979**, *174* (3), C59-C62.
(79) Johnson, T. C.; Morris, D. J.; Wills, M. Hydrogen Generation from Formic Acid and Alcohols Using Homogeneous Catalysts. *Chem. Soc. Rev.* **2010**, *39* (1), 81-88.
(80) Gao, Y.; Kuncheria, J. K.; Jenkins, H. A.; Puddephatt, R. J.; Yap, G. P. A. The Interconversion of Formic Acid and Hydrogen/Carbon Dioxide Using a Binuclear Ruthenium Complex Catalyst. *Journal of the Chemical Society, Dalton Transactions* **2000**, (18), 3212-3217.

(81) Gao, Y.; Kuncheria, J.; Yap, G. P. A.; Puddephatt, R. J. An Efficient Binuclear Catalyst for Decomposition of Formic Acid. *Chem. Commun.* **1998**, 2365-2366.
(82) Junge, H.; Boddien, A.; Capitta, F.; Loges, B.; Noyes, J. R.; Gladiali, S.; Beller, M. Improved Hydrogen Generation from Formic Acid. *Tetrahedron Lett.* **2009**, *50* (14), 1603-1606.
(83) Loges, B.; Boddien, A.; Junge, H.; Beller, M. Controlled Generation of Hydrogen from Formic Acid Amine Adducts at Room Temperature and Application in H_2/O_2 Fuel Cells. *Angew. Chem. Int. Ed.* **2008**, *47* (21), 3962-3965.
(84) Boddien, A.; Loges, B.; Junge, H.; Beller, M. Hydrogen Generation at Ambient Conditions: Application in Fuel Cells. *ChemSusChem* **2008**, *1* (8-9), 751-758.
(85) Boddien, A.; Loges, B.; Junge, H.; Gärtner, F.; Noyes, J. R.; Beller, M. Continuous Hydrogen Generation from Formic Acid: Highly Active and Stable Ruthenium Catalysts. *Adv. Synth. Catal.* **2009**, *351* (14-15), 2517-2520.
(86) Sponholz, P.; Mellmann, D.; Junge, H.; Beller, M. Towards a Practical Setup for Hydrogen Production from Formic Acid. *ChemSusChem* **2013**, *6* (7), 1172-1176.
(87) Fellay, C.; Dyson, P. J.; Laurenczy, G. A Viable Hydrogen-Storage System Based on Selective Formic Acid Decomposition with a Ruthenium Catalyst. *Angew. Chem. Int. Ed.* **2008**, *47* (21), 3966-3968.
(88) Gan, W.; Fellay, C.; Dyson, P. J.; Laurenczy, G. Influence of Water-Soluble Sulfonated Phosphine Ligands on Ruthenium Catalyzed Generation of Hydrogen from Formic Acid. *J. Coord. Chem.* **2010**, *63* (14-16), 2685-2694.
(89) Fellay, C.; Yan, N.; Dyson, P. J.; Laurenczy, G. Selective Formic Acid Decomposition for High-Pressure Hydrogen Generation: A Mechanistic Study. *Chem. Eur. J.* **2009**, *15* (15), 3752-3760.
(90) Gan, W.; Snelders, D. J. M.; Dyson, P. J.; Laurenczy, G. Ruthenium(II)-Catalyzed Hydrogen Generation from Formic Acid Using Cationic, Ammoniomethyl-Substituted Triarylphosphine Ligands. *ChemCatChem* **2013**, *5* (5), 1126-1132.
(91) Fukuzumi, S.; Kobayashi, T.; Suenobu, T. Unusually Large Tunneling Effect on Highly Efficient Generation of Hydrogen and Hydrogen Isotopes in Ph-Selective Decomposition of Formic Acid Catalyzed by a Heterodinuclear Iridium-Ruthenium Complex in Water. *J. Am. Chem. Soc.* **2010**, *132* (5), 1496–1497.
(92) Fukuzumi, S. Bioinspired Energy Conversion Systems for Hydrogen Production and Storage. *Eur. J. Inorg. Chem.* **2008**, *2008* (9), 1351-1362.
(93) Fukuzumi, S.; Kobayashi, T.; Suenobu, T. Efficient Catalytic Decomposition of Formic Acid for the Selective Generation of H_2 and H/D Exchange with a Water-Soluble Rhodium Complex in Aqueous Solution. *ChemSusChem* **2008**, *1* (10), 827-834.
(94) Himeda, Y. Highly Efficient Hydrogen Evolution by Decomposition of Formic Acid Using an Iridium Catalyst with 4,4′-Dihydroxy-2,2′-Bipyridine. *Green Chem.* **2009**, *11* (12), 2018-2022.
(95) Himeda, Y.; Miyazawa, S.; Hirose, T. Interconversion between Formic Acid and H_2/CO_2 Using Rhodium and Ruthenium Catalysts for CO_2 Fixation and H_2 Storage. *ChemSusChem* **2011**, *4* (4), 487-493.
(96) Wang, W. H.; Hull, J. F.; Muckerman, J. T.; Fujita, E.; Hirose, T.; Himeda, Y. Highly Efficient D_2 Generation by Dehydrogenation of Formic Acid in D_2O through H^+/D^+ Exchange on an Iridium Catalyst: Application to the Synthesis of Deuterated Compounds by Transfer Deuterogenation. *Chem. Eur. J.* **2012**, *18* (30), 9397-9404.
(97) Boddien, A.; Mellmann, D.; Gartner, F.; Jackstell, R.; Junge, H.; Dyson, P. J.; Laurenczy, G.; Ludwig, R.; Beller, M. Efficient Dehydrogenation of Formic Acid Using an Iron Catalyst. *Science* **2011**, *333* (6050), 1733-1736.
(98) Mellone, I.; Peruzzini, M.; Rosi, L.; Mellmann, D.; Junge, H.; Beller, M.; Gonsalvi, L. Formic Acid Dehydrogenation Catalysed by Ruthenium Complexes Bearing the Tripodal Ligands Triphos and NP_3. *Dalton Trans.* **2013**, *42* (7), 2495-2501.
(99) Rieckborn, T. P.; Huber, E.; Karakoc, E.; Prosenc, M. H. Platinum Complex Catalyzed Decomposition of Formic Acid. *Eur. J. Inorg. Chem.* **2010**, *2010* (30), 4757-4761.
(100) Bertini, F.; Mellone, I.; Ienco, A.; Peruzzini, M.; Gonsalvi, L. Iron(II) Complexes of the Linear *rac*-Tetraphos-1 Ligand as Efficient Homogeneous Catalysts for Sodium Bicarbonate Hydrogenation and Formic Acid Dehydrogenation. *ACS Catal.* **2015**, *5* (2), 1254-1265.
(101) Tanaka, R.; Yamashita, M.; Chung, L. W.; Morokuma, K.; Nozaki, K. Mechanistic Studies on the Reversible Hydrogenation of Carbon Dioxide Catalyzed by an Ir-PNP Complex. *Organometallics* **2011**, *30* (24), 6742-6750.
(102) Filonenko, G. A.; van Putten, R.; Schulpen, E. N.; Hensen, E. J. M.; Pidko, E. A. Highly Efficient Reversible Hydrogenation of Carbon Dioxide to Formates Using a Ruthenium PNP-Pincer Catalyst. *ChemCatChem* **2014**, *6* (6), 1526-1530.
(103) Hsu, S. F.; Rommel, S.; Eversfield, P.; Muller, K.; Klemm, E.; Thiel, W. R.; Plietker, B. A Rechargeable Hydrogen Battery Based on Ru Catalysis. *Angew. Chem. Int. Ed.* **2014**, *53* (27), 7074-7078.
(104) Kothandaraman, J.; Czaun, M.; Goeppert, A.; Haiges, R.; Jones, J. P.; May, R. B.; Prakash, G. K.; Olah, G. A. Amine-Free Reversible Hydrogen Storage in Formate Salts Catalyzed by Ruthenium Pincer Complex without pH Control or Solvent Change. *ChemSusChem* **2015**, *8* (8), 1442-1451.

(105) Agapova, A.; Alberico, E.; Kammer, A.; Junge, H.; Beller, M. Catalytic Dehydrogenation of Formic Acid with Ruthenium-PNP-Pincer Complexes: Comparing N-Methylated and NH-Ligands. *ChemCatChem* **2019**, *11* (7), 1910-1914.
(106) Pan, Y.; Pan, C. L.; Zhang, Y.; Li, H.; Min, S.; Guo, X.; Zheng, B.; Chen, H.; Anders, A.; Lai, Z.; *et al.* Selective Hydrogen Generation from Formic Acid with Well-Defined Complexes of Ruthenium and Phosphorus-Nitrogen PN^3-Pincer Ligand. *Chem. Asian J.* **2016**, *11* (9), 1357-1360.
(107) Piccirilli, L.; Rabell, B.; Padilla, R.; Riisager, A.; Das, S.; Nielsen, M. Versatile CO_2 Hydrogenation-Dehydrogenation Catalysis with a Ru-PNP/Ionic Liquid System. *J. Am. Chem. Soc.* **2023**, *145* (10), 5655-5663.
(108) Zell, T.; Butschke, B.; Ben-David, Y.; Milstein, D. Efficient Hydrogen Liberation from Formic Acid Catalyzed by a Well-Defined Iron Pincer Complex under Mild Conditions. *Chem. Eur. J.* **2013**, *19* (25), 8068-8072.
(109) Bielinski, E. A.; Lagaditis, P. O.; Zhang, Y.; Mercado, B. Q.; Wurtele, C.; Bernskoetter, W. H.; Hazari, N.; Schneider, S. Lewis Acid-Assisted Formic Acid Dehydrogenation Using a Pincer-Supported Iron Catalyst. *J. Am. Chem. Soc.* **2014**, *136* (29), 10234-10237.
(110) Mellone, I.; Gorgas, N.; Bertini, F.; Peruzzini, M.; Kirchner, K.; Gonsalvi, L. Selective Formic Acid Dehydrogenation Catalyzed by Fe-PNP Pincer Complexes Based on the 2,6-Diaminopyridine Scaffold. *Organometallics* **2016**, *35* (19), 3344-3349.
(111) Tondreau, A. M.; Boncella, J. M. 1,2-Addition of Formic or Oxalic Acid to $^-N\{CH_2CH_2(PiPr_2)\}_2$-Supported Mn(I) Dicarbonyl Complexes and the Manganese-Mediated Decomposition of Formic Acid. *Organometallics* **2016**, *35* (12), 2049-2052.
(112) Anderson, N. H.; Boncella, J.; Tondreau, A. M. Manganese-Mediated Formic Acid Dehydrogenation. *Chem. Eur. J.* **2019**, *25* (45), 10557-10560.
(113) Wei, D.; Sang, R.; Sponholz, P.; Junge, H.; Beller, M. Reversible Hydrogenation of Carbon Dioxide to Formic Acid Using a Mn-Pincer Complex in the Presence of Lysine. *Nat. Energy* **2022**, *7* (5), 438-447.
(114) Myers, T. W.; Berben, L. A. Aluminium–Ligand Cooperation Promotes Selective Dehydrogenation of Formic Acid to H_2 and CO_2. *Chem. Sci.* **2014**, *5* (7), 2771-2777.
(115) Enthaler, S.; Brück, A.; Kammer, A.; Junge, H.; Irran, E.; Gülak, S. Exploring the Reactivity of Nickel Pincer Complexes in the Decomposition of Formic Acid to CO_2/H_2 and the Hydrogenation of $NaHCO_3$ to HCOONa. *ChemCatChem* **2014**, *7* (1), 65-69.
(116) Younus, H. A.; Ahmad, N.; Su, W.; Verpoort, F. Ruthenium Pincer Complexes: Ligand Design and Complex Synthesis. *Coord. Chem. Rev.* **2014**, *276*, 112-152.
(117) Kawatsura, M.; Hartwig, J. F. Transition Metal-Catalyzed Addition of Amines to Acrylic Acid Derivatives. A High-Throughput Method for Evaluating Hydroamination of Primary and Secondary Alkylamines. *Organometallics* **2001**, *20*, 1960-1964.
(118) Müller, G.; Klinga, M.; Leskelä, M.; Rieger, B. Iron and Cobalt Complexes of a Series of Tridentate P,N,P Ligands - Synthesis, Characterization, and Application in Ethene Polymerization Reactions. *Z. Anorg. Allg. Chem.* **2002**, *628* (13), 2839-2846.
(119) McGuinness, D. S.; Wasserscheid, P.; Keim, W.; Hu, C.; Englert, U.; Dixon, J. T.; Grove, C. Novel Cr-PNP Complexes as Catalysts for the Trimerisation of Ethylene. *Chem. Commun.* **2003**, (3), 334-335.
(120) Wasserscheid, P.; Grimm, S.; Köhn, Randolf D.; Haufe, M. Synthesis of Synthetic Lubricants by Trimerization of 1-Decene and 1-Dodecene with Homogeneous Chromium Catalysts. *Adv. Syn. Catal.* **2001**, *343* (8), 814-818.
(121) Abdur-Rashid, K.; Goussev, D. G. Tansfer Hydrogenation Processes and Catalysts. WO/2004/096735, 2004.
(122) Zhang, J.; Gandelman, M.; Shimon, L. J. W.; Rozenberg, H.; Milstein, D. Electron-Rich, Bulky Ruthenium PNP-Type Complexes. Acceptorless Catalytic Alcohol Dehydrogenation. *Organometallics* **2004**, *23*, 4026-4033.
(123) Zhang, J.; Leitus, G.; Ben-David, Y.; Milstein, D. Facile Conversion of Alcohols into Esters and Dihydrogen Catalyzed by New Ruthenium Complexes. *J. Am. Chem. Soc.* **2005**, *127*, 10840-10841.
(124) Benito-Garagorri, D.; Becker, E.; Wiedermann, J.; Lackner, W.; Pollak, M.; Mereiter, K.; Kisala, J.; Kirchner, K. Achiral and Chiral Transition Metal Complexes with Modularly Designed Tridentate PNP Pincer-Type Ligands Based on N-Heterocyclic Diamines. *Organometallics* **2006**, *25*, 1900-1913.
(125) Benito-Garagorri, D.; Wiedermann, J.; Pollak, M.; Mereiter, K.; Kirchner, K. Iron(II) Complexes Bearing Tridentate PNP Pincer-Type Ligands as Catalysts for the Selective Formation of 3-Hydroxyacrylates from Aromatic Aldehydes and Ethyldiazoacetate. *Organometallics* **2007**, *26*, 217-222.
(126) Langer, R.; Leitus, G.; Ben-David, Y.; Milstein, D. Efficient Hydrogenation of Ketones Catalyzed by an Iron Pincer Complex. *Angew. Chem. Int. Ed.* **2011**, *50* (9), 2120-2124.
(127) Kuriyama, W.; Matsumoto, T.; Ogata, O.; Ino, Y.; Aoki, K.; Tanaka, S.; Ishida, K.; Kobayashi, T.; Sayo, N.; Saito, T. Catalytic Hydrogenation of Esters. Development of an Efficient Catalyst and Processes for Synthesising (*R*)-1,2-Propanediol and 2-(*l*-Menthoxy)Ethanol. *Org. ProcessRes. Dev.* **2012**, *16* (1), 166-171.

(128) Kempf, H. A.; Both, N. F.; Stein, C. A. M.; Spannenberg, A.; Junge, K.; Junge, H.; Beller, M. Synthesis of Guanamine-Based Ruthenium Pincer Complexes and Their Application in Catalytic (De)Hydrogenation Reactions. *Organometallics* **2024**, *43* (20), 2450-2457.
(129) Chen, L.; Ai, P.; Gu, J.; Jie, S.; Li, B.-G. Stereospecific Polymerization of 1,3-Butadiene Catalyzed by Cobalt Complexes Bearing N-Containing Diphosphine PNP Ligands. *J. Organomet. Chem.* **2012**, *716*, 55-61.
(130) Zhang, G.; Scott, B. L.; Hanson, S. K. Mild and Homogeneous Cobalt-Catalyzed Hydrogenation of C=C, C=O, and C=N Bonds. *Angew. Chem. Int. Ed.* **2012**, *51* (48), 12102-12106.
(131) He, L.-P.; Chen, T.; Xue, D.-X.; Eddaoudi, M.; Huang, K.-W. Efficient Transfer Hydrogenation Reaction Catalyzed by a Dearomatized PN_3P Ruthenium Pincer Complex under Base-Free Conditions. *J. Organomet. Chem.* **2012**, *700*, 202-206.
(132) Michlik, S.; Kempe, R. A Sustainable Catalytic Pyrrole Synthesis. *Nat. Chem.* **2013**, *5* (2), 140-144.
(133) Rösler, S.; Obenauf, J.; Kempe, R. A Highly Active and Easily Accessible Cobalt Catalyst for Selective Hydrogenation of C=O Bonds. *J. Am. Chem. Soc.* **2015**, *137* (25), 7998-8001.
(134) Mukherjee, A.; Nerush, A.; Leitus, G.; Shimon, L. J.; Ben David, Y.; Espinosa Jalapa, N. A.; Milstein, D. Manganese-Catalyzed Environmentally Benign Dehydrogenative Coupling of Alcohols and Amines to Form Aldimines and H_2: A Catalytic and Mechanistic Study. *J. Am. Chem. Soc.* **2016**, *138* (13), 4298-4301.
(135) Mastalir, M.; Glatz, M.; Gorgas, N.; Stöger, B.; Pittenauer, E.; Allmaier, G.; Veiros, L. F.; Kirchner, K. Divergent Coupling of Alcohols and Amines Catalyzed by Isoelectronic Hydride Mn(I) and Fe(II) PNP Pincer Complexes. *Chem. Eur. J.* **2016**, *22* (35), 12316-12320.
(136) Kallmeier, F.; Irrgang, T.; Dietel, T.; Kempe, R. Highly Active and Selective Manganese C=O Bond Hydrogenation Catalysts: The Importance of the Multidentate Ligand, the Ancillary Ligands, and the Oxidation State. *Angew. Chem. Int. Ed.* **2016**, *55* (39), 11806-11809.
(137) Mastalir, M.; Stöger, B.; Pittenauer, E.; Puchberger, M.; Allmaier, G.; Kirchner, K. Air Stable Iron(II) PNP Pincer Complexes as Efficient Catalysts for the Selective Alkylation of Amines with Alcohols. *Adv. Syn. Catal.* **2016**, *358* (23), 3824-3831.
(138) Li, H.; Al-Dakhil, A.; Lupp, D.; Gholap, S. S.; Lai, Z.; Liang, L. C.; Huang, K. W. Cobalt-Catalyzed Selective Hydrogenation of Nitriles to Secondary Imines. *Org. Lett.* **2018**, *20* (20), 6430-6435.
(139) Jia, G.; Lee, H. M.; Xia, H. P.; Williams, I. D. Coupling Reactions of Terminal Acetylenes with a Cyclometalated Aryl Ligand. *Organometallics* **1996**, *15*, 5453-5455.
(140) Lee, H. M.; Yao, J.; Jia, G. Coupling Reactions of Terminal Acetylenes with Ruthenium Complexes Containing the Ortho-Metalated Ligand 2,6-$(PPh_2CH_2)_2C_6H_3$. *Organometallics* **1997**, *16*, 3927-3933.
(141) Kempf, H. A.; López Robledo, G.; Spannenberg, A.; Junge, K.; Jiao, H.; Junge, H.; Beller, M. Synthesis of Ru-Pnpc Pincer Complexes and Applications in Catalytic Hydrogenation and Dehydrogenation Reactions. *ChemCatChem* **2024**, e202401481.
(142) Gagliardo, M.; Chase, P. A.; Brouwer, S.; van Klink, G. P. M.; van Koten, G. Electronic Effects in PCP-Pincer Ru(II)-Based Hydrogen Transfer Catalysis. *Organometallics* **2006**, *26*, 2219-2227.
(143) Dijkstra, H. P.; Albrecht, M.; Medici, S.; van Klink, G. P. M.; van Koten, G. Hexakis(PCP-Platinum and -Ruthenium) Complexes by the Transcyclometalation Reaction and Their Use in Catalysis. *Adv. Syn. Catal.* **2002**, *344* (10), 1135-1141.
(144) Dani, P.; Karlen, T.; Gossage, R. A.; Gladiali, S.; van Koten, G. Hydrogen-Transfer Catalysis with Pincer-Aryl Ruthenium(II) Complexes. *Angew. Chem. Int. Ed.* **2000**, *39* (4), 743-745.
(145) Takaya, J.; Hartwig, J. F. Mechanistic Studies of Ruthenium-Catalyzed Anti-Markovnikov Hydroamination of Vinylarenes: Intermediates and Evidence for Catalysis through Π-Arene Complexes. *J. Am. Chem. Soc.* **2005**, *127*, 5756-5757.
(146) Otsuka, M.; Endo, K.; Shibata, T. Catalytic S_NAr Reaction of Non-Activated Fluoroarenes with Amines *via* Ru η^6-Arene Complexes. *Chem. Commun.* **2010**, *46* (2), 336-338.
(147) Musa, S.; Ghosh, A.; Vaccaro, L.; Ackermann, L.; Gelman, D. Efficient E-Selective Transfer Semihydrogenation of Alkynes by Means of Ligand-Metal Cooperating Ruthenium Catalyst. *Adv. Syn. Catal.* **2015**, *357* (10), 2351-2357.
(148) Musa, S.; Ackermann, L.; Gelman, D. Dehydrogenative Cross-Coupling of Primary and Secondary Alcohols. *Adv. Syn. Catal.* **2013**, *355* (14-15), 3077-3080.
(149) Musa, S.; Fronton, S.; Vaccaro, L.; Gelman, D. Bifunctional Ruthenium(II) PCP Pincer Complexes and Their Catalytic Activity in Acceptorless Dehydrogenative Reactions. *Organometallics* **2013**, *32* (10), 3069-3073.
(150) Kallmeier, F.; Fertig, R.; Irrgang, T.; Kempe, R. Chromium-Catalyzed Alkylation of Amines by Alcohols. *Angew. Chem. Int. Ed.* **2020**, *59* (29), 11789-11793.
(151) Lu, S.-M.; Han, X.-W.; Zhou, Y.-G. An Efficient Catalytic System for the Hydrogenation of Quinolines. *J. Organomet. Chem.* **2007**, *692* (14), 3065-3069.
(152) Ogata, O. Cationic Ruthenium Complex, and Production Method Therefor, and Use Thereof. WO2018181865A1, 2018.
(153) Neumann, J.; Bornschein, C.; Jiao, H.; Junge, K.; Beller, M. Hydrogenation of Aliphatic and Aromatic Nitriles Using a Defined Ruthenium PNP Pincer Catalyst. *Eur. J. Org. Chem.* **2015**, (27), 5944-5948.

(154) Budweg, S.; Wei, Z.; Jiao, H.; Junge, K.; Beller, M. Iron-PNP-Pincer-Catalyzed Transfer Dehydrogenation of Secondary Alcohols. *ChemSusChem* **2019**, *12* (13), 2988-2993.
(155) Lo, H. K.; Copéret, C. CO_2 Hydrogenation to Formate with Immobilized Ru-Catalysts Based on Hybrid Organo-Silica Mesostructured Materials. *ChemCatChem* **2019**, *11* (1), 430-434.
(156) Pyykkö, P. Additive Covalent Radii for Single-, Double-, and Triple-Bonded Molecules and Tetrahedrally Bonded Crystals: A Summary. *J. Phys. Chem. A* **2015**, *119*, 2326-2337.
(157) Allen, F. H.; Kennard, O.; Watson, D. G.; Brammer, L.; Orpen, A. G.; Taylor, R. Tables of Bond Lengths Determined by X-Ray and Neutron Diffraction. Part 1. Bond Lengths in Organic Compounds. *J. Chem. Soc. Perkin Trans. II* **1987**, S1-S19.
(158) Subaramanian, M.; Sivakumar, G.; Landge, V. G.; Kumar, R.; Natte, K.; Jagadeesh, R. V.; Balaraman, E. General and Selective Homogeneous Ru-Catalyzed Transfer Hydrogenation, Deuteration, and Methylation of Functional Compounds Using Methanol. *J. Catal.* **2023**, *425*, 386-405.
(159) Nair, A. G.; McBurney, R. T.; Walker, D. B.; Page, M. J.; Gatus, M. R.; Bhadbhade, M.; Messerle, B. A. Ruthenium(II) Complexes of Hemilabile Pincer Ligands: Synthesis and Catalysing the Transfer Hydrogenation of Ketones. *Dalton Trans* **2016**, *45* (36), 14335-14342.
(160) Curley, J. B.; Hert, C.; Bernskoetter, W. H.; Hazari, N.; Mercado, B. Q. Control of Catalyst Isomers Using an *N*-Phenyl-Substituted $RN(CH_2CH_2P^iPr_2)_2$ Pincer Ligand in CO_2 Hydrogenation and Formic Acid Dehydrogenation. *Inorg. Chem.* **2022**, *61* (1), 643-656.
(161) Curley, J. B.; Smith, N. E.; Bernskoetter, W. H.; Hazari, N.; Mercado, B. Q. Catalytic Formic Acid Dehydrogenation and CO_2 Hydrogenation Using Iron PN^RP Pincer Complexes with Isonitrile Ligands. *Organometallics* **2018**, *37* (21), 3846-3853.
(162) Bellows, S. M.; Chakraborty, S.; Gary, J. B.; Jones, W. D.; Cundari, T. R. An Uncanny Dehydrogenation Mechanism: Polar Bond Control over Stepwise or Concerted Transition States. *Inorg. Chem.* **2017**, *56* (10), 5519-5524.
(163) Qu, S.; Dai, H.; Dang, Y.; Song, C.; Wang, Z.-X.; Guan, H. Computational Mechanistic Study of Fe-Catalyzed Hydrogenation of Esters to Alcohols: Improving Catalysis by Accelerating Precatalyst Activation with a Lewis Base. *ACS Catal.* **2014**, *4* (12), 4377-4388.
(164) Elangovan, S.; Wendt, B.; Topf, C.; Bachmann, S.; Scalone, M.; Spannenberg, A.; Jiao, H.; Baumann, W.; Junge, K.; Beller, M. Improved Second Generation Iron Pincer Complexes for Effective Ester Hydrogenation. *Adv. Synth. Catal.* **2016**, *358* (5), 820-825.
(165) Chakraborty, S.; Lagaditis, P. O.; Förster, M.; Bielinski, E. A.; Hazari, N.; Holthausen, M. C.; Jones, W. D.; Schneider, S. Well-Defined Iron Catalysts for the Acceptorless Reversible Dehydrogenation-Hydrogenation of Alcohols and Ketones. *ACS Catal.* **2014**, *4* (11), 3994-4003.

6 APPENDIX

6.1 Literature overview over methanol APR

Table adapted from ref[52].

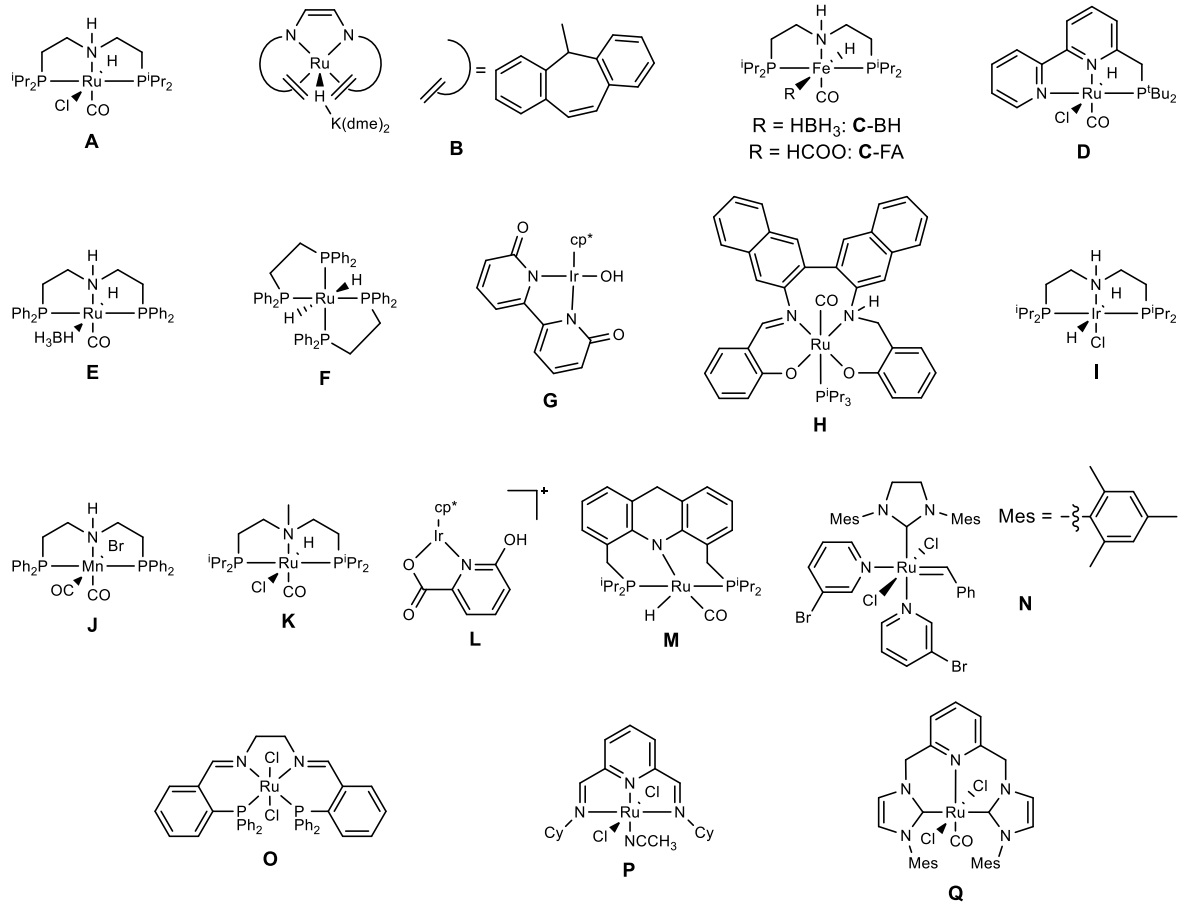

Author, year	Catalyst	Solvent	Additives	T in °C	CO impurities	TON; TOF
Beller[48] 2013[a)]	**A**	–	8 M KOH	95	<10 ppm	350,000; 4,700 h^{-1}
Trincado, Grützmacher[49] 2013[b)]	**B**	Toluene	10 mol% NEt_3	90	No detection limit	540; 54 h^{-1}
Milstein[53] 2014[a)]	**D**	Toluene	8.3 M KOH	100	No detection limit	2,900; 50 h^{-1}
Beller[50] 2014[b)]	**E** + **F**	Triglyme	–	93.5	<8 ppm	4,200; 94 h^{-1}
de Bruin, Reek[55] 2016[a)]	**H**	Dioxane	8 M KOH	82	No detection limit	– ; 55 h^{-1}
Beller[51] 2019[b)]	**A** + **K**	Triglyme	0.33 M KOH	92.5	<10 ppm	13,400; 194 h^{-1}

	A	Triglyme	0.33 M KOH	92.5	<10 ppm	– ; 142 h^{-1}
	K	Triglyme	0.33 M KOH	92.5	<10 ppm	– ; 168 h^{-1}
Milstein[57] 2021[b)]	**M**	–	0,625 mM 1–Hexanethiol	150	20 ppm	130,000; 643 h^{-1}
Qin, Chung, Zheng[58] 2022[a)]	**N**	–	8 M KOH	97	<1 ppm	11,400; 158 h^{-1}
Qin, Zhu, Zheng[56] 2023[a)]	**O**	Triglyme	8 M KOH	120	<10 ppm	12,600; 158 h^{-1}
Kumar[29] 2023[c)]	**P**	–	1.5 eq. KO^{t}Bu	100	–	81% yield
Qin, Yu, Zheng[54] 2024[c)]	**Q**	–	8 M KOH	94	–	14,500; 89 h^{-1}
		–	8 M KOH	91	<10 ppm	10,000; 702 h^{-1}
Beller[63] 2013[a)]	**C**-BH	–	4 M KOH	79	<10 ppm	177; 59 h^{-1}
		–	0.5 M KOH	72	<10 ppm	25; 10.3 h^{-1}
Bernskoetter, Hazari, Holthausen[64] 2015[b)]	**C**-FA	EtOAc	10 mol% $LiBF_4$	77	<0.1%	51,000; 542 h^{-1}
Beller[62] 2017[a)]	**J**	Triglyme	8 M KOH, 10 eq. ligand	92	Not reported	20,000; 14 h^{-1}
Fujita, Yamaguchi[59] 2015[b)]	**G**	–	0.44 M NaOH	65	Not reported	10,500; 70 h^{-1}
Beller[60] 2017[b)]	**I**	–	0,5 M KOH	70	Not reported	1,400; 326 h^{-1}
Zhou[61] 2020[b)]	**L**	–	1.58 mM Na_2CO_3	89	No detection limit	235 491h^{-1}

a) Initiation phase TON/TOF. b) Working phase TON/TOF. c) No full dehydrogenation of methanol was performed. The reaction product was formic acid or potassium formate.

6.2 Publications

6.2.1 Synthesis of Guanamine-Based Ruthenium Pincer Complexes and Their Application in Catalytic (De)hydrogenation Reactions

Hendrik A. Kempf, Niklas, F. Both, Carolin, A. M. Stein, Anke Spannenberg, Kathrin Junge, Henrik Junge and Matthias Beller

Organometallics **2024**, *43*, *20*, 2450-2457

DOI: 10.1021/acs.organomet.3c00523

Author contributions:

In this manuscript, I synthesized all ligands and complexes. Their analytical characterization was carried out together with A. S. I carried out all dehydrogenation reactions and investigations into the catalyst stability. The manuscript was prepared, edited and peer reviewed by all authors. My overall contribution to this work accounts to approximately 60%.

Signature of the student — Signature of the supervisor

(Hendrik Kempf) — **(Prof. Matthias Beller)**

ORGANOMETALLICS

pubs.acs.org/Organometallics Article

Synthesis of Guanamine-Based Ruthenium Pincer Complexes and Their Application in Catalytic (De)hydrogenation Reactions

Hendrik A. Kempf, Niklas F. Both, Carolin A. M. Stein, Anke Spannenberg, Kathrin Junge,* Henrik Junge,* and Matthias Beller*

Cite This: *Organometallics* 2024, 43, 2450−2457 Read Online

ACCESS | Metrics & More | Article Recommendations | Supporting Information

ABSTRACT: Reaction of [RuHCl(CO)(PPh_3)$_3$] with ligand *N*,*N*′-bis(diisopropylphosphino)-benzoguanamine leads to the formation of monomeric and dimeric ruthenium complexes. Investigations of the stability of these guanamine-based PNP-pincer complexes reveals that no interconversion between both species is taking place under reaction conditions employed. Hence, both species are tested in different model reactions and compared to state-of-the-art systems. The new complexes show good to excellent performance in the dehydrogenation of formic acid and the hydrogenation of CO_2. Notably, in the former reaction, the monomeric complex is more active than all so far reported systems. Additionally, both complexes are utilized in the hydrogenation of different functional groups (ketone, nitrile, ester, N-heteroarene), important in organic synthesis. Generally, the monomeric species is more active than the dimeric one, which can be attributed to the difference in steric shielding of the metal center.

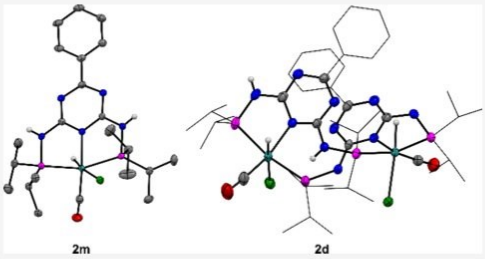

INTRODUCTION

A key challenge for the chemical industry in the next decade is to realize the feedstocks transformation from fossil to renewable resources.[1−5] For this process, catalysts are of utmost importance, as they enable new and more selective reactions with lower energy consumption.[1,5−8] Moreover, catalytic reactions present a cornerstone of the chemical industry, as the manufacturing of over 80% of products includes at least one catalytic step.[1,9−11] Hence, the continuous development of new catalysts is essential for existing and new processes in a future, green chemical industry.[7]

Historically, milestones of the chemical industry came hand in hand with the development of new catalysts. Important examples of heterogeneous catalysts include iron-based systems in the Haber−Bosch process[12] or Cu/ZnO/Al_2O_3 in the methanol synthesis.[13] In contrast, homogeneous complexes are preferred for fine chemical synthesis, e.g., palladium-catalyzed coupling,[14] metathesis,[15−17] and (de)hydrogenation reactions.[18−21] More specifically, metal PNP-pincer complexes have become state-of-the-art catalysts for the latter and related reactions over the past two decades (Figure 1).[18,22−25] For example, Ru-MACHO was recently used for the reduction of 2.2 t of methyl (*R*)-lactate to the corresponding diol at room temperature.[26] As evident from this exceptional result, pincer ligands are very promising for future applications in industry.

The first homogeneous catalytic applications of PNP-pincer ligands with an aliphatic backbone were performed by McGuinness, Wasserscheid, and co-workers utilizing a chromium pincer complex in the trimerization of ethylene.[27] Shortly after, Kamaluddin patented the respective iridium and ruthenium catalysts for the transfer hydrogenation of various functional groups.[28] In 2011, Kuriyama and co-workers introduced the famous Ru-MACHO complex for the hydrogenation of esters.[26] Starting in 2012, further pincer complexes based on earth-abundant metals were introduced and applied in a variety of (de)hydrogenation and polymerization reactions.[9,29−31] Pincer ligands with a pyridyl-group in their backbone were applied in an *in situ* system by Kawatsura and Hartwig for the addition of amines to acrylic acid derivatives.[32] One year later, a defined cobalt complex was utilized in ethylene polymerization by Rieger and co-workers.[33] Afterwards, Milstein and co-workers described multiple defined complexes with exceptional reactivity in (de)hydrogenation reactions.[34−37] Further variations of the ligand backbone were performed by Kirchner and co-workers, who applied the respective palladium complexes in Suzuki−Miyaura cross-coupling and iron complexes for the synthesis of 3-hydro-

Special Issue: Applied Organometallic Chemistry

Received: December 19, 2023
Revised: February 6, 2024
Accepted: February 7, 2024
Published: February 24, 2024

https://doi.org/10.1021/acs.organomet.3c00523
Organometallics 2024, 43, 2450−2457

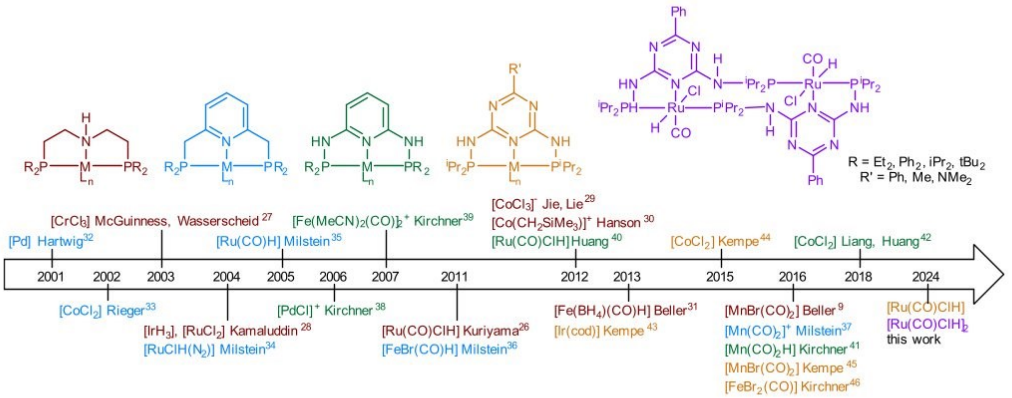

Figure 1. Timeline for the development of metal PNP-pincer complexes applied in catalysis. Colors symbolize the kind of ligand backbone.

Scheme 1. Synthesis of Monomeric and Dimeric Ruthenium Complexes 2m and 2d

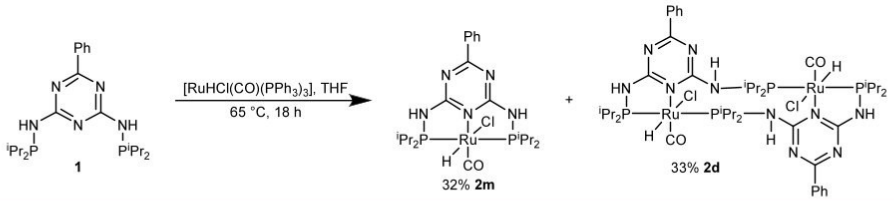

acrylates.[38,39] In addition, Huang and co-workers studied the corresponding ruthenium complex in transfer hydrogenations.[40] Later, manganese[41] and cobalt[42] complexes were investigated in the alkylation of amines with alcohols and the hydrogenation of nitriles.

The first applications of pincer ligands based on guanamine were shown by Michlik and Kempe in 2013.[43] Utilizing the corresponding Ir complexes, they synthesized pyrroles form amino alcohols and secondary alcohols. In 2015 and 2016, the corresponding cobalt,[44] manganese,[45] and iron complexes[46] were synthesized and applied in hydrogenation and alkylation reactions.

This latter subclass of ligands can easily be varied in the triazine ring of the ligand backbone (Figure 1, R′). Modification at this position allows for fine-tuning of electronic properties of the catalyst, thereby permitting the optimization of the catalyst for a chosen reaction. To the best of our knowledge, ruthenium complexes bearing this subclass of pincer ligands have not been reported to this date, although related ruthenium pincer catalysts have shown exceptionally high activity in, e.g., (de)hydrogenation reactions.[18,22,23] Therefore, we aimed to synthesize the respective guanamine-based Ru pincer complexes and explore their performance in selected model reactions.

RESULTS AND DISCUSSION

Complex Synthesis. The parent ruthenium guanamine-based pincer complex was synthesized starting from [RuHCl(CO)(PPh_3)$_3$] and ligand **1** (*N*,*N*′-bis(diisopropylphosphino)-benzoguanamine) as shown in Scheme 1, following a general reaction protocol previously applied for a different complex (Figure 1) by Huang and co-workers.[40] However, complexation of the ligand with the metal precursor resulted in the formation of multiple products, which could be separated by column chromatography. Initial NMR analysis of the obtained fractions did not lead to clear structural determination. However, high resolution mass spectrometry suggested the formation of a monomeric and dimeric species. Full structural resolution could then be obtained by SC-XRD (Figures 2 and 3). Crystals of complexes **2m** and **2d** suitable for X-ray structural analysis were obtained by vapor diffusion of pentane into a saturated THF-solution of the corresponding complex. In both complexes, **2m** and **2d**, the metal centers are coordinated by two phosphorus and one nitrogen atom of the pincer ligand(s), as well as a carbonyl, hydrido, and chlorido ligand, forming a distorted octahedral coordination geometry. The pincer ligand coordinates meridionally in **2m**, as reported for similar complexes.[35,40,43−48] In **2d**, both pincers act as bridging ligands, leading to the formation of a dimeric complex. The metal centers are each coordinated by one phosphorus and one nitrogen atom of one pincer ligand and another phosphorus atom of a second ligand. To the best of our knowledge, this type of coordination is unknown for guanamine-based PNP-pincer ligands.

The distortion of the octahedral coordination geometry is most pronounced in the P−Ru−P angles (**2m** P1−Ru1−P2 = 160.03(3); **2d** P1−Ru1−P4 = 162.867(19)/P3−Ru2−P2 = 162.76(2)°), which differ from the expected 180° angle. It is worth noting that the triazine units strongly deviate from planarity in **2d** (mean deviation of the best plane = 0.06 and 0.07 Å). Additionally, the Ru and N atoms neighboring the

https://doi.org/10.1021/acs.organomet.3c00523
Organometallics 2024, 43, 2450−2457

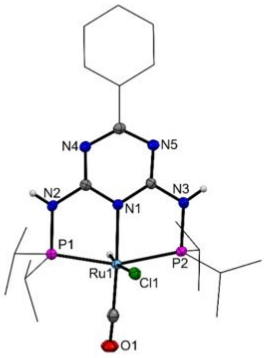

Figure 2. Molecular structure of monomeric complex **2m**. Displacement ellipsoids are drawn at 50% probability at 110 K. Hydrogen atoms are omitted for clarity, except those on Ru and N. Phenyl and isopropyl groups are displayed as wire frames for better graphical representation.

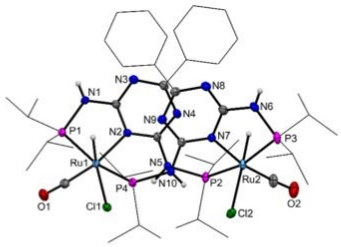

Figure 3. Molecular structure of dimeric complex **2d**. Displacement ellipsoids are drawn at 30% probability at 110 K. Hydrogen atoms are omitted for clarity, except those on Ru and N. Disordered parts of the molecule are shown in only one position. Phenyl and isopropyl groups are displayed as wire frames for better graphical representation.

ring are out of the formed plane (Ru1: 0.75, N1: 0.21, N5: 0.35 Å/Ru2: 0.84, N6: 0.22, N10: 0.33 Å). In **2m**, the triazine unit is nearly planar (mean deviation of the best plane = 0.006 Å), and the displacement of the substituents of the ring is less pronounced (largest deviation for C4(phenyl ring) = 0.06 Å).

Catalytic Applications. Having related monomeric and dimeric complexes **2m** and **2d** in hand, we became interested in the comparison of the catalytic performance of both systems. Notably, detailed examinations of such related mono- and bimetallic complexes are scarce. Typically, dimeric complexes, like the Shvo catalyst, are converted to the catalytically active monomeric species during initiation of the catalytic reaction.[49,50] To prove the integrity of both species, the interconversion between them was examined. Therefore, a solution of each compound was heated in THF-d_8 to 115 °C for 18 h. For **2m**, no change could be observed, whereas 8% of **2d** was converted into **2m** (SI Figure S10). As (de)-hydrogenation catalysis is often performed under basic conditions, the interconversion in the presence of base was investigated, too. However, addition of NEt_3 to a solution of **2d** or **2m** led to no reaction, even at elevated temperature (90 °C, 2 h, see SI Figure S11). Additionally, no interconversion could be observed in the presence of formic acid at room temperature. Comparing the activity of **2m** with **2d** during catalysis (see below), significantly different reactivities were observed, indicating no interconversion of the complexes. Overall, it can be assumed that only at elevated temperatures (>100 °C) slow formation of **2m** from **2d** is taking place, and interconversion of the complexes is unlikely in the model reactions presented vide infra.

To earn insights into the catalytic behavior of both complexes, **2d** and **2m** were examined in six different model reactions, i.e., (i) dehydrogenation of formic acid, (ii) hydrogenation of carbon dioxide, and (iii) hydrogenation of four unsaturated organic model compounds.

Dehydrogenation of Formic Acid. Over the past two decades, formic acid has attracted a lot of attention as a promising hydrogen carrier.[51−54] For this technology, the hydrogenation of CO_2 to formic acid and its dehydrogenation to hydrogen gas are necessary. First, the decomposition of formic acid was investigated. Screening of different reaction conditions previously reported for Ru pincer catalysts[55−57] revealed the DMSO/NEt_3 system to provide the best results (SI Table S3). Therefore, these reaction conditions were chosen for further experiments (Table 1). For comparison, other recently reported high-performance Ru-based pincer complexes **3**−**6** were included in the catalytic tests.[55−57]

Applying batch conditions, dimeric complex **2d** displayed a maximum activity of 54,000 h^{-1} in formic acid dehydrogenation (Table 1, entry 1). When the reaction was continued by addition of more formic acid, the result was improved to 112,000 h^{-1}. This behavior was attributed to the poor solubility of **2d** in DMSO in the first run. Interestingly, significantly higher activity could be observed for monomeric complex **2m** (470,000 h^{-1}; Table 1, entry 2), resulting in a very short reaction time of 3 min. When comparing to catalysts previously described in literature for formic acid dehydrogenation with weak bases,[55,57] **2m** is significantly more reactive (155,000 h^{-1} for **3** and 200,000 h^{-1} for **4**, Table 1, entries 3 and 4). It is worth noting that an essential improvement was achieved for complex **4** in comparison to reported values (200,000 h^{-1} to 7,333 h^{-1}) due to slight alterations in the catalyst structure, i.e. changing from P^tBu_2 to P^iPr_2.[55] Furthermore, complex **5** and its methylated variant **6** were evaluated (Table 1, entries 5 and 6). Whereas **5** showed little activity (38,500 h^{-1}), **6** proved to be the second most active catalyst after **2m** (280,000 h^{-1}).

The best catalysts were further examined in reactions with continuous formic acid addition. To determine the maximum activity, the formic acid dosage rate was slowly increased, until a drop in gas evolution was observed. Here, **2d** yielded a maximum activity of 130,000 h^{-1} (Table 1, entry 1). Similar to the batch reactions, **2m** proved to be the most active one (350,000 h^{-1}; Table 1, entry 2) with a gas evolution rate of up to 17 L/h, corresponding to a space-time yield of 14 g_{H2} L^{-1} h^{-1}, followed by **6** (230,000 h^{-1}, Table 1, entry 6). Catalyst **3** gave a TOF_{max} of 185,000 h^{-1} (Table 1, entry 3).

Hydrogenation of Carbon Dioxide. Inspired by the excellent results of **2m** and **2d** in formic acid dehydrogenation, the second important reaction for the application of formic acid as a hydrogen carrier—the hydrogenation of CO_2 to formic acid and formate—was investigated. In the presence of NEt_3, **2m** showed a higher activity for CO_2 hydrogenation than the state-of-the-art catalyst **3**, while no reaction occurred applying **2d** (6,345 h^{-1}; Table 2, entries 1−4). Higher yields were obtained for both catalysts, **2d** and **2m**, applying DBU

https://doi.org/10.1021/acs.organomet.3c00523
Organometallics 2024, 43, 2450−2457

Table 1. Activity of Ruthenium Pincer Complexes in Formic Acid Dehydrogenation

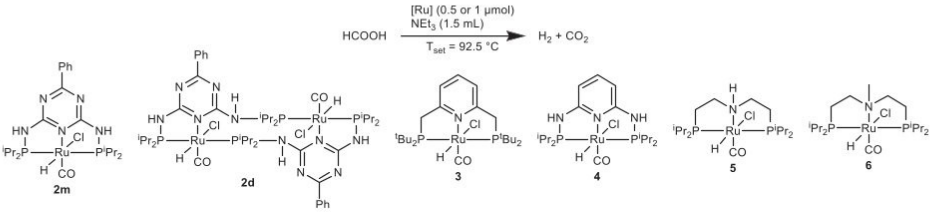

		Batch reactions[a]			Continuous addition[b]		
Entry	Catalyst	Reaction time until full conv. [min]	TOF_{max} [h^{-1}]	TON	Reaction time [min]	TOF_{max} [h^{-1}]	TON
1	**2d**	40	54,000	23,000	150	130,000	250,000
		16[c]	112,000[c]	23,000[c]			
2	**2m**	3	470,000	23,000	62	350,000	240,000
3	**3**	13	155,000	23,000	80	185,000	175,000
4	**4**	9	200,000	23,000	n. t.	n. t.	n. t.
5	**5**	50	38,500	23,000	n. t.	n. t.	n. t.
6	**6**	6	280,000	23,000	60	230,000	125,000

[a]Reaction conditions: formic acid (0.41 mL, 10.8 mmol), NEt_3 (1.5 mL), DMSO (5.0 mL), catalyst (0.5 μmol Ru), T_{set} = 92.5 °C. Reactions were started by catalyst addition. Batch reactions were reproduced at least twice with a standard deviation of <10%. [b]Reaction conditions: formic acid (4.6−13 mL/h), NEt_3 (1.5 mL), DMSO (5.0 mL), catalyst (1.0 μmol Ru), T_{set} = 92.5 °C. TOF_{max} was determined by variation of formic acid dosage rate as described in SI Figures S14−S17 and calculated according to eq 7 in SI 1.3. [c]Data after continuation of the experiment by addition of formic acid (0.41 mL, 10.8 mmol). n. t.: not tested.

Table 2. Catalytic CO_2 Hydrogenation with Different Ruthenium Pincer Complexes

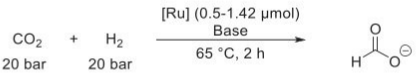

Entry	Catalyst	Amount of Ru metal [μmol]	TOF [h^{-1}]	Yield [mmol]
1	**2d**[a]	2.00	0	0
2	**2d**[a]	1.00	0	0
3	**2m**[a]	1.00	6,345	13
4	**3**[a]	1.00	4,601	9
5	**2d**[b]	2.84	20,941	59
6	**2d**[b]	1.40	27,286	38
7	**2m**[b]	1.42	7,313	21
8	**3**[b]	1.42	36,000[57]	102

[a]All reactions were done in a 300 mL stainless steel autoclave with 12 mL glass vials. NEt_3 (1.5 mL), DMSO (5 mL), H_2 (20 bar), CO_2 (20 bar), T_{set} = 65 °C, 2 h. Yields were determined by ^1H NMR with DMF as internal standard. [b]conditions analogous to ref 57. All reactions were done in a 100 mL stainless steel autoclave. DBU (5.0 mL), DMF (30.0 mL), catalysts (1.42 μmol Ru unless noted otherwise), H_2 (20 bar), CO_2 (20 bar), T_{set} = 65 °C, 2 h. Yields were determined by ^1H NMR with toluene as internal standard. All experiments were repeated at least once.

instead of NEt_3 under conditions recently used for complex **3** (Table 2, entries 5−7).[57] Interestingly, opposite to the NEt_3 system, the dimeric species **2d** showed higher activity than the monomeric complex **2m** by a factor of almost four (ca. 27,000 h^{-1} vs 7,300 h^{-1}). As expected, an increase in catalyst loading of **2d** led to a lower activity (21,000 h^{-1}, Table 2, entry 5). Nevertheless, **3** provides the highest activity within this comparison (36,000 h^{-1}, Table 2, entry 8).

Hydrogenation of Unsaturated Organic Compounds. Hydrogenation of functional groups is a widely applied methodology for the synthesis of bulk and fine chemicals.[58,59] Therefore, the ability of **2d** and **2m** to hydrogenate different unsaturated C−O and C−N bonds in, e.g., ketones, nitriles, esters, and N-heteroarenes was investigated (Scheme 2). For this purpose, acetophenone, 4-phenylbenzonitrile, methyl benzoate, and quinoline were chosen as benchmark substrates. In all cases, KO^{t}Bu was applied as a base for precatalyst activation. To our delight, hydrogenation of the model substrates was observed in all cases for the monomeric as well as the dimeric complex under conditions typically used in

Scheme 2. Hydrogenation of Different Substrates by Monomeric and Dimeric Ru Complexes 2m and 2d[a]

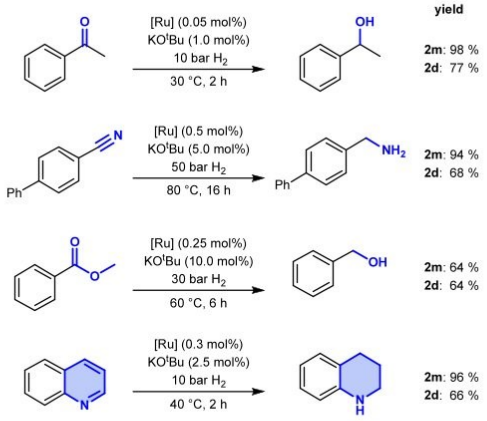

[a]Reaction conditions: Substrate (0.5 mmol), THF (2 mL). yields were determined by GC analysis using hexadecane as internal standard, conversions provided in SI Table S5−8. Catalyst concentration is reported as the amount of Ru metal employed.

https://doi.org/10.1021/acs.organomet.3c00523
Organometallics 2024, 43, 2450−2457

homogeneous Ru hydrogenation catalysis.[22,26,60−62] As described in Scheme 2, in the case of acetophenone, 4-phenylbenzonitrile, and quinoline hydrogenation, higher activities were obtained for the monomeric complex **2m** (94% to 98% yield) than for the dimeric complex **2d** (68% to 77% yield). However, methyl benzoate hydrogenation resulted in same yield for both complexes (64%).

CONCLUSION

Two new Ru pincer complexes, **2d** and **2m**, containing the guanamine moiety in the backbone were synthesized and fully characterized including SC-XRD. Interestingly, the synthesis resulted in a monomeric and a dimeric ruthenium species whose interconversion is only possible to a certain extent under harsh conditions. This inherent stability offered the possibility to compare the catalytic performance of related mono- and bimetallic complexes.

More specifically, the ability of the two new organometallic complexes to act as catalysts was examined in six different model reactions, i.e., (i) dehydrogenation of formic acid, (ii) hydrogenation of carbon dioxide, and (iii) hydrogenation of unsaturated organic compounds resulting in good to excellent yields and activities, especially for the monomeric species **2m**, while **2d** was observed to be mostly less active. In formic acid dehydrogenation, **2m** even outperforms state-of-the-art catalysts. Thus, the new complexes **2m** and **2d** provide an extension of the class of available ruthenium pincer catalysts for (de)hydrogenation reactions and might inspire researchers for further developments in this area.

EXPERIMENTAL SECTION

General Methods. Column chromatography was performed under protective gas atmosphere with silica by Macherey-Nagel MN Kieselgel 60 (0.04−0.063 mm). The column was filled dry. Solvent mixtures are reported in volume percent. TLCs were performed using Merck TLC-plates with fluorescence indicator (silica gel 60, F_{254}). 1% $KMnO_4$ solution was used as a coloring agent. NMR spectra were recorded at room temperature at one of the following devices: 300 MHz (Bruker AV-III 300), 300 MHz (Bruker AV-III HD 300), or 400 MHz (Bruker AV-III HD 400). ^{31}P spectra were recorded at 122 or 162 MHz. ^{13}C spectra were recorded at 75 or 101 MHz. Chemical shifts are reported in the δ-scale. The resonance signal of the remaining protons or carbon atoms of the solvent was used as an internal standard. The following abbreviations were used to describe the signals: s = singlet, d = doublet, t = triplet, sept. = septet, m = multiplet. The coupling constant J is reported in Hz. GC analysis for the hydrogenation of organic molecules was performed on an Agilent 7890A chromatograph equipped with a HP-5 column (30 m × 250 μm × 0.25 μm). GC-MS analyses were carried out using an Agilent 8890 chromatograph equipped with a HP-5 column (30 m × 250 μm × 0.25 μm) connected to an Agilent 5977B GC/MSD. Diffraction data were collected on a Bruker Kappa APEX II Duo diffractometer using Mo Kα for **2d** and Cu Kα radiation for **2m**. The structures were solved by direct methods[63] and refined by full-matrix least-squares procedures on F^2.[64] XP (Bruker AXS) or MERCURY[65] were used for graphical representations. Contributions of disordered solvent in complex **2d** were removed from the diffraction data using the SQUEEZE procedure in PLATON.[66] Mass spectrometry was performed on an XEVO G2-XS TOF using ESI for ionization. All experiments were carried out under an inert gas atmosphere using standard Schlenk and glovebox techniques. Triglyme, formic acid, and water were degassed by bubbling argon for 1 h. Formic acid was distilled before use. Other solvents and liquid reagents were dried and degassed with a solvent purification system (SPS) or according to literature[67] and stored on molecular sieves (3 Å) under argon atmosphere. Chemicals and catalysts RuPN^{H}P^{i}Pr were purchased from chemical companies and used without further purification. Catalysts RuPN^{Me}P^{i}Pr,[68] RuPN^{Pyr}P^{t}Bu,[35] RuPN$_3$P^{i}Pr,[40] and ligand **1**[43,44] were synthesized according to literature procedures. All catalysts and air-sensitive compounds were stored under argon atmosphere.

Synthesis of Complexes [Ru(CO)ClH(*N*,*N*′-bis-(diisopropylphosphino)-benzoguanamine)] 2m and [Ru(CO)-ClH(*N*,*N*′-bis(diisopropylphosphino)-benzoguanamine)]$_2$ 2d. To a solution of ligand **1** (1.26 g, 3.00 mmol, 1.00 equiv) in THF (22.5 mL), [RuHCl(CO)(PPh$_3$)$_3$] (2.86 g, 3.00 mmol, 1.00 equiv) was added. The reaction mixture was refluxed at 65 °C for 18 h. After removal of the solvent in vacuo, the crude product was purified by column chromatography under protective gas atmosphere (heptane/Et_2O 9:1 to pentane/EtOAc 6:4 to DCM/MeOH 9:1). The monomeric and dimeric complex **2m** and **2d** were collected in two fractions as a yellow solid.

Monomeric complex **2m**: Yield: 32% (556 mg, 0.951 mmol). ^{1}H NMR (300 MHz, THF-d_8): δ = 8.37−8.26 (m, 2H, C*H*CHC), 7.51−7.44 (m, 1H, C*H*CHCHC), 7.44−7.35 (m, 2H, C*H*C), 3.26−3.05 (m, 2H, CH^{iPr}), 2.50−2.35 (m, 2H, CH^{iPr}), 1.60−1.39 (m, 12H, CH_3), 1.21 (dt, J = 6.9, 9.4 Hz, 6H, CH_3), 1.11 (dd, J = 7.0, 15.3 Hz, 6H, CH_3), −14.78 (t, J = 19.3 Hz, 1H, RuH) ppm. ^{31}P NMR (122 MHz, THF-d_8): δ = 123.8 ppm. ^{13}C NMR (75 MHz, THF-d_8): δ = 208.4 (CO), 171.4 (CPh), 170.7 (t, J = 11.5 Hz, CN_3), 137.4 ($C(C)_3$), 132.9 (*C*HCHCHC), 129.4 (CH*C*HC), 129.1 (CH*C*), 29.4 (t, J = 11.7 Hz, $CHCH_3$), 27.4 (t, J = 13.3 Hz, $CHCH_3$), 20.6 (t, J = 4.6 Hz, CH_3), 19.4−18.7 (m, CH_3), 17.4 (CH_3) ppm. ESI-HRMS (m/z pos): Calculated for [$C_{22}H_{36}N_5OP_2Ru$]: 550.1439; found: 550.1453 [M−Cl]$^+$. X-ray structural analysis: Crystals suitable for X-ray analysis were grown by vapor diffusion of *n*-pentane into a saturated THF-solution. Crystal data of **2m** (CCDC: 2313386): $C_{22}H_{36}ClN_5OP_2Ru$, M = 585.02, orthorhombic, space group $Pna2_1$, a = 18.9902(16), b = 13.0446(11), c = 10.8083(9) Å, V = 2677.4(4) Å^3, T = 110(2) K, Z = 4, 60170 reflections measured, 6466 independent reflections (R_{int} = 0.0362), final R values ($I > 2\sigma(I)$): R_1 = 0.0228, wR_2 = 0.0531, final R values (all data): R_1 = 0.0243, wR_2 = 0.0539, 307 parameters.

Dimeric complex **2d**: Yield: 33% (585 mg, 0.500 mmol). ^{1}H{^{31}P} NMR (400 MHz, THF-d_8): δ = 8.05−7.99 (m, 4H, C*H*C), 7.47−7.39 (m, 2H, C*H*CHCHC), 7.26 (t, J = 7.7 Hz, 4H, C*H*CHC), 3.01 (sept, J = 7.1 Hz, 2H, CH^{iPr}), 2.68 (sept, J = 7.2 Hz, 2H, CH^{iPr}), 2.61−2.46 (m, 2H, CH^{iPr}), 2.39 (sept, J = 6.9 Hz, 2H, CH^{iPr}), 1.69 (d, J = 7.1 Hz, 6H, CH_3), 1.68 (d, J = 7.0 Hz, 6H, CH_3), 1.53 (d, J = 6.9 Hz, 6H, CH_3), 1.50 (d, J = 7.1 Hz, 6H, CH_3), 1.36 (d, J = 7.0 Hz, 6H, CH_3), 1.26 (d, J = 7.1 Hz, 6H, CH_3), 1.22 (d, J = 7.0 Hz, 6H, CH_3), 1.17 (d, J = 7.2 Hz, 6H, CH_3), −13.86 (s, 2H, RuH) ppm. For the integration data from a ^{1}H NMR (300 MHz, THF-d_8) spectrum were used. ^{31}P NMR (122 MHz, THF-d_8): δ = 119.31 (d, J = 322.5 Hz), 102.07 (d, J = 322.8 Hz) ppm. ^{13}C NMR (101 MHz, THF-d_8): δ = 207.6 (t, J = 15.2 Hz, CO), 171.5 (d, J = 15.2 Hz, CN_3), 169.6 (C^{Ph}), 167.7 (CN_3), 136.3 ($C(C)_3$), 132.6 (CHCHCHC), 130.1 (CHC), 128.5 (CHCHC), 33.4 (d, J = 20.4 Hz, CH^{iPr}), 33.1 (t, J = 8.7 Hz, CH^{iPr}), 31.4 (d, J = 18.1 Hz, CH^{iPr}), 27.4 (d, J = 34.0 Hz, CH^{iPr}), 22.5 (CH_3), 21.4 (d, J = 10.8 Hz, CH_3), 20.8 (d, J = 7.1 Hz, CH_3), 19.8 (CH_3), 19.1 (CH_3), 18.8 (d, J = 6.2 Hz, CH_3), 17.5 (d, J = 6.6 Hz, CH_3), 17.4 (CH_3) ppm. ESI-HRMS (m/z pos): Calculated for [$C_{44}H_{72}N_{10}O_2P_4ClRu_2$]: 1135.2566; found: 1135.2546 [M−Cl]$^+$. Crystals suitable for X-ray analysis were grown by vapor diffusion of *n*-pentane into a saturated THF-solution. Crystal data of **2d** (CCDC: 2313385): $C_{44}H_{72}Cl_2N_{10}O_2P_4Ru_2$, M = 1170.03, monoclinic, space group $P2_1/n$, a = 12.6107(6), b = 24.1527(11), c = 21.7434(9) Å, b = 100.682(2)°, V = 6507.9(5) Å^3, T = 110(2) K, Z = 4, 79942 reflections measured, 11557 independent reflections (R_{int} = 0.0542), final R values ($I > 2\sigma(I)$): R_1 = 0.0257, wR_2 = 0.0621, final R values (all data): R_1 = 0.0306, wR_2 = 0.0648, 663 parameters.

Formic Acid Dehydrogenation. A double-walled, thermostatically controlled reaction vessel is connected via a reflux condenser to a manual buret. The reaction vessel was charged with all solid reagents except the catalyst and repeatedly evacuated and purged with argon (three times). The valve for extraction of gas samples was closed, and

https://doi.org/10.1021/acs.organomet.3c00523
Organometallics 2024, 43, 2450−2457

another three evacuation and purge cycles were carried out. The buret was flushed with argon three times. After addition of all liquid reagents under argon stream, the reaction vessel was brought to reaction temperature with a thermostat (a set temperature of 92.5 °C corresponds to 90 °C internal temperature). Once the reaction temperature was reached, the setup was equilibrated for 20 min. The reaction was started by addition of the catalyst stock solution (for reactions with <2 μmol catalyst) through a septum. In reactions with >2 μmol catalyst, the reaction was started by catalyst addition with a Teflon crucible under slight argon stream. The evolved gas volume was measured at set time points. At the end of the reaction, a gas sample was taken for GC analysis. The reaction setup used is shown in SI Figure S12.

In reactions with continuous formic acid addition, a syringe pump was used. The formic acid dosage was accelerated after the gas evolution rate matched the addition rate. After reaching the maximum activity, indicated by stable or decreased gas evolution, the reaction was stopped. By subtracting the consumed formic acid (calculated from the evolved gas) from the added formic acid, the amount of formic acid in the reaction vessel can roughly be calculated.

Batch reactions were reproduced at least twice with a standard deviation of <10%. CO content was below 10 ppm.

Hydrogenation of CO_2. Hydrogenations of carbon dioxide for reaction conditions a) were carried out in a Parr Instruments autoclave (300 mL) with an aluminum inlet. The autoclave was purged with argon before usage, and 12 mL glass vials were equipped with a stirring bar and closed with a screw cap containing a septum. Under an argon atmosphere, the vials were charged with 5 mL of DMSO (dry) and 1.5 mL of NEt_3 (dry). The septum was punctured with a needle to allow gas exchange, and the vials were transferred to the autoclave. The autoclave was purged 3 times with 5−10 bar H_2. First, it was pressurized with 20 bar CO_2, then with 20 bar H_2 and heated in a preheated aluminum block at 65 °C for 2 h. Afterward, the autoclave was cooled to 0 °C, and the pressure was released. DMF was added to the reaction vials as an internal standard, and the yield was determined by ^{1}H NMR.

Hydrogenations of carbon dioxide for reaction conditions b) were carried out in a Parr Instruments autoclave (100 mL) equipped with a glass inlet. The autoclave was purged with argon prior to the reaction. DMF (30 mL in total, dry), then a stock solution of the catalysts and 5.0 mL of DBU were added under an argon atmosphere. The autoclave was closed and purged with 10−20 bar H_2 three times. It was pressurized with 20 bar CO_2, then with 20 bar H_2. The reaction was heated at 65 °C for 2 h with overhead stirring. The pressure was released at 0 °C. Toluene was added as an internal standard, and the yield was determined by ^{1}H NMR. All reactions were repeated at least one time.

Hydrogenation of Unsaturated Organic Molecules. Hydrogenations were carried out in a Parr Instruments autoclave (300 mL) with an aluminum inlet for 8 mL vials. Under an argon atmosphere, a vial was charged with the respective precatalyst and solvent (2 mL), before KO^{t}Bu was added. The mixture was stirred for approximately 5 min, and the corresponding substrate (0.5 mmol) was added. The vial was closed with a screw cap containing a septum, which was punctured with a needle to allow for the exchange of atmosphere, and the vial was transferred into the autoclave. Once sealed, the autoclave was purged five times with 5 to 10 bar of hydrogen, then pressurized with the desired pressure and heated in a preheated aluminum block for the respective reaction time. Afterward, the autoclave was cooled to RT, and the pressure was carefully released. The reaction mixture was diluted with Et_2O, hexadecane was added as an internal standard, and the mixture was filtered through a pad of Celite and analyzed by GC and GC-MS.

■ ASSOCIATED CONTENT

Supporting Information

The Supporting Information is available free of charge at https://pubs.acs.org/doi/10.1021/acs.organomet.3c00523.

General methods, experimental details, and analytical data (PDF)

Accession Codes

CCDC 2313385−2313386 contain the supplementary crystallographic data for this paper. These data can be obtained free of charge via www.ccdc.cam.ac.uk/data_request/cif, or by emailing data_request@ccdc.cam.ac.uk, or by contacting The Cambridge Crystallographic Data Centre, 12 Union Road, Cambridge CB2 1EZ, UK; fax: +44 1223 336033.

■ AUTHOR INFORMATION

Corresponding Authors

Kathrin Junge − *Leibniz-Institut für Katalyse e.V., 18059 Rostock, Germany*; orcid.org/0000-0001-7044-8888; Email: Kathrin.Junge@catalysis.de

Henrik Junge − *Leibniz-Institut für Katalyse e.V., 18059 Rostock, Germany*; orcid.org/0000-0002-7603-1984; Email: Henrik.Junge@catalysis.de

Matthias Beller − *Leibniz-Institut für Katalyse e.V., 18059 Rostock, Germany*; orcid.org/0000-0001-5709-0965; Email: Matthias.Beller@catalysis.de

Authors

Hendrik A. Kempf − *Leibniz-Institut für Katalyse e.V., 18059 Rostock, Germany*; orcid.org/0009-0002-8780-4361

Niklas F. Both − *Leibniz-Institut für Katalyse e.V., 18059 Rostock, Germany*; orcid.org/0000-0002-0565-4164

Carolin A. M. Stein − *Leibniz-Institut für Katalyse e.V., 18059 Rostock, Germany*

Anke Spannenberg − *Leibniz-Institut für Katalyse e.V., 18059 Rostock, Germany*

Complete contact information is available at: https://pubs.acs.org/10.1021/acs.organomet.3c00523

Notes

The authors declare no competing financial interest.

■ ACKNOWLEDGMENTS

This work was funded by the German Federal Ministry for Economic Affairs and Climate Action within the project "MEGA" (FKZ: 03EN5006A). We thank Anja Kammer for analytical support and valuable discussions.

■ REFERENCES

(1) Bai, S. T.; De Smet, G.; Liao, Y.; Sun, R.; Zhou, C.; Beller, M.; Maes, B. U. W.; Sels, B. F. Homogeneous and Heterogeneous Catalysts for Hydrogenation of CO_2 to Methanol Under Mild Conditions. *Chem. Soc. Rev.* **2021**, *50* (7), 4259−4298.

(2) Ranjekar, A. M.; Yadav, G. D. Steam Reforming of Methanol for Hydrogen Production: A Critical Analysis of Catalysis, Processes, and Scope. *Ind. Eng. Chem. Res.* **2021**, *60* (1), 89−113.

(3) Klankermayer, J.; Wesselbaum, S.; Beydoun, K.; Leitner, W. Selective Catalytic Synthesis Using the Combination of Carbon Dioxide and Hydrogen: Catalytic Chess at the Interface of Energy and Chemistry. *Angew. Chem., Int. Ed.* **2016**, *55* (26), 7296−7343.

(4) Gallezot, P. Conversion of Biomass to Selected Chemical Products. *Chem. Soc. Rev.* **2012**, *41* (4), 1538−1558.

(5) Anastas, P. T.; Warner, J. C. *Green Chemistry: Theory and Practice*; Oxford University Press, 1998.

(6) Mitsudome, T.; Sheng, M.; Nakata, A.; Yamasaki, J.; Mizugaki, T.; Jitsukawa, K. A Cobalt Phosphide Catalyst for the Hydrogenation of Nitriles. *Chem. Sci.* **2020**, *11* (26), 6682−6689.

(7) Trunschke, A.; Bellini, G.; Boniface, M.; Carey, S. J.; Dong, J.; Erdem, E.; Foppa, L.; Frandsen, W.; Geske, M.; Ghiringhelli, L. M.;

et al. Towards Experimental Handbooks in Catalysis. *Top. Catal.* **2020**, *63* (19−20), 1683−1699.
(8) Horváth, I. T.; Anastas, P. T. Innovations and Green Chemistry. *Chem. Rev.* **2007**, *107*, 2169−2173.
(9) Elangovan, S.; Topf, C.; Fischer, S.; Jiao, H.; Spannenberg, A.; Baumann, W.; Ludwig, R.; Junge, K.; Beller, M. Selective Catalytic Hydrogenations of Nitriles, Ketones, and Aldehydes by Well-Defined Manganese Pincer Complexes. *J. Am. Chem. Soc.* **2016**, *138* (28), 8809−8814.
(10) Zybert, M. Applied Catalysis in Chemical Industry: Synthesis, Catalyst Design, and Evaluation. *Catalysts* **2023**, *13* (3), 607.
(11) Heaeus Precious Metals. *Chemical Process Catalysts*. 2023. https://www.heraeus.com/en/hpm/hmp_products_solutions/heterogeneous_catalysts/chemical_process_catalysts/process_catalysts.html#tabs-1235788-2 (accessed September 5, 2023).
(12) Humphreys, J.; Lan, R.; Tao, S. Development and Recent Progress on Ammonia Synthesis Catalysts for Haber−Bosch Process. *Adv. Energy Sustainability Res.* **2021**, *2* (1), 2000043.
(13) Behrens, M.; Studt, F.; Kasatkin, I.; Kühl, S.; Hävecker, M.; Abild-Pedersen, F.; Zander, S.; Girgsdies, F.; Kurr, P.; Kniep, B.-L.; et al. The Active Site of Methanol Synthesis over $Cu/ZnO/Al_2O_3$ Industrial Catalysts. *Science* **2012**, *336*, 893−897.
(14) Johansson Seechurn, C. C. C.; Kitching, M. O.; Colacot, T. J.; Snieckus, V. Palladium-Catalyzed Cross-Coupling: A Historical Contextual Perspective to the 2010 Nobel Prize. *Angew. Chem., Int. Ed.* **2012**, *51* (21), 5062−5085.
(15) Schrock, R. R.; Basset, J.-M.; Callens, E.; Riache, N.; Keitz, B. K.; Weinberger, D. S.; Lavallo, V.; Allen, D. P.; Solans-Monfort, X.; Copéret, C.; et al. *Handbook of Metathesis Vol. 1: Catalyst Development and Mechanism*; Wiley-VCH Verlag GmbH & Co. KGaA, 2015.
(16) Hanson, P. R.; Maitra, S.; Chegondi, R.; Markley, J. L.; O'Leary, D. J.; O'Neil, G. W.; Lin, Y. A.; Davis, B. G.; Nam, Y. H.; Snapper, M. L.; et al. *Handbook of Metathesis Vol. 2: Applications in Organic Synthesis*; Wiley-VCH Verlag GmbH & Co. KGaA, 2015.
(17) Slugovc, C.; Héroguez, V.; Chemtob, A.; Quemener, D.; Hanik, N.; Kilbinger, A. F. M.; Elacqua, E.; Brummelhuis, N. t.; Weck, M.; Miyake, G. M.; et al. *Handbook of Metathesis Vol. 3: Polymer Synthesis*; Wiley-VCH Verlag GmbH & Co. KGaA, 2015.
(18) Kallmeier, F.; Kempe, R. Manganese Complexes for (De)-Hydrogenation Catalysis: A Comparison to Cobalt and Iron Catalysts. *Angew. Chem., Int. Ed.* **2018**, *57* (1), 46−60.
(19) Das, K.; Waiba, S.; Jana, A.; Maji, B. Manganese-Catalyzed Hydrogenation, Dehydrogenation, and Hydroelementation Reactions. *Chem. Soc. Rev.* **2022**, *51* (11), 4386−4464.
(20) Wang, D.; Astruc, D. The Golden Age of Transfer Hydrogenation. *Chem. Rev.* **2015**, *115* (13), 6621−6686.
(21) Gunanathan, C.; Milstein, D. Applications of Acceptorless Dehydrogenation and Related Transformations in Chemical Synthesis. *Science* **2013**, *341* (6143), No. 1229712.
(22) Younus, H. A.; Ahmad, N.; Su, W.; Verpoort, F. Ruthenium Pincer Complexes: Ligand Design and Complex Synthesis. *Coord. Chem. Rev.* **2014**, *276*, 112−152.
(23) Kumar, A.; Daw, P.; Milstein, D. Homogeneous Catalysis for Sustainable Energy: Hydrogen and Methanol Economies, Fuels from Biomass, and Related Topics. *Chem. Rev.* **2022**, *122* (1), 385−441.
(24) Piccirilli, L.; Lobo Justo Pinheiro, D.; Nielsen, M. Recent Progress with Pincer Transition Metal Catalysts for Sustainability. *Catalysts* **2020**, *10* (7), 773.
(25) Lawrence, M. A. W.; Green, K.-A.; Nelson, P. N.; Lorraine, S. C. Review: Pincer Ligands—Tunable, Versatile and Applicable. *Polyhedron* **2018**, *143*, 11−27.
(26) Kuriyama, W.; Matsumoto, T.; Ogata, O.; Ino, Y.; Aoki, K.; Tanaka, S.; Ishida, K.; Kobayashi, T.; Sayo, N.; Saito, T. Catalytic Hydrogenation of Esters. Development of an Efficient Catalyst and Processes for Synthesising (*R*)-1,2-Propanediol and 2-(*l*-Menthoxy)-ethanol. *Org. ProcessRes. Dev.* **2012**, *16* (1), 166−171.
(27) McGuinness, D. S.; Wasserscheid, P.; Keim, W.; Hu, C.; Englert, U.; Dixon, J. T.; Grove, C. Novel Cr-PNP Complexes as Catalysts for the Trimerisation of Ethylene. *Chem. Commun.* **2003**, *3*, 334−335.
(28) Kamaluddin, A.-R. Transfer Hydrogenation Processes and Catalysts. WO2004096735A2, 2004.
(29) Chen, L.; Ai, P.; Gu, J.; Jie, S.; Li, B.-G. Stereospecific Polymerization of 1,3-butadiene Catalyzed by Cobalt Complexes Bearing N-Containing Diphosphine PNP Ligands. *J. Organomet. Chem.* **2012**, *716*, 55−61.
(30) Zhang, G.; Scott, B. L.; Hanson, S. K. Mild and Homogeneous Cobalt-Catalyzed Hydrogenation of C = C, C = O, and C = N Bonds. *Angew. Chem., Int. Ed.* **2012**, *51* (48), 12102−12106.
(31) Alberico, E.; Sponholz, P.; Cordes, C.; Nielsen, M.; Drexler, H. J.; Baumann, W.; Junge, H.; Beller, M. Selective Hydrogen Production from Methanol with a Defined Iron Pincer Catalyst under Mild Conditions. *Angew. Chem., Int. Ed.* **2013**, *52* (52), 14162−14166.
(32) Kawatsura, M.; Hartwig, J. F. Transition Metal-Catalyzed Addition of Amines to Acrylic Acid Derivatives. A High-Throughput Method for Evaluating Hydroamination of Primary and Secondary Alkylamines. *Organometallics* **2001**, *20*, 1960−1964.
(33) Müller, G.; Klinga, M.; Leskelä, M.; Rieger, B. Iron and Cobalt Complexes of a Series of Tridentate P,N,P Ligands - Synthesis, Characterization, and Application in Ethene Polymerization Reactions. *Z. Anorg. Allg. Chem.* **2002**, *628* (13), 2839−2846.
(34) Zhang, J.; Gandelman, M.; Shimon, L. J. W.; Rozenberg, H.; Milstein, D. Electron-Rich, Bulky Ruthenium PNP-Type Complexes. Acceptorless Catalytic Alcohol Dehydrogenation. *Organometallics* **2004**, *23*, 4026−4033.
(35) Zhang, J.; Leitus, G.; Ben-David, Y.; Milstein, D. Facile Conversion of Alcohols into Esters and Dihydrogen Catalyzed by New Ruthenium Complexes. *J. Am. Chem. Soc.* **2005**, *127*, 10840−10841.
(36) Langer, R.; Leitus, G.; Ben-David, Y.; Milstein, D. Efficient Hydrogenation of Ketones Catalyzed by an Iron Pincer Complex. *Angew. Chem., Int. Ed.* **2011**, *50* (9), 2120−2124.
(37) Mukherjee, A.; Nerush, A.; Leitus, G.; Shimon, L. J.; Ben David, Y.; Espinosa Jalapa, N. A.; Milstein, D. Manganese-Catalyzed Environmentally Benign Dehydrogenative Coupling of Alcohols and Amines to Form Aldimines and H_2: A Catalytic and Mechanistic Study. *J. Am. Chem. Soc.* **2016**, *138* (13), 4298−4301.
(38) Benito-Garagorri, D.; Becker, E.; Wiedermann, J.; Lackner, W.; Pollak, M.; Mereiter, K.; Kisala, J.; Kirchner, K. Achiral and Chiral Transition Metal Complexes with Modularly Designed Tridentate PNP Pincer-Type Ligands Based on N-Heterocyclic Diamines. *Organometallics* **2006**, *25*, 1900−1913.
(39) Benito-Garagorri, D.; Wiedermann, J.; Pollak, M.; Mereiter, K.; Kirchner, K. Iron(II) Complexes Bearing Tridentate PNP Pincer-Type Ligands as Catalysts for the Selective Formation of 3-Hydroxyacrylates from Aromatic Aldehydes and Ethyldiazoacetate. *Organometallics* **2007**, *26*, 217−222.
(40) He, L.-P.; Chen, T.; Xue, D.-X.; Eddaoudi, M.; Huang, K.-W. Efficient Transfer Hydrogenation Reaction Catalyzed by a Dearomatized PN_3P Ruthenium Pincer Complex under Base-Free Conditions. *J. Organomet. Chem.* **2012**, *700*, 202−206.
(41) Mastalir, M.; Glatz, M.; Gorgas, N.; Stöger, B.; Pittenauer, E.; Allmaier, G.; Veiros, L. F.; Kirchner, K. Divergent Coupling of Alcohols and Amines Catalyzed by Isoelectronic Hydride Mn(I) and Fe(II) PNP Pincer Complexes. *Chem.—Eur. J.* **2016**, *22* (35), 12316−12320.
(42) Li, H.; Al-Dakhil, A.; Lupp, D.; Gholap, S. S.; Lai, Z.; Liang, L. C.; Huang, K. W. Cobalt-Catalyzed Selective Hydrogenation of Nitriles to Secondary Imines. *Org. Lett.* **2018**, *20* (20), 6430−6435.
(43) Michlik, S.; Kempe, R. A Sustainable Catalytic Pyrrole Synthesis. *Nat. Chem.* **2013**, *5* (2), 140−144.
(44) Rösler, S.; Obenauf, J.; Kempe, R. A Highly Active and Easily Accessible Cobalt Catalyst for Selective Hydrogenation of C = O Bonds. *J. Am. Chem. Soc.* **2015**, *137* (25), 7998−8001.
(45) Kallmeier, F.; Irrgang, T.; Dietel, T.; Kempe, R. Highly Active and Selective Manganese C = O Bond Hydrogenation Catalysts: The

Importance of the Multidentate Ligand, the Ancillary Ligands, and the Oxidation State. *Angew. Chem., Int. Ed.* **2016**, *55* (39), 11806−11809.
(46) Mastalir, M.; Stöger, B.; Pittenauer, E.; Puchberger, M.; Allmaier, G.; Kirchner, K. Air Stable Iron(II) PNP Pincer Complexes as Efficient Catalysts for the Selective Alkylation of Amines with Alcohols. *Adv. Syn. Catal.* **2016**, *358* (23), 3824−3831.
(47) Kallmeier, F.; Fertig, R.; Irrgang, T.; Kempe, R. Chromium-Catalyzed Alkylation of Amines by Alcohols. *Angew. Chem., Int. Ed.* **2020**, *59* (29), 11789−11793.
(48) Mastalir, M.; Stoger, B.; Pittenauer, E.; Allmaier, G.; Kirchner, K. Air-Stable Triazine-Based Ni(II) PNP Pincer Complexes As Catalysts for the Suzuki-Miyaura Cross-Coupling. *Org. Lett.* **2016**, *18* (13), 3186−3189.
(49) Conley, B. L.; Pennington-Boggio, M. K.; Boz, E.; Williams, T. J. Discovery, Applications, and Catalytic Mechanisms of Shvo's Catalyst. *Chem. Rev.* **2010**, *110*, 2294−2312.
(50) Karvembu, R.; Prabhakaran, R.; Natarajan, K. Shvo's Diruthenium Complex: A Robust Catalyst. *Coord. Chem. Rev.* **2005**, *249* (9−10), 911−918.
(51) Mellmann, D.; Sponholz, P.; Junge, H.; Beller, M. Formic Acid as a Hydrogen Storage Material - Development of Homogeneous Catalysts for Selective Hydrogen Release. *Chem. Soc. Rev.* **2016**, *45* (14), 3954−3988.
(52) Eppinger, J.; Huang, K.-W. Formic Acid as a Hydrogen Energy Carrier. *ACS Energy Lett.* **2017**, *2* (1), 188−195.
(53) Dutta, I.; Chatterjee, S.; Cheng, H.; Parsapur, R. K.; Liu, Z.; Li, Z.; Ye, E.; Kawanami, H.; Low, J. S. C.; Lai, Z.; et al. Formic Acid to Power towards Low-Carbon Economy. *Adv. Energy Mater.* **2022**, *12* (15), 2103799.
(54) Piccirilli, L.; Rabell, B.; Padilla, R.; Riisager, A.; Das, S.; Nielsen, M. Versatile CO_2 Hydrogenation-Dehydrogenation Catalysis with a Ru-PNP/Ionic Liquid System. *J. Am. Chem. Soc.* **2023**, *145* (10), 5655−5663.
(55) Pan, Y.; Pan, C. L.; Zhang, Y.; Li, H.; Min, S.; Guo, X.; Zheng, B.; Chen, H.; Anders, A.; Lai, Z.; et al. Selective Hydrogen Generation from Formic Acid with Well-Defined Complexes of Ruthenium and Phosphorus-Nitrogen PN_3-Pincer Ligand. *Chem.—Asian J.* **2016**, *11* (9), 1357−1360.
(56) Agapova, A.; Alberico, E.; Kammer, A.; Junge, H.; Beller, M. Catalytic Dehydrogenation of Formic Acid with Ruthenium-PNP-Pincer Complexes: Comparing N-Methylated and NH-Ligands. *ChemCatChem.* **2019**, *11* (7), 1910−1914.
(57) Filonenko, G. A.; van Putten, R.; Schulpen, E. N.; Hensen, E. J. M.; Pidko, E. A. Highly Efficient Reversible Hydrogenation of Carbon Dioxide to Formates Using a Ruthenium PNP-Pincer Catalyst. *ChemCatChem.* **2014**, *6* (6), 1526−1530.
(58) Andersson, P. G.; Munslow, I. J. *Modern Reduction Methods*; Wiley-VCH, 2008.
(59) Blaser, H.-U.; Spindler, F.; Thommen, M. Chapter 34: Industrial Application. In *The Handbook of Homogeneous Hydrogenation*; Wiley-VCH, 2006.
(60) Lu, S.-M.; Han, X.-W.; Zhou, Y.-G. An efficient catalytic system for the hydrogenation of quinolines. *J. Organomet. Chem.* **2007**, *692* (14), 3065−3069.
(61) Ogata, O. Cationic Ruthenium Complex, and Production Method Therefor, and Use Thereof. WO2018181865A1, 2018.
(62) Neumann, J.; Bornschein, C.; Jiao, H.; Junge, K.; Beller, M. Hydrogenation of Aliphatic and Aromatic Nitriles Using a Defined Ruthenium PNP Pincer Catalyst. *Eur. J. Org. Chem.* **2015**, *27*, 5944−5948.
(63) Sheldrick, G. M. A Short History of SHELX. *Acta Crystallogr.* **2008**, *A64*, 112−122.
(64) Sheldrick, G. M. Crystal Structure Refinement with SHELXL. *Acta Crystallogr.* **2015**, *C71*, 3−8.
(65) Macrae, C. F.; Sovago, I.; Cottrell, S. J.; Galek, P. T. A.; McCabe, P.; Pidcock, E.; Platings, M.; Shields, G. P.; Stevens, J. S.; Towler, M.; et al. Mercury 4.0: from Visualization to Analysis, Design and Prediction. *J. Appl. Crystallogr.* **2020**, *53*, 226−235.
(66) Spek, A. L. PLATON SQUEEZE: a Tool for the Calculation of the Disordered Solvent Contribution to the Calculated Structure Factors. *Acta Crystallogr.* **2015**, *C71*, 9−18.
(67) Armarego, W. L. F.; Chai, C. *Purification of Laboratory Chemicals*; Butterworth-Heineman, 2009.
(68) Alberico, E.; Lennox, A. J.; Vogt, L. K.; Jiao, H.; Baumann, W.; Drexler, H. J.; Nielsen, M.; Spannenberg, A.; Checinski, M. P.; Junge, H.; et al. Unravelling the Mechanism of Basic Aqueous Methanol Dehydrogenation Catalyzed by Ru-PNP Pincer Complexes. *J. Am. Chem. Soc.* **2016**, *138* (45), 14890−14904.

https://doi.org/10.1021/acs.organomet.3c00523
Organometallics 2024, 43, 2450−2457

6.2.2 Synthesis of Ru-PNPC Pincer Complexes and Applications in Catalytic Hydrogenation and Dehydrogenation Reactions

Hendrik A. Kempf, Germán López Robledo, Anke Spannenberg, Kathrin Junge, Haijun Jiao, Henrik Junge and Matthias Beller

ChemCatChem **2024**, e202401481

DOI: 10.1002/cctc.202401481

Author contributions:

In this manuscript, I synthesized all ligands and complexes. Their analytical characterization was carried out by me, except for SC-XRD. I performed all dehydrogenation reactions, as well as experimental mechanistic investigations. The manuscript was prepared, edited and peer reviewed by all authors. My overall contribution to this work accounts to approximately 60%.

Signature of the student — Signature of the supervisor

(Hendrik Kempf) — **(Prof. Matthias Beller)**

Check for updates

ChemCatChem

Research Article
doi.org/10.1002/cctc.202401481

Chemistry Europe
European Chemical Societies Publishing

www.chemcatchem.org

Synthesis of Ru-PNPC Pincer Complexes and Applications in Catalytic Hydrogenation and Dehydrogenation Reactions

Hendrik A. Kempf,[a] Germán López Robledo,[a] Anke Spannenberg,[a] Kathrin Junge,[a] Haijun Jiao,*[a] Henrik Junge,*[a] and Matthias Beller*[a]

The reaction of *N*,*N*-bis(2-(diisopropylphosphaneyl)ethyl)prop-2-yn-1-amine **1** with [Ru(CO)ClH(PPh_3)$_3$] leads to the formation of a new class of cyclometallated PNPC pincer complexes. Several examples of this class of compounds are synthesized and characterized. They, specifically complexes **2** and **3**, show good to excellent activity and selectivity in additive-free formic acid dehydrogenation, and transfer (de)hydrogenation reactions of different functional groups (ketone, alkyne, and alcohol). Theoretical and experimental studies reveal two competing pathways for the dehydrogenation of formic acid. The Ru-H pathway proceeds via the coordination site trans to the propylene arm of the ligand, whereas in the Ru-C pathway, a de-coordination of the propylene arm is observed.

1. Introduction

The development of new catalysts and improved chemical processes over the past century contributed significantly to global progress in medicine,[1] agriculture,[2] and industrialization.[3] The achieved improvements allowed for a raise in our standard of living,[4] becoming evident in an increase in the global population as well as a longer life expectancy at birth, especially between 1950 and 1985.[3,5] The development of novel organometallic complexes and homogeneous catalysts went hand in hand with these advancements.[6] For example, the invention of molecularly defined Ziegler-Natta catalysts, a milestone in polymer chemistry, continues to have a major impact on all kinds of materials used in our daily lives.[6b,7] In addition to bulk chemical processes, organometallic catalysis, specifically with phosphine metal complexes, plays a major role in the development and synthesis of pharmaceuticals, agrochemicals, and many specialty chemicals.[1,8] As a result, there is an ongoing interest in the synthesis and research of new types of organometallic complexes both in the chemical industry and in academic science. These can not only be used to improve existing chemical processes, i.e., make them more (cost) efficient and applicable, but they also offer opportunities to discover completely new transformations and will therefore eventually lead to a rise in our standard of living.

One example of this is the class of so-called pincer complexes, which have recently become interesting as active catalysts for various applications, as highlighted in Figure 1.[9] Pincer complexes are usually structured in such a way that they can bind to the respective metal center with several ligand donor atoms (e.g., P, N, or S).[9,10] One of the most important subclasses are PNP pincer complexes, which are formed by most transition metals.[10,11] Among various metals, specifically ruthenium-based complexes, attracted significant attention in the past two decades. The respective Ru-pincer complexes were successfully applied in various hydrogenation,[10,12] coupling[12d,e,13] as well as dehydrogenation reactions.[9d,12d,e,14] Selected examples are provided vide infra. Especially in the dehydrogenation of formic acid and methanol, they proved to give higher activities than analogue complexes containing other metal centers, like iron, iridium, or manganese.[9d,12a,14a,c,15] Overall, ruthenium PNP-pincer complexes were mostly applied in hydrogenation, dehydrogenation, and transfer hydrogenation reactions.[10,12c,13,14] Examples of such complexes are displayed in Figure 2 and their applications highlighted in the following paragraphs.

Originally, ruthenium PNP-pincer complexes were first applied by Abdur-Rashid and Goussev in 2004 for the transfer hydrogenation of ketones and imines.[16] In 2011, the now famous Ru-MACHO complex was invented by Takasago chemists, which is also reported to be industrially applied for the hydrogenation of esters.[17] An interesting sub-class of PNP-pincer complexes with a pyridine-based backbone was first introduced by Milstein and coworkers and applied in the green synthesis of imines from alcohols and amines via acceptorless dehydrogenative coupling.[18] Later, they were used in many other interesting transformations, including the reversible hydrogenation of CO_2 to formate salts by Pidko and coworkers.[19]

Interesting variations of the PNP-ligand were performed by the utilization of aminophosphines in the ligand backbone

[a] H. A. Kempf, G. López Robledo, Dr. A. Spannenberg, Dr. K. Junge, Dr. H. Jiao, Dr. H. Junge, Prof. Dr. M. Beller
Leibniz-Institut für Katalyse e. V., Albert-Einstein-Str. 29a 18059, Rostock, Germany
E-mail: haijun.jiao@catalysis.de
henrik.junge@catalysis.de
matthias.beller@catalysis.de

Supporting information for this article is available on the WWW under https://doi.org/10.1002/10.1002/cctc.202401481

ChemCatChem
Research Article
doi.org/10.1002/cctc.202401481
Chemistry Europe
European Chemical Societies Publishing

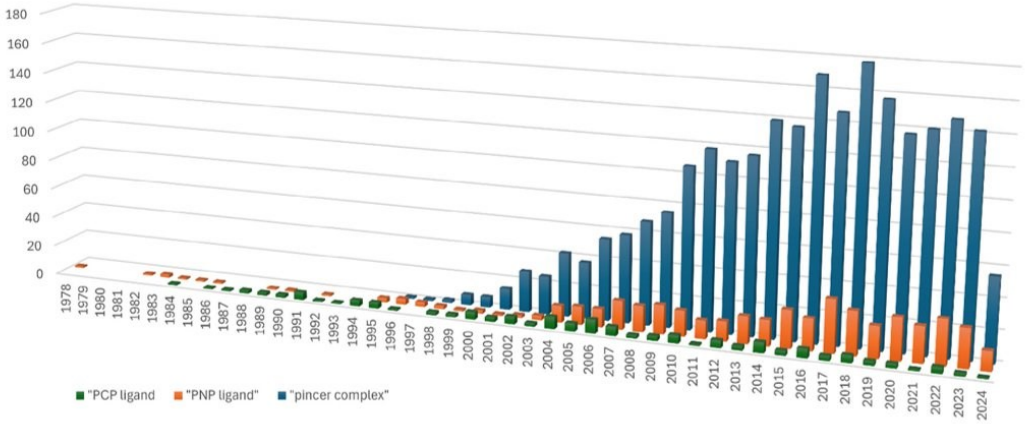

Figure 1. Number of publications about "pincer complex" (blue), "PNP ligand" (orange), and "PCP ligand" (green) in each year as found by SciFinder. It is worth noting that pincer complexes were first synthesized in 1976 but not named as such.

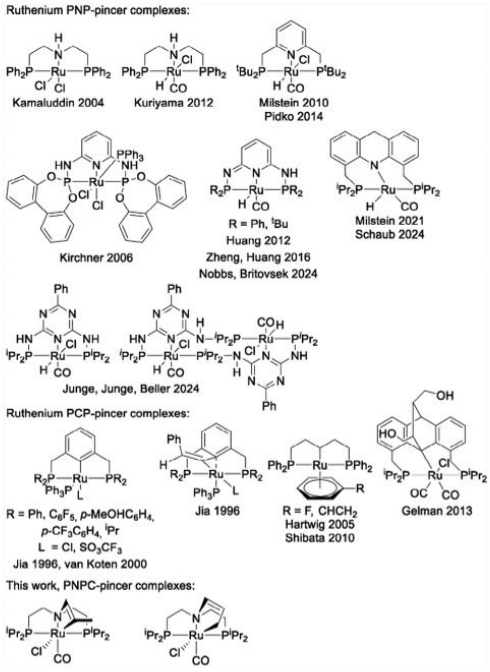

Figure 2. Selected examples of ruthenium-PNP and PCP pincer complexes.

by Kirchner and coworkers.[20] First catalytic applications were shown by Huang and coworkers, Zheng, Huang and coworkers, as well as Nobbs, Britovsek, and coworkers.[21] Utilizing this subclass of PNP-pincer complexes, notable catalyst activities were observed in different hydrogenation and dehydrogenation reactions, including transfer hydrogenation of ketones,[21a] ester synthesis from alcohols,[21b] imine formation from primary amines,[21b] formic acid dehydrogenation,[21c] and hydrogenation of CO_2.[21d] In addition, Ru PNP-pincer complexes with an acridine-based ligand backbone were employed by Milstein and coworkers, as well as Schaub and coworkers.[22] This complex was utilized for methanol reformation and the Guerbert reaction.[22] Most recently, some of us synthesized the first ruthenium complexes with a guanamine-based ligand backbone, a ligand typically used by the group of Kempe.[11,23] In general, good activity in hydrogenation and dehydrogenation reactions was observed in the presence of such complexes, too.

Another interesting subclass of pincer ligands are the so-called PCP ones, in which two phosphine and one carbon donor atom coordinate with the metal center. Compared to PNP ligands, in such complexes, additional reactivity at the metal—carbon bond can be expected. Indeed, as an example, Jia and coworkers observed the incorporation of phenylacetylene into the Ru—C bond of a ruthenium PCP-pincer complex already in 1996.[24] The first catalytic applications of ruthenium-PCP complexes were shown by van Koten and coworkers.[25] They reduced ketones to alcohols in transfer hydrogenation reactions. Later on, other PCP-pincer ligands based on dpppent-ligands have been disclosed. These latter metal complexes were prepared and characterized by Hartwig and coworkers and applied in the hydroamination of vinylarenes.[26] Further applications include catalytic nucleophilic aromatic substitution reactions.[27] Finally, it should be mentioned that an anthracene-based PCP-pincer complex was synthesized by Gelman and coworkers, which was utilized in different dehydrogenative coupling reactions and in transfer hydrogenations.[28]

Based on our interest in developing pincer complexes for (de)hydrogenation reactions,[29] we recently started investigating the potential immobilization of such complexes. For this purpose, we envisioned the synthesis of PNP-ligands with suitable

ChemCatChem
Research Article
doi.org/10.1002/cctc.202401481
Chemistry Europe
European Chemical Societies Publishing

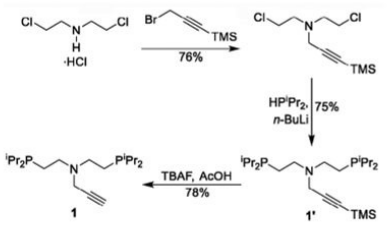

Scheme 1. Synthesis of ligands **1** and **1′**.

substituents attached to the nitrogen atom. During our studies, we serendipitously discovered the synthesis of a new type of pincer complex with PNPC ligands. The resulting complexes showed unexpected stability and allowed for several interesting catalytic applications.

2. Results and Discussion

2.1. Complex Synthesis

According to our original plan, we envisioned ligand **1** as a suitable precursor for immobilization of pincer complexes via Sharpless-type click reactions, as demonstrated by Lo and Copéret for a NHC-based ruthenium pincer complex.[30] Hence, **1** was synthesized in a straightforward manner, starting with the alkylation of bis-(2-chloroethyl)-ammonium chloride with 3-(trimethylsilyl)-propargylbromide, yielding the desired product in 76% (Scheme 1). Subsequent phosphination gave the TMS-protected ligand **1′** in 75% yield. Final deprotection was successfully performed in 78% yield, producing ligand **1**.

Next, the reaction of **1** with $[Ru(CO)ClH(PPh_3)_3]$ provided the corresponding ruthenium-PNPC complex. Notably, running the reaction at 60 °C, 6 d were needed to reach full conversion (Scheme 2). Unfortunately, a mixture of complexes was formed under these conditions, from which it was not possible to isolate pure products. To decrease reaction time and increase selectivity, the reaction temperature was increased to 120 °C, leading to a decrease in reaction time to 3 h. To our surprise, instead of the expected ruthenium-PNP complex **6**, ruthenium-PNPC complexes **2** and **4** were formed, which could be isolated in 15% yield by column chromatography. To further increase selectivity and yield, tetra-*n*-butylammonium acetate was tested as an additive. At 60 °C, reaction time was decreased to 36 h providing ruthenium-PNPC complexes **2** and **3**. Increasing the reaction temperature to 120 °C and further optimization of the reaction conditions led to the formation of PNPC complexes **2** and **3** in 66% isolated yield after 3 h.

Structural elucidation of PNPC complexes **2** and **3** was achieved by a combination of NMR and SC-XRD. Crystals suitable for X-ray structural analysis were obtained from a concentrated solution of **2** and **3** in ethyl acetate.[31] In this way, a mixed crystal of both species was formed (Figures 3 and 4). In both complexes, the metal center is coordinated by two phosphorus, one nitrogen, and one carbon atom of ligand **1**, as well as a carbonyl and a chlorido ligand, forming a distorted octahedral coordination environment.

In **2** (Figure 3), the chemical shift of C19B in the ^{13}C NMR spectrum suggests coordination to the metal center (^{13}C NMR: 160.0 ppm). Additionally, the chemical shifts of H18B (^1H NMR: 4.98 ppm), C18B (^{13}C NMR: 120.3 ppm), and C19B (^{13}C NMR: 160.0 ppm) indicate the presence of a double bond at this position. The latter agrees with the observed bond length between C18B and C19B, which is in the range of a typical $C(sp^2)$-$C(sp^2)$ double bond (C18B to C19B: 1.336(10) Å).[32] Furthermore, the splitting pattern indicates the presence of a CH and CH_3 group with a coupling constant of 2.0 Hz fitting with a ^4J coupling.

In **3** (Figure 4), the chemical shift of C18A (^{13}C NMR: 141.2 ppm), C19A (^{13}C NMR: 137.1 ppm), and the corresponding hydrogen atoms (^1H NMR of H18A: 5.70 ppm, H19A: 4.45 ppm), as well as the bond length of 1.352(7) Å indicate the presence of a double bond at this position. Furthermore, splitting pattern and DEPT measurement reveal the presence of two CH and one CH_2 groups, suggesting a N—CH═CH—CH_2 fragment. Consequently, C20A is coordinated to Ru1, which is additionally supported by the crystal structure.

Despite multiple attempts, it was not possible to obtain crystals suitable for X-ray structural analysis of PNPC complex **4**. However, NMR measurements suggest the formation of the assigned structure (see Scheme 2 for numbering of carbon atoms). The chemical shift of C20 (^{13}C NMR: 157.1 ppm) and H20 (^1H NMR: 7.27 ppm) suggests the coordination of the terminal carbon to the metal center and the presence of a double bond to C19 (^{13}C NMR: C19: 124.5 ppm, ^1H NMR: H19: 5.45 ppm). The chemical shift of C18 (^{13}C NMR: 64.5 ppm) and H18 (^1H NMR: 2.69 ppm) can be assigned to the NCH_2 fragment. C20 is coordinated to Ru1. Splitting pattern and coupling constants further support the assigned structure.

Furthermore, the protected ligand **1′** was used to synthesize ruthenium PNP complex **5** in 42% yield (Scheme 3). Here, the formation of the *cis*- and *trans*-isomers could be observed. The deprotection of **5** yielded an unknown main product whose structural elucidation was not possible. Moreover, **5**-*trans* is computed to be more stable than **5**-*cis* by 1.25 kcal/mol, corresponding to an expected ratio of 89:11, close to the determined 81:19.

To get further insights into the formation of the complexes, DFT calculations were performed using B3PW91/TZVP for full structural optimization and energy calculations (Figure 5). During the complex synthesis, the triple bond of ligand **1** is partially reduced by the hydrido ligand of the metal precursor, enabling the coordination of one carbon atom to the metal center. This reaction is strongly exergonic with ΔG of roughly −30 kcal/mol (Figure 5, difference between **6** and **4**, **7**). Subsequent isomerization of the double bond leads to the formation of **2** and **3**. In addition, the exocyclic isomer **7** is much less stable than the endocyclic isomers. Hence, its experimental observation was not possible. The difference in Gibbs free energy between **2** and **3** of 0.96 kcal/mol corresponds to a ratio of 17:83. Experimentally, a ratio of 41:59 was found (determined by NMR).

ChemCatChem
Research Article
doi.org/10.1002/cctc.202401481
Chemistry Europe
European Chemical Societies Publishing

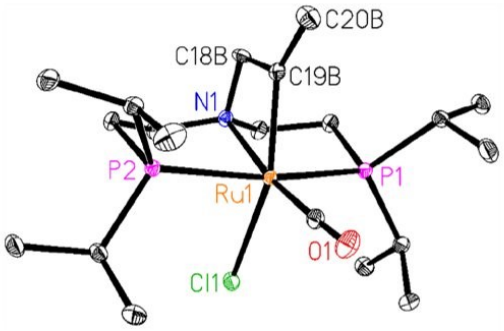

Figure 3. Crystal structure of the mixed crystal of **2** and **3**, showing only the former complex. Therefore, atoms with the suffix A are omitted. Displacement ellipsoids are drawn at 30% probability at 110 K. Hydrogen atoms are omitted for clarity.

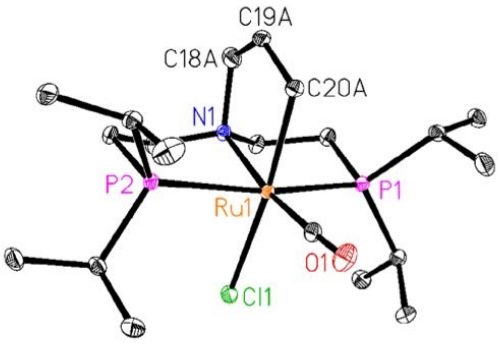

Figure 4. Crystal structure of the mixed crystal of **2** and **3**, showing only the latter complex. Therefore, atoms with suffix B are omitted. Displacement ellipsoids are drawn at 30% probability at 110 K. Hydrogen atoms are omitted for clarity.

Since the synthesis of the mixture of PNPC complexes **2** and **3** showed the highest yield and good selectivity, we decided to further investigate this mixture as catalysts. To enable the use in base-free reactions, they were transformed into the hydrido PNPC complexes **8** and **9** in 33% yield utilizing $NaBHEt_3$, whilst retaining the isomeric ratio between both structures (Scheme 4).

2.2. Catalytic Applications

2.2.1. Dehydrogenation Reactions

As mentioned above, PNP-pincer metal complexes have been well established in many dehydrogenation reactions.[9d,11,14a,33] Thus, having the PNPC pincer hydride complexes **8** and **9** in hand, their performance in additive-free formic acid dehydrogenation was investigated. This reaction is of general interest as part of hydrogen storage technologies.[14b,c,34] In a previous publication, some of us showed that in formic acid dehydrogenation base concentration has no significant influence on activity below a certain threshold.[35] Indeed, similar activity and productivity were observed between a mixture of PNPC complexes **8** and **9** (Table 1, entry 2, TOF: 598 h^{-1}, TON: 1610) and the activated PNPC complexes **2** and **3** (Table 1, entry 1, TOF: 540 h^{-1}, TON: 1500). Additionally, similar activities for PNP complexes **10** and **11** were observed, compared to the literature.[35] As expected, catalyst **11** showed the highest turnover number (Table 1, entry 4, TON: 1727) of the known catalysts in the literature. To our delight, with the new complex mixture of **8** and **9**, the activity and productivity were very similar (Table 1, entry 2, TOF: 598 h^{-1}, TON: 1610). Furthermore, PNPC complexes **8** and **9** were shown to be active in additive-free methanol dehydrogenation. However, in this latter case, poor reproducibility was observed (Table S5).

2.2.2. Transfer (De)Hydrogenation of Organic Compounds

After observing good activity in dehydrogenation reactions, we decided to investigate transfer dehydrogenation and transfer hydrogenation reactions. In general, both ruthenium PCP- and PNP-pincer complexes are known to be appropriate transfer hydrogenation catalysts.[36] Therefore, good activity can be expected for the novel PNPC complexes.

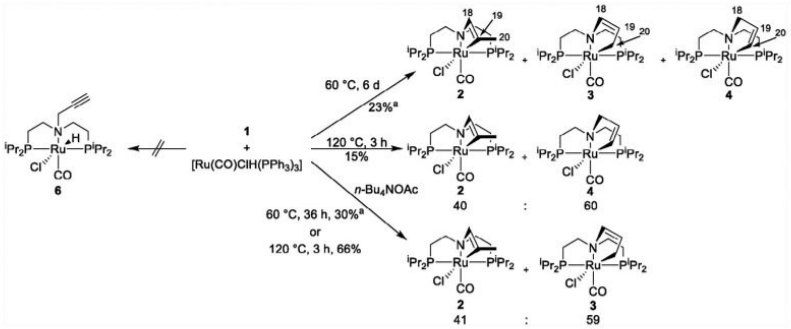

Scheme 2. Synthesis of different ruthenium-PNPC complexes using ligand **1**. [a] Yield determined by ^{31}P NMR.

ChemCatChem
Research Article
doi.org/10.1002/cctc.202401481
Chemistry Europe
European Chemical Societies Publishing

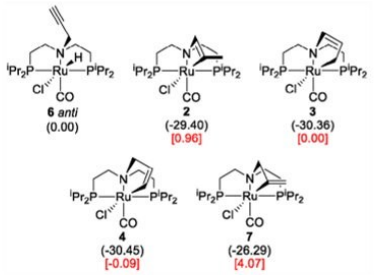

Figure 5. Calculated relative Gibbs free energy (ΔG, kcal/mol) of different ruthenium-PNPC complexes **2**–**4**, **6**, and **7**.

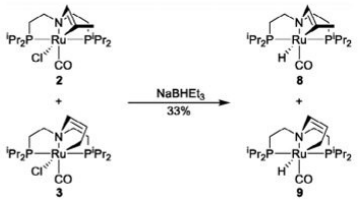

Scheme 4. Synthesis of hydrido PNPC complexes **8** and **9**.

Table 1. Additive-free formic acid dehydrogenation of PNPC complexes **8** and **9** and their comparison to state-of-the-art PNP-pincer complexes.[a]

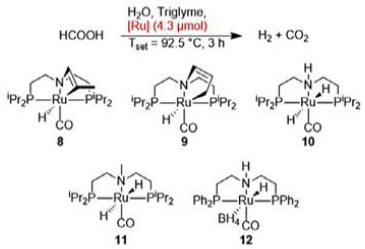

Entry	Catalyst	TOF_{1h} (h^{-1})	TON_{3h}	CO Content (ppm)
1[b]	**2** + **3**	540	1500	3
2	**8** + **9**	598	1610	<1
3	**10**	378	1035	4
4	**11**	584	1727	2
5	**12**	415	1275	3

Reaction conditions:
[a]Formic acid (32 mmol, 1.2 mL), H_2O (8.8 mL), triglyme (4 mL), catalyst (4.3 µmol), 92.5 °C. Reactions were performed at least twice with a standard deviation < 15%, except for entry 3.
[b]The complex was activated with 1.6 equiv of KOH prior to the reaction.

First, the transfer dehydrogenation of 1-phenylethanol to acetophenone was evaluated (Scheme 5). Since the reactions were performed in the presence of base, PNPC complexes **2** + **3** were utilized as the precatalysts. When performing this reaction in THF/acetone (1:1), after 4.5 h, the substrate showed almost 50% conversion and 44% yield (Scheme 5a). Extending the reaction time to 72 h led to full conversion and 92% yield (Scheme 5b). For Ru-MACHO, 98% yield was already achieved after 4.5 h (Scheme 5c). In all cases, the main byproducts were related to the expected aldol addition (4-hydroxypentan-2-one) and condensation (pent-3-en-2-one) reactions. Notably, the presence of the hydrogen acceptor is essential, as the catalyst mixture was also tested in pure THF in an open system (Scheme 5d). After 16 h, almost no product formation was observed.

Reaction conditions: Substrate: 0.25 mmol; (a, b, c) THF/acetone 1:1 (10 mL); (d) THF (10 mL). Yields were determined by GC-FID analysis using hexadecane as an internal standard. Conversions are provided in Table S3. Catalyst concentration is reported as the amount of complex mixture employed. Equivalents refer to the substrate.

Having observed good catalytic activity, the focus was switched to the transfer hydrogenation of benchmark unsaturated organic molecules. The tests involved common functional groups such as ketones, alkenes, and alkynes (Scheme 6), using conditions reported in the literature.[25,37] When using ^{i}PrOH as the hydrogen source, both aromatic and aliphatic ketones (Scheme 6a,b) were hydrogenated in quantitative yields within short reaction times (≤4 h). These observed results are similar compared to the Ru-MACHO catalyst under the same conditions (Figure S6). Comparing both catalysts at a shorter reaction time (15 min), the classical Ru-MACHO, however, outperformed the new Ru-PNPC system (Figure S7).

Reaction conditions: (a and b) Substrate: 0.25 mmol, ^{i}PrOH (10 mL); (c) substrate: 0.25 mmol, MeOH (2 mL); (d) substrate: 0.25 mmol, MeOH/H_2O 2:1 (2 mL). Yields were determined by GC-FID analysis using hexadecane as an internal standard. Conversions are provided in Table S2. Catalyst concentration is reported as the amount of complex mixture employed. Equivalents refer to the substrate.

Having detected activity in methanol dehydrogenation, its use as a hydrogen source in the transfer hydrogenation of unsaturated aliphatic compounds became of interest. Testing the catalyst using diphenylacetylene (Scheme 6c) mainly produced

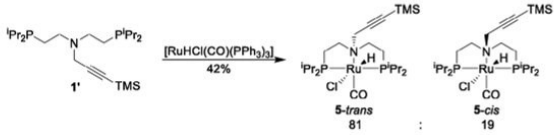

Scheme 3. Synthesis of PNP complex **5**. The *trans*- and *cis*-isomers were observed in an 81:19 ratio (determined by ^{1}H NMR, assigned by NOESY measurement).

ChemCatChem
Research Article
doi.org/10.1002/cctc.202401481
Chemistry Europe
European Chemical Societies Publishing

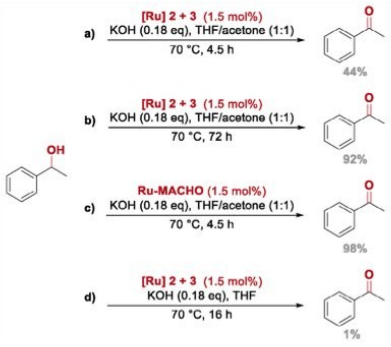

Scheme 5. Transfer dehydrogenation of 1-phenylethanol.

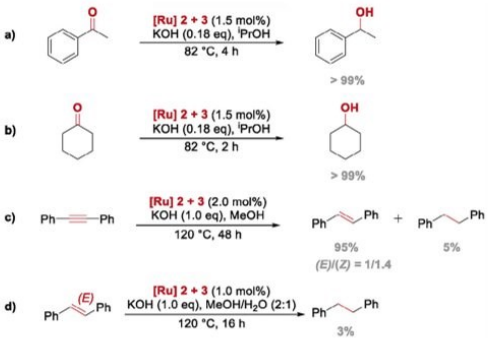

Scheme 6. Transfer hydrogenations of benchmark substrates utilizing a mixture of Ru complexes **2** and **3**.

the internal olefin (95%), with the (*Z*) isomer slightly favored over the (*E*) isomer (*E*/*Z* = 1/1.4). This selective behavior was also reported for Ru-MACHO by Subaramanian et al. under the same reaction conditions.[23] Here, the stereoselectivity was considerably better, as the reaction produced mainly the (*E*) isomer. However, while the use of Ru-PNPC led to the formation of only 5% of the over-reduced product after 48 h, Ru-MACHO yielded 10% after just 12 h. Further evidence of the improved chemoselectivity of the novel system over the Ru-PNP system was provided by an additional experiment. When applying the optimized conditions for the reduction of alkenes described by the same group,[23] it was revealed that (*E*)-stilbene (Scheme 6d) was practically not hydrogenated after 16 h. Diazobenzene and methyl benzoate were also tested under previously reported conditions, but with no success (Figure S8).

2.2.3. Mechanistic Investigations

Having observed good catalytic activity in various (de)hydrogenation reactions, we became interested in elucidating the reaction mechanism of this novel class of catalysts. In this respect, especially the stability of the cyclometalated com-

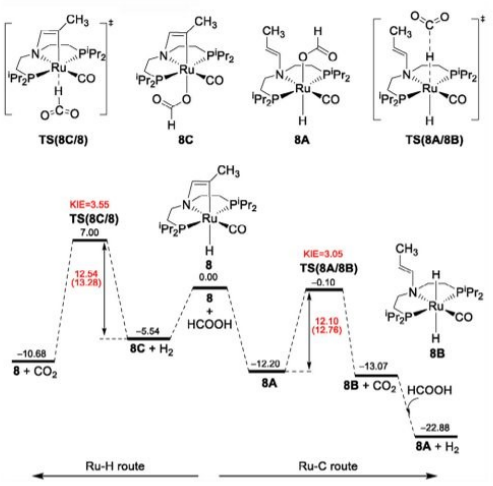

Figure 6. Ru-H (left) and Ru-C (right) routes for the dehydrogenation of formic acid with complex **8**. Relative Gibbs free energies are given in kcal/mol.

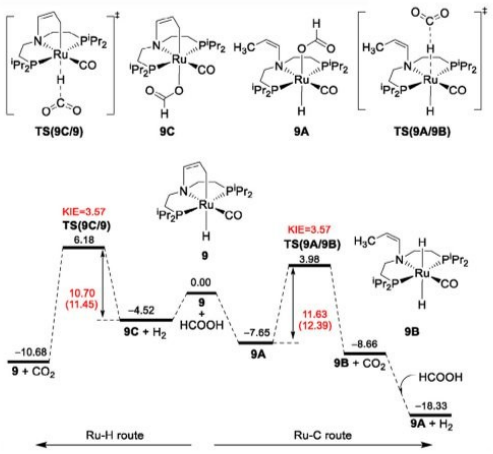

Figure 7. Ru-H (left) and Ru-C (right) routes for the dehydrogenation of formic acid with complex **9**. Relative Gibbs free energies are given in kcal/mol.

plexes is of interest. Focusing on formic acid dehydrogenation, a reaction via an inner sphere mechanism can be expected due to the tertial amine backbone, as postulated earlier on.[38] In general, two different reaction pathways utilizing this mechanism are possible. Both were calculated for PNPC complexes **8** and **9** by DFT (Figures 6 and 7). In the first route (Ru-C route, Ru—C bond cleavage), the reaction starts with the formal metathesis of the Ru—C bond with the O—H bond of formic acid resulting, in the hydrido formate complex (**8A** and **9A**), followed by CO_2 release and the formation of the dihydrido complex (**8B** and

ChemCatChem
Research Article
doi.org/10.1002/cctc.202401481
Chemistry Europe
European Chemical Societies Publishing

9B). In the second route (Ru-H route, Ru-C remaining intact), the formal acid and base reaction between formic acid and the hydrido ligand in **8** and **9** results in the formate complex (**8C** and **9C**) and the release of H_2. It is noted that complexes **8** and **9** are isoenergetic computationally, and this enables a direct comparison of their activity.

For complex **8** (Figure 6), the Ru-C route (**8** to **8A**) is energetically more favored (−12.20 kcal/mol) than the Ru-H route (**8** to **8C** + H_2, −5.54 kcal/mol), indicating that the Ru-C breaking is more favored thermodynamically than Ru-H breaking by 6.66 kcal/mol.

Starting from intermediate **8A**, CO_2 elimination via the C—H activation (**TS(8A/8B)**), resulting in the formation of the dihydrido complex **8B**, has a Gibbs free energy barrier of 12.10 kcal/mol and is exergonic by 0.87 kcal/mol. The subsequent regeneration of **8A** with one equivalent formic acid and the release of one equivalent H_2 is exergonic by 9.81 kcal/mol. Starting from intermediate **8C**, the CO_2 elimination via the C—H activation (**TS(8C/8)**) resulting in the regeneration of **8B** has a Gibbs free energy barrier of 12.54 kcal/mol and is exergonic by 5.14 kcal/mol. Considering both routes independently, they have close Gibbs free energy barriers (12.10 and 12.54 kcal/mol, respectively). Considering the stability of **8A** and **8C**, however, the Ru-C route via dihydrido complex **8B** should be more favorable based on the Curtin-Hammett principle.

Similar results have been found for complex **9** (Figure 7). For example, the formation of complex **9A** is more favored thermodynamically than that of complex **9C** (−7.65 vs. −4.52 kcal/mol). Starting from **9A**, the C—H activation (**TS(9A/9B)**) has a Gibbs free energy barrier of 11.63 kcal/mol and is slightly exergonic by 1.01 kcal/mol for the formation of the dihydrido complex **9B** and the release of CO_2. Starting from **9C**, CO_2 release and the regeneration of **9** have a Gibbs free energy barrier of 10.70 kcal/mol and are exergonic by 6.16 kcal/mol.

Considering both routes independently for complexes **8** and **9**, they have close Gibbs free energy barriers (12.10/11.63 and 12.54/10.70 kcal/mol, respectively). Taking into account the stability of **8A/9A** and **8C/9C**, however, the Ru-C route via dihydrido complex **8B/9B** should be more favorable based on the Curtin-Hammett principle. In addition, we also computed the kinetic isotopic effect (KIE) for deuterated formic acid (DCOOH) and found KIE (3.05 and 3.57, respectively) for the Ru-C route for **8** and **9**.

To check a possible inner-sphere mechanism via β-hydride elimination based on the de-coordination of the phosphine ligand, the de-coordination of one phosphine ligand for **8** and **9** was computed. It is found that the de-coordination of one phosphine ligand costs over 29 kcal/mol, which is much higher than the apparent barriers for formic acid dehydrogenation. Therefore, this possible mechanism can simply be discarded.

To distinguish between both pathways, the reaction of a mixture of **8** and **9** with stoichiometric amounts of formic acid was performed. It was monitored by NMR. Overall, five major products were observed. After 6 h of reaction time, the formation of one product dominates the reaction. Based on the presence of a formate signal (^{1}H NMR: 9.02 (s) ppm), the absence of a hydride signal, and the chemical shift of the propylic protons and the phosphorus atoms (^{1}H NMR: 5.66 (dt, J = 5.1, 3.3 Hz), 4.39 (dt, J = 4.8, 2.3 Hz) ppm; ^{31}P NMR: 60.09 ppm), the structure of **9C** was assigned. The analytical data show similar characteristic signals as related formate PNP complex **15** (Scheme 7).[38] After keeping the reaction solution for 5 days at room temperature, the amount of **9C** decreased by 44%.

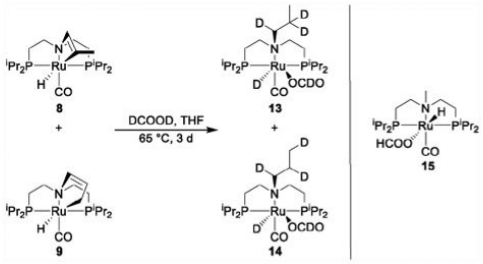

Scheme 7. Reaction of 8 + 9 with deuterated formic acid (left). Structure of complex **15** (right).

The other four major products form slowly over the course of the reaction and are most prominent after 5 days. They show similar signals in NMR, likely corresponding to four hydrido formate complexes (^{1}H NMR: 9.27 (s), 9.24 (s), 9.19 (s), 9.17 (s), −16.84 (t, J = 18.6 Hz), −16.90 (t, J = 18.2 Hz), −16.99 (t, J = 18.7 Hz), −17.17 (t, J = 18.8 Hz) ppm; ^{31}P NMR: 71.84, 71.14, 69.61, 69.37 ppm), matching with the chemical shift of **15**.[38] Hence, the structures of **8A**, **9A**, and the two corresponding *cis* orientated complexes (referring to the orientation of the propylic arm and the hydrido ligand) were assigned.

To confirm the presence of the Ru-C pathway, catalysis with deuterated formic acid (DCOOD) was performed (Scheme 7). In the presence of the Ru-C pathway, incorporation of deuterium into the propylene arm is expected. After reacting a catalyst solution with deuterated formic acid for 3 days at 65 °C, the reaction solution was analyzed by ^{2}H NMR. Similar to the reaction with stoichiometric amounts of formic acid, the presence of formate and hydride signals (^{2}H NMR: 8.43 (s, br), −17.19 (s, br) ppm), as well as the chemical shift of the phosphorus atoms (^{31}P NMR: 71.59, 69.69 ppm), indicate the formation of a hydrido formate complex. Furthermore, signals in the alkyl region were observed (^{2}H NMR: 3.60 (s, br), 2.79 (s, br), 1.76 (s, br), 1.55 (s, br), 1.28 (s, br), 0.75 (s, br) ppm) and, in combination with TOCSY and 2D-measurements, assigned to a propylic group. Therefore, the formation of **13** and **14** is likely.

Based on the DFT and experimental results, we assume that upon the addition of formic acid, the preferred formation of **8C** and **9C** should be kinetically controlled, and the subsequent formation of other products can be thermodynamically controlled. Consequently, in the beginning of the reaction, catalysis preferentially proceeds via the Ru-H route, and with ongoing time, the concentration of **8A** and **9A** increases, and the Ru-C pathway should become the dominant one.

ChemCatChem
Research Article
doi.org/10.1002/cctc.202401481
Chemistry Europe
European Chemical Societies Publishing

3. Conclusion

The reaction of ligand **1** with a suitable ruthenium precursor leads to a new subclass of organometallic pincer complexes. Here, the PNPC ligand coordinates with two phosphorus, one nitrogen, and one carbon atom to the metal center. The resulting complexes were characterized by a combination of NMR-spectroscopy and SC-XRD. The complexes were employed in base-free formic acid dehydrogenation as well as in transfer dehydrogenation and transfer hydrogenation reactions of organic molecules. Similar activities to other state-of-the-art pincer complexes were observed. Mechanistic investigations revealed two competing pathways for the dehydrogenation of formic acid either, with or without Ru–C bond cleavage. Both pathways are proceeding at different times of the reaction.

4. Experimental Section

4.1. General Methods

Column chromatography was performed under a protective gas atmosphere with silica by Macherey-Nagel MN Kieselgel 60 (0.04–0.063 mm). The column was filled dry. Solvent mixtures are reported in volume percent. TLCs were performed using Merck TLC-plates with fluorescence indicators (silica gel 60, F_{254}). A 1% $KMnO_4$ solution was used as a coloring agent.

NMR spectra were recorded at room temperature at one of the following devices: 300 MHz (Bruker AV-III 300), 300 MHz (Bruker AV-III HD 300), or 400 MHz (Bruker AV-III HD 400). ^{31}P spectra were recorded at 122 MHz and 162 MHz. ^{13}C spectra were recorded at 75 MHz and 101 MHz. Chemical shift is reported in the δ-scale. The resonance signal of the remaining protons of the solvent was used as an internal standard. For ^{13}C spectra, the resonance signal of the carbon atom of the solvent was used. The following abbreviations were used to describe the signals: s = singlet, d = doublet, t = triplet, q = quartet, qint. = quintet, sept. = septet, m = multiplet, br = broad. The coupling constant *J* is reported in Hz.

GC analysis for the transfer hydrogenation of organic molecules was performed on a HP 6890 Series chromatograph, equipped with a HP-5 column (30 m x 250 um x 0.25 um) and flame-ionization detector. GC-MS spectra were recorded on an Agilent 7890A with an 5975C inert XL MSD mass detector.

Diffraction data were collected on a Bruker Kappa APEX II Duo diffractometer. The structures were solved by direct methods[39] and refined by full-matrix least-squares procedures on F^2.[40] XP (Bruker AXS) was used for graphical representations.

CCDC 2378636 contains the supplementary crystallographic data for this paper. These data are provided free of charge by the joint Cambridge Crystallographic Data Centre and Fachinformationszentrum Karlsruhe Access Structures service, www.ccdc.cam.ac.uk/structures.

All experiments were carried out under an inert gas atmosphere (Ar) using standard Schlenk (and glovebox) techniques. Triglyme, formic acid, and water were degassed by bubbling argon for 1 h. Formic acid was distilled before use. Other solvents and liquid reagents were dried and degassed with a solvent purification system (SPS) or according to literature[41] and stored on molecular sieves (3 Å) under argon atmosphere. Chemicals and catalysts **10** were purchased from chemical companies and used without further purification. Catalyst **11** was synthesized according to literature procedures.[38] All catalysts and air sensitive compounds were stored under an argon atmosphere.

The choice of the computational methods was based on our previous study on the stepwise steam reforming of methanol (CH_3OH) to carbon dioxide (CO_2) and hydrogen (H_2) via methanol dehydrogenation to formaldehyde [$CH_3OH = CH_2O + H_2$], methanediol [$CH_2O + H_2O = CH_2(OH)_2$] and formic acid [$CH_2(OH)_2 = HCOOH + H_2$] and finally to CO_2 and H_2 [$HCOO = CO_2 + H_2$] by using the standard Ru-PN^{H}P complex (also complex **10** in current work for testing).[38] It has been found that among several functionals along with solvent and van der Waals dispersion correction (B3PW91, B3LYP, BP86, and M06), the B3PW91 functional can best and quantitatively reproduce the experimentally observed kinetics and thermodynamics, while other methods, including dispersion and solvation corrections, either overestimate the activation barriers or the reaction energies. Especially, benchmark calculations for the reaction of $HCOOH = CO_2 + H_2$ show the B3PW91 computed reaction enthalpy and reaction free energy (−3.86 and −10.68 kcal/mol, respectively) are in perfect agreement with the experimental values (−3.56 and −10.39 kcal/mol, respectively). For the reaction of $CH_3OH = CH_2O + H_2$, the B3PW91 computed reaction enthalpy of 21.62 kcal/mol is also in perfect agreement with the experimental value (21.29 ± 2.39 kcal/mol). These agreements also validate the B3PW91 method to be reasonable.

All calculations were carried out by using the Gaussian 16 program.[42] All structures were optimized at the B3PW91[43] level of DFT with the TZVP[44] basis set (LANL2DZ for Ru[45]). Each optimized structure was characterized either as an energy minimum without imaginary frequencies or a transition state with only one imaginary frequency by frequency calculations, and the imaginary model connects the initial and final states. The thermal corrections to Gibbs free energy at 298 K from the frequency analysis are added to the total electronic energy, and we therefore used the corrected Gibbs free energy (ΔG) at 298 K for our energetic discussion and comparison.

4.2. Complex Synthesis

4.2.1. Synthesis of a mixture of complexes 2 and 4

In a Young-NMR tube, to a solution of ligand **1** (60.0 mg, 175 µmol, 1.00 equiv) in toluene (0.5 mL) and C_6D_6 (0.15 mL), [Ru(CO)ClH(PPh_3)$_3$] (166 mg, 175 µmol, 1.00 equiv) was added. The reaction mixture was heated at 120 °C for 3 h without stirring. After cooling to room temperature, the product mixture was purified by column chromatography (Pentane/EtOAc 8:2 → 1:1).

Yield: 15% (13.6 mg, 26.7 µmol) of a 2:3 mixture of complexes **2** and **4**.

4.2.2. Synthesis of a mixture of complexes 2 and 3

To a solution of ligand **1** (0.970 g, 2.82 mmol, 1.00 equiv) in toluene (45 mL), [Ru(CO)ClH(PPh_3)$_3$] (4.57 g, 4.80 mmol, 1.70 equiv), and *n*-Bu_4NOAc (1.00 g, 3.33 mmol, 1.18 equiv) were added. The reaction mixture was refluxed at 120 °C for 3 h. After cooling to room temperature, the crude product was purified by column chromatography (Pentane/EtOAc: 8:2 → 1:1) yielding a light brown 41:59 mixture of complexes **2** and **3**.

Yield: 66% (949 mg, 1.86 mmol)

ESI-HRMS (m/z pos): Calculated for [$C_{20}H_{40}NOP_2RuCl$]: 509.1317; found: 474.1636 [M-Cl]$^+$.

Crystals suitable for X-ray analysis were grown from a concentrated solution of **2** and **3** in ethyl acetate. Complexes **2** and **3** crystallized as mixed crystals, where these two complexes overlayed each other in a ratio of 1:1. SADI instruction was used to equalize

ChemCatChem
Research Article
doi.org/10.1002/cctc.202401481
Chemistry Europe
European Chemical Societies Publishing

the bond lengths N1-C18A and N1-C18B. The anisotropic displacement parameters of C18A and C18B, as well as C19B and C20B, were restrained to be equal (EADP). Crystal data of the mixed crystals of **2** + **3**: $C_{20}H_{40}ClNOP_2Ru$, $M = 508.99$, monoclinic, space group $P2_1/c$, $a = 14.643(3)$, $b = 12.355(2)$, $c = 14.618(3)$ Å, $\beta = 117.420(3)°$, $V = 2347.4(7)$ Å^3, $T = 110(2)$ K, $Z = 4$, 60417 reflections measured, 6857 independent reflections ($R_{int} = 0.0509$), final R values ($I > 2\sigma(I)$): $R_1 = 0.0282$, $wR_2 = 0.0641$, final R values (all data): $R_1 = 0.0387$, $wR_2 = 0.0699$, 259 parameters.

4.2.3. NMR data

Since the signals of the ^{i}Pr- and the CH_2-groups of both complexes overlap, integration and assignment of those groups remain ambiguous.

Complex 2:

^{1}H NMR (400 MHz, C_6D_6) $\delta = 4.98$ (q, $J = 2.0$ Hz, 1H), 3.68–3.57 (m, 2H), 3.15–3.04 (m, 2H), 3.00–2.78 (m, 2H), 2.36–2.11 (m, 4H), 1.87 (q, $J = 1.5$ Hz, 3H), 1.82–1.67 (m, 2H), 1.67–1.55 (m, 6H), 1.44–1.32 (m, 6H), 1.21 (q, $J = 7.4$ Hz, 6H), 1.00–0.92 (m, 6H) ppm.

^{31}P NMR (162 MHz, C_6D_6) $\delta = 59.40$ ppm.

^{13}C NMR (101 MHz, C_6D_6) $\delta = 210.4$, 208.9, 160.0, 120.3, 56.9, 53.2, 29.2, 25.8, 24.6, 24.3, 23.8, 22.7, 22.7, 21.0, 20.8, 20.7, 20.1, 19.9, 18.6, 17.9 ppm.

Complex 3:

^{1}H NMR (400 MHz, C_6D_6) $\delta = 5.70$ (dt, $J = 5.0$, 3.2 Hz, 1H), 4.45 (dt, $J = 4.8$, 2.2 Hz, 1H), 3.68–3.57 (m, 2H), 3.15–3.04 (m, 2H), 3.00–2.78 (m, 2H), 2.36–2.11 (m, 4H), 1.82–1.67 (m, 2H), 1.67–1.55 (m, 8H), 1.44–1.32 (m, 6H), 1.21 (q, $J = 7.4$ Hz, 6H), 1.00–0.92 (m, 6H) ppm.

^{31}P NMR (162 MHz, C_6D_6) $\delta = 59.46$ ppm.

^{13}C NMR (101 MHz, C_6D_6) $\delta = 210.4$, 208.9, 141.2, 137.1, 56.9, 53.2, 29.2, 25.8, 24.6, 24.3, 22.7, 22.7, 21.0, 20.8, 20.7, 20.1, 19.9, 18.6, 17.9, 10.0 ppm.

Complex 4:

^{1}H NMR (300 MHz, C_6D_6) $\delta = 7.27$ (dsept., $J = 9.1$, 1.0 Hz, 1H), 5.45 (dquint., $J = 9.1$, 2.2 Hz, 1H), 3.75–3.61 (m, 2H), 2.99–2.80 (m, 2H), 2.69 (quint., $J = 2.3$ Hz, 2H), 2.31–2.03 (m, 4H), 1.80–1.66 (m, 2H), 1.66–1.55 (m, 6H), 1.48–1.26 (m, 14H), 1.26–1.16 (m, 6H), 1.02–0.88 (m, 6H) ppm.

^{31}P NMR (122 MHz, C_6D_6) $\delta = 62.92$ ppm.

^{13}C NMR (75 MHz, C_6D_6) $\delta = 157.1$, 124.5 (t, $J = 3.3$ Hz), 64.5, 60.0 (t, $J = 5.8$ Hz), 53.1, 32.3, 30.3–30.1 (m), 29.9, 29.3 (t, $J = 11.7$ Hz), 26.2 (t, $J = 7.8$ Hz), 25.8 (t, $J = 11.8$ Hz), 24.5 (t, $J = 8.8$ Hz), 23.4–22.9 (m), 22.7 (d, $J = 10.1$ Hz), 21.0, 20.9–20.6 (m), 20.1–19.8 (m), 19.5, 18.7–18.5 (m).

4.2.4. Synthesis of a mixture of complex 5

To a solution of $[Ru(CO)ClH(PPh_3)_3]$ (952 mg, 1.00 mmol, 1.00 equiv) in toluene (10 mL), a solution of ligand **1′** (416 mg, 1.00 mmol, 1.00 equiv) in toluene (1 mL) was added. After refluxing at 120 °C for 3 h, the reaction mixture was cooled to room temperature and the solvent removed *in vacuo*. The crude product was purified by column chromatography (Pentane/EtOAc 9:1 → 0:1), yielding complex **5** as a light brown solid.

Yield: 42% (247 mg, 424 µmol)

A 19:81 mixture of *cis* and *trans* isomers was obtained by ^{1}H NMR.

ESI-HRMS (m/z pos): Calculated for $[C_{23}H_{48}NOP_2RuSiCl]$: 581.1712; found: 546.2022 $[M\text{-}Cl]^+$.

Major isomer (*trans*):

^{1}H NMR (300 MHz, C_6D_6) $\delta = 4.05$ (s, 2H), 3.31–3.07 (m, 2H), 2.76–2.60 (m, 2H), 2.08–1.93 (m, 2H), 1.93–1.80 (m, 2H), 1.64–1.53 (m, 8H), 1.54–1.43 (m, 2H), 1.22–1.11 (dt, $J = 8.9$, 6.9 Hz, 6H), 1.00–0.89 (m, 12H), 0.21 (s, 9H), −15.23 (t, $J = 17.9$ Hz, 1H), ppm.

^{31}P NMR (122 MHz, C_6D_6) $\delta = 70.24$ ppm.

^{13}C NMR (75 MHz, C_6D_6) $\delta = 207.6$, 99.2, 93.2, 59.9 (t, $J = 4.7$ Hz), 44.8, 27.8 (t, $J = 8.8$ Hz), 27.4 (t, $J = 10.8$ Hz), 24.9 (t, $J = 12.7$ Hz), 20.9–20.5 (m), 19.1, 17.2, 0.1 ppm.

The carbonyl group could only be observed in an HMBC spectrum. No signal is observed between hydride and CH_2-protons of the propargylic chain in an NOESY spectrum, indicating a *trans* orientation of these groups.

Minor isomer (*cis*):

^{1}H NMR (300 MHz, C_6D_6) $\delta = 3.58$ (s, 1H), 3.31–3.07 (m, 2H), 2.76–2.60 (m, 2H), 2.08–1.93 (m, 2H), 1.93–1.80 (m, 2H), 1.64–1.53 (m, 8H), 1.54–1.43 (m, 2H), 1.22–1.11 (dt, $J = 8.9$, 6.9 Hz, 6H), 1.00–0.89 (m, 12H), 0.18 (s, 9H), −15.27 (t, $J = 18.2$ Hz, 1H), ppm.

^{31}P NMR (122 MHz, C_6D_6) $\delta = 72.61$ ppm.

^{13}C NMR (75 MHz, C_6D_6) $\delta = 99.2$, 93.2, 59.9 (t, $J = 4.7$ Hz), 44.8, 27.8 (t, $J = 8.8$ Hz), 27.4 (t, $J = 10.8$ Hz), 24.9 (t, $J = 12.7$ Hz), 20.9–20.5 (m), 19.1, 17.2, −0.0 ppm.

A signal is observed between hydride and CH_2-protons of the propargylic chain in an NOESY spectrum, indicating a *cis* orientation of these groups.

4.2.5. Synthesis of a mixture of complexes 8 and 9

To a solution of complexes **2** and **3** (255 mg, 0.500 mmol, 1.00 equiv) in toluene (25 mL), $NaBHEt_3$ (0.6 mL of a 1 M solution on toluene, 0.600 mmol, 1.20 equiv) was added. The reaction solution was stirred for 18 h at RT and filtered over celite. After removal of the solvent *in vacuo*, a mixture of complexes **8** and **9** was obtained as a light brown solid.

Yield: 33% (77.3 mg, 163 µmol)

ESI-HRMS (m/z pos): Calculated for $[C_{20}H_{41}NOP_2Ru]$: 475.1707; found: 474.1633 $[M - H]^+$.

Since the signals of the ^{i}Pr- and the CH_2-groups of both complexes overlap, integration and assignment of those groups remain ambiguous. Upon prolonged storage at RT complex **8** very slowly converts into **9**.

NMR data of complex **8**:

^{1}H NMR (300 MHz, C_6D_6) $\delta = 5.47$–5.41 (m, 1H), 2.51–2.34 (m, 5H), 2.32–1.80 (m, 10H), 1.55–1.39 (m, 6H), 1.39–1.13 (m, 12H), 1.13–1.03 (m, 6H), 1.00–0.91 (m, 6H), −8.93 (t, $J = 19.5$ Hz, 1H) ppm.

^{31}P NMR (162 MHz, C_6D_6): $\delta = 78.84$ ppm.

^{13}C NMR (101 MHz, C_6D_6): $\delta = 211.5$, 168.1, 58.1, 31.1 (t, $J = 11.2$ Hz), 28.0 (t, $J = 9.0$ Hz), 24.9, 24.2 (t, $J = 12.1$ Hz), 21.4 (t, $J = 3.5$ Hz), 20.2 (t, $J = 4.3$ Hz), 18.6, 18.1 ppm.

NMR data of complex **9**:

^{1}H NMR (300 MHz, C_6D_6) $\delta = 6.40$ (td, $J = 4.3$, 3.2 Hz, 1H), 4.13 (dt, $J = 4.6$, 2.3 Hz, 1H), 2.51–2.34 (m, 2H), 2.32–1.80 (m, 12H), 1.55–1.39 (m, 6H), 1.39–1.13 (m, 12H), 1.00–0.91 (m, 6H), −7.51 (t, $J = 20.4$ Hz, 1H) ppm.

^{31}P NMR (162 MHz, C_6D_6): $\delta = 80.15$ ppm.

^{13}C NMR (101 MHz, C_6D_6): $\delta = 211.5$, 168.1, 58.1, 31.1 (t, $J = 11.2$ Hz), 28.0 (t, $J = 9.0$ Hz), 24.9, 24.2 (t, $J = 12.1$ Hz), 21.4 (t, $J = 3.5$ Hz), 20.2 (t, $J = 4.3$ Hz), 18.6, 18.1 ppm.

4.3. Formic Acid Dehydrogenation

A double-walled, thermostatically controlled reaction vessel is connected via a reflux condenser to a manual burette. The reaction vessel was repeatedly evacuated and purged with argon (three times). The valve for extraction of gas samples was closed, and another three evacuation and purge cycles were carried out. The burette was flushed with argon three times. After the addition of H_2O (8.8 mL), triglyme (3.8 mL for complexes **10** and **11**, otherwise 4 mL), and FA (32 mmol, 1.2 mL) under an argon stream, the reac-

ChemCatChem | Research Article doi.org/10.1002/cctc.202401481 | Chemistry Europe European Chemical Societies Publishing

tion vessel was brought to reaction temperature with a thermostat (a set temperature of 92.5 °C corresponds to a 90 °C internal temperature). Once the reaction temperature was reached, the setup was equilibrated for 20 min. The reaction was started for complexes **10** and **11** by addition of the catalyst stock solution (215 µL of a 20 mM solution in triglyme, 4.3 µmol). In the case of complexes **8** + **9** and **12**, the reaction was started by catalyst addition (4.3 µmol) with a teflon crucible under a slight argon stream. The evolved gas volume was measured at set time points. At the end of the reaction, a gas sample was taken for GC analysis. CO content was below 10 ppm. Reactions were reproduced at least twice with a standard deviation of <15%, except with complex **11**.

4.4. Transfer Dehydrogenation

A 25 mL Schlenk pressure tube with screw cap, together with a stirring bar, was transferred to a glovebox. Inside, precatalysts **2** + **3** mixture (2.0 mg, or 2.3 mg of Ru-MACHO, 1.5 mol%) and KOH (2.5 mg, 0.045 mmol, 0.18 equiv) were added. Outside the glovebox, 10 mL of acetone/THF 1:1 mixture (or pure THF) was added under argon flow, together with 1-phenylethanol (30.5 mg, 0.25 mmol, 1.00 equiv). The Schlenk tube was closed and placed inside a preheated oil bath (70 °C). Once the time had elapsed, the reaction was stopped by placing the flask inside an ice bath. Internal standard (hexadecane) was added, and the solution was analyzed by GC-FID.

4.5. Transfer Hydrogenation

A 25 mL Schlenk pressure tube with screw cap, together with a stirring bar, was transferred to a glovebox. Inside, 2.0 mg of precatalysts **2** + **3** mixture (or Ru-MACHO, 1–2 mol%) and KOH (0.18–1.00 equiv) were added. Outside the glovebox, 10 mL of ^{i}PrOH or 1.3 mL of MeOH and 0.7 mL of H_2O were added under argon flow, together with the substrate (0.25 mmol, 1.00 equiv). The Schlenk tube was closed and placed inside a preheated oil bath (82 or 120 °C). Once the desired reaction time had elapsed, the reaction was stopped by placing the flask inside an ice bath. Internal standard (hexadecane) was added, and the solution was analyzed by GC-FID.

4.6. Stoichiometric Reaction with Formic Acid

In a Young-NMR tube, to a solution of **8** + **9** (24.8 mg, 52.3 µmol, 1.00 equiv) in C_6D_6, formic acid (2.40 µL, 63.6 µmol, 1.20 equiv) was added. After 6 h and 5 days, the reaction was analyzed by NMR. GC-analysis of the headspace revealed the formation of trace amounts of H_2 and CO_2.

4.7. Reaction with Deuterated Formic Acid

In a pressure tube, to a solution of **8** + **9** (10.2 mg, 20.0 µmol, 1.00 equiv) in THF (1 mL), formic acid d_2 (37.7 µL, 1.00 mmol, 50.0 equiv) was added. The reaction mixture was stirred at 65 °C for 3 days and subsequently analyzed by NMR.

Supporting Information

The Supporting Information contains all experimental methods, analytical data, and computational information.

Acknowledgments

This work was funded by the German Federal Ministry for Economic Affairs and Climate Action within the project "MEGA" (FKZ: 03EN5006A). The authors thank Anja Kammer for analytical support and valuable discussions, as well as Mahmoud Kanaan for experimental assistance.

Open access funding enabled and organized by Projekt DEAL.

Conflict of Interests

The authors declare no conflict of interest.

Data Availability Statement

The data that support the findings of this study are available in theSupporting Information of this article.

Keywords: Computational chemistry · Dehydrogenation · Homogeneous catalysis · Ruthenium-pincer complex · Transfer hydrogenation

[1] K. C. Nicolaou, S. Rigol, *J. Antibiot.* **2018**, *71*, 153–184.
[2] M. van Dijk, T. Morley, M. L. Rau, Y. Saghai, *Nat. Food* **2021**, *2*, 494–501.
[3] Department for International Development, Growth: Building Jobs and Prosperity in Developing Countries, United Kingdom 2008.
[4] a) M. Barreiro-Gen, *Decent Work and Economic Growth* (Eds: W. Leal Filho, A. M. Azul, L. Brandli, P. G. Özuyar, T. Wall), Springer, Cham **2019**, pp. 1–15; b) P. Conceição, Human Development Report 2023/2024, United Nations Development Programme, New York 2024.
[5] World Population Prospects 2019, I: Comprehensive Tables, United Nations Department of Economic and Social Affairs Population Division, New York 2019.
[6] a) J. Wisniak, *Educ. Quím.* **2010**, *21*, 60–69; b) R. van Santen, *Catalysis: From Principles to Applications*, 1st ed., Wiley-VCH, Weinheim, Germany **2012**.
[7] J. Kumawat, V. K. Gupta, *Polym. Chem.* **2020**, *11*, 6107–6128.
[8] a) K. C. Nicolaou, *J. Org. Chem.* **2005**, *70*, 7007–7027; b) C. C. C. Johansson Seechurn, M. O. Kitching, T. J. Colacot, V. Snieckus, *Angew. Chem., Int. Ed.* **2012**, *51*, 5062–5085.
[9] a) D. Morales-Morales, *Pincer Compounds: Chemistry and Applications*, Elsevier, Amsterdam **2018**; b) K. J. Szabó, O. F. Wendt, *Pincer and Pincer-Type Complexes: Applications in Organic Synthesis and Catalysis*, Wiley-VCH, Weinheim **2014**; c) G. van Koten, R. A. Gossage, *The Privileged Pincer-Metal Platform: Coordination Chemistry & Applications*, Springer, Cham, Switzerland **2016**; d) L. Piccirilli, D. L. J. Pinheiro, M. Nielsen, *CatalystsCatalysts* **2020**, *10*, 773.
[10] H. A. Younus, N. Ahmad, W. Su, F. Verpoort, *Coord. Chem. Rev.* **2014**, *276*, 112–152.
[11] F. Kallmeier, R. Kempe, *Angew. Chem., Int. Ed.* **2018**, *57*, 46–60.
[12] a) W. H. Wang, Y. Himeda, J. T. Muckerman, G. F. Manbeck, E. Fujita, *Chem. Rev.* **2015**, *115*, 12936–12973; b) D. Wang, D. Astruc, *Chem. Rev.* **2015**, *115*, 6621–6686; c) S. T. Bai, G. De Smet, Y. Liao, R. Sun, C. Zhou, M. Beller, B. U. W. Maes, B. F. Sels, *Chem. Soc. Rev.* **2021**, *50*, 4259–4298; d) H. A. Younus, W. Su, N. Ahmad, S. Chen, F. Verpoort, *Adv. Syn. Catal.* **2015**, *357*, 283–330; e) C. Gunanathan, D. Milstein, *Chem. Rev.* **2014**, *114*, 12024–12087.
[13] C. Gunanathan, D. Milstein, *Science* **2013**, *341*, 1229712.
[14] a) A. Kumar, P. Daw, D. Milstein, *Chem. Rev.* **2022**, *122*, 385–441; b) J. Eppinger, K.-W. Huang, *ACS Energy Lett.* **2017**, *2*, 188–195; c) D. Mellmann, P. Sponholz, H. Junge, M. Beller, *Chem. Soc. Rev.* **2016**, *45*, 3954–3988.

ChemCatChem
Research Article
doi.org/10.1002/cctc.202401481
Chemistry Europe
European Chemical Societies Publishing

[15] M. Trincado, D. Banerjee, H. Grützmacher, *Energy Environ. Sci.* **2014**, *7*, 2464–2503.
[16] K. Abdur-Rashid, D. G. Goussev, WO/2004/096735, **2004**.
[17] W. Kuriyama, T. Matsumoto, O. Ogata, Y. Ino, K. Aoki, S. Tanaka, K. Ishida, T. Kobayashi, N. Sayo, T. Saito, *Org. Process. Res. Dev.* **2012**, *16*, 166–171.
[18] B. Gnanaprakasam, J. Zhang, D. Milstein, *Angew. Chem., Int. Ed.* **2010**, *49*, 1468–1471.
[19] G. A. Filonenko, R. van Putten, E. N. Schulpen, E. J. M. Hensen, E. A. Pidko, *ChemCatChem* **2014**, *6*, 1526–1530.
[20] D. Benito-Garagorri, E. Becker, J. Wiedermann, W. Lackner, M. Pollak, K. Mereiter, J. Kisala, K. Kirchner, *Organometallics* **2006**, *25*, 1900–1913.
[21] a) L.-P. He, T. Chen, D.-X. Xue, M. Eddaoudi, K.-W. Huang, *J. Organomet. Chem.* **2012**, *700*, 202–206; b) L.-P. He, T. Chen, D. Gong, Z. Lai, K.-W. Huang, *Organometallics* **2012**, *31*, 5208–5211; c) Y. Pan, C. L. Pan, Y. Zhang, H. Li, S. Min, X. Guo, B. Zheng, H. Chen, A. Anders, Z. Lai, J. Zheng, K. W. Huang, *Chem. Asian J.* **2016**, *11*, 1357–1360; d) M. D. Morton, B. Y. Tay, J. J. Q. Mah, A. J. P. White, J. D. Nobbs, M. van Meurs, G. J. P. Britovsek, *Inorg. Chem.* **2024**, *63*, 3393–3401.
[22] a) J. Luo, S. Kar, M. Rauch, M. Montag, Y. Ben-David, D. Milstein, *J. Am. Chem. Soc.* **2021**, *143*, 17284–17291; b) M. R. Jungfer, J. L. Schwarz, F. Rominger, T. Oeser, R. Paciello, A. S. K. Hashmi, T. Schaub, *ChemCatChem* **2024**, *16*, e202301588.
[23] a) S. Michlik, R. Kempe, *Nat. Chem.* **2013**, *5*, 140–144; b) S. Rösler, J. Obenauf, R. Kempe, *J. Am. Chem. Soc.* **2015**, *137*, 7998–8001; c) F. Freitag, T. Irrgang, R. Kempe, *J. Am. Chem. Soc.* **2019**, *141*, 11677–11685; d) F. Kallmeier, R. Fertig, T. Irrgang, R. Kempe, *Angew. Chem., Int. Ed.* **2020**, *59*, 11789–11793.
[24] a) G. Jia, H. M. Lee, H. P. Xia, I. D. Williams, *Organometallics* **1996**, *15*, 5453–5455; b) H. M. Lee, J. Yao, G. Jia, *Organometallics* **1997**, *16*, 3927–3933.
[25] a) P. Dani, T. Karlen, R. A. Gossage, S. Gladiali, G. van Koten, *Angew. Chem., Int. Ed.* **2000**, *39*, 743–745; b) H. P. Dijkstra, M. Albrecht, S. Medici, G. P. M. van Klink, G. van Koten, *Adv. Syn. Catal.* **2002**, *344*, 1135–1141; c) M. Gagliardo, P. A. Chase, S. Brouwer, G. P. M. van Klink, G. van Koten, *Organometallics* **2006**, *26*, 2219–2227.
[26] J. Takaya, J. F. Hartwig, *J. Am. Chem. Soc.* **2005**, *127*, 5756–5757.
[27] M. Otsuka, K. Endo, T. Shibata, *Chem. Commun.* **2010**, *46*, 336–338.
[28] a) S. Musa, L. Ackermann, D. Gelman, *Adv. Syn. Catal.* **2013**, *355*, 3077–3080; b) S. Musa, S. Fronton, L. Vaccaro, D. Gelman, *Organometallics* **2013**, *32*, 3069–3073; c) S. Musa, A. Ghosh, L. Vaccaro, L. Ackermann, D. Gelman, *Adv. Syn. Catal.* **2015**, *357*, 2351–2357.
[29] a) M. Nielsen, E. Alberico, W. Baumann, H. J. Drexler, H. Junge, S. Gladiali, M. Beller, *Nature* **2013**, *495*, 85–89; b) S. Elangovan, C. Topf, S. Fischer, H. Jiao, A. Spannenberg, W. Baumann, R. Ludwig, K. Junge, M. Beller, *J. Am. Chem. Soc.* **2016**, *138*, 8809–8814; c) H. A. Kempf, N. F. Both, C. A. M. Stein, A. Spannenberg, K. Junge, H. Junge, M. Beller, *Organometallics* **2024** *43*, 2450–2457.
[30] H. K. Lo, C. Copéret, *ChemCatChem* **2018**, *11*, 430–434.
[31] CCDC 2378636 contains the supplementary crystallographic data for this paper. These data are provided free of charge by the joint Cambridge Crystallographic Data Centre and Fachinformationszentrum Karlsruhe Access Structures service www.ccdc.cam.ac.uk/structures.
[32] a) P. Pyykkö, *J. Phys. Chem. A* **2015**, *119*, 2326–2337; b) F. H. Allen, O. Kennard, D. G. Watson, L. Brammer, A. G. Orpen, R. Taylor, *J. Chem. Soc. Perkin Trans. II* **1987**, S1–S19.
[33] K. Das, S. Waiba, A. Jana, B. Maji, *Chem. Soc. Rev.* **2022**, *51*, 4386–4464.
[34] I. Dutta, S. Chatterjee, H. Cheng, R. K. Parsapur, Z. Liu, Z. Li, E. Ye, H. Kawanami, J. S. C. Low, Z. Lai, X. J. Loh, K. W. Huang, *Adv. Energy Mater.* **2022**, *12*, 2103799.
[35] A. Agapova, E. Alberico, A. Kammer, H. Junge, M. Beller, *ChemCatChem* **2019**, *11*, 1910–1914.
[36] a) H. Schratzberger, B. Stoger, L. F. Veiros, K. Kirchner, *ACS Catal.* **2023**, *13*, 14012–14022; b) R. Padilla, Z. Ni, D. Mihrin, R. W. Larsen, M. Nielsen, *ChemCatChem* **2022**, *15*, e202200819.
[37] a) M. Subaramanian, G. Sivakumar, V. G. Landge, R. Kumar, K. Natte, R. V. Jagadeesh, E. Balaraman, *J. Catal.* **2023**, *425*, 386–405; b) A. G. Nair, R. T. McBurney, D. B. Walker, M. J. Page, M. R. Gatus, M. Bhadbhade, B. A. Messerle, *Dalton Trans.* **2016**, *45*, 14335–14342.
[38] E. Alberico, A. J. Lennox, L. K. Vogt, H. Jiao, W. Baumann, H. J. Drexler, M. Nielsen, A. Spannenberg, M. P. Checinski, H. Junge, M. Beller, *J. Am. Chem. Soc.* **2016**, *138*, 14890–14904.
[39] G. M. Sheldrick, *Acta Cryst.* **2008**, *A64*, 112–122.
[40] G. M. Sheldrick, *Acta Cryst.* **2015**, *C71*, 3–8.
[41] W. L. F. Armarego, C. Chai, *Purification of Laboratory Chemicals*, 6 ed., Butterworth-Heineman, Oxford, UK **2009**.
[42] M. J. Frisch, G. W. Trucks, H. B. Schlegel, G. E. Scuseria, M. A. Robb, J. R. Cheeseman, Scalmani, G., V. Barone, B. Mennucci, G. A. Petersson, H. Nakatsuji, M. Caricato, X. Li, H. P. Hratchian, A. F. Izmaylov, J. Bloino, G. Zheng, J. L. Sonnenberg, M. Hada, M. Ehara, K. Toyota, R. Fukuda, J. Hasegawa, M. Ishida, T. Nakajima, Y. Honda, O. Kitao, H. Nakai, T. Vreven, J. A. Montgomery Jr., J. E. Peralta, F. Ogliaro, M. Bearpark, J. J. Heyd, E. Brothers, K. N. Kudin, V. N. Staroverov, R. Kobayashi, J. Normand, K. Raghavachari, A. Rendell, J. C. Burant, S. S. Iyengar, J. Tomasi, M. Cossi, N. Rega, J. M. Millam, M. Klene, J. E. Knox, J. B. Cross, V. Bakken, C. Adamo, J. Jaramillo, R. Gomperts, R. E. Stratmann, O. Yazyev, A. J. Austin, R. Cammi, C. Pomelli, J. W. Ochterski, R. L. Martin, K. Morokuma, V. G. Zakrzewski, G. A. Voth, P. Salvador, J. J. Dannenberg, S. Dapprich, A. D. Daniels, Ö. Farkas, J. B. Foresman, J. V. Ortiz, J. Cioslowski, D. J. Fox, *Gaussian 09*, Revision D.01, Gaussian, Inc., Wallingford, CT, **2009**.
[43] A. D. Becke, *J. Chem. Phys.* **1993**, *98*, 5648–5652.
[44] A. Schaefer, C. Huber, R. Ahlrichs, *J. Chem. Phys.* **1994**, *100*, 5829–5835.
[45] P. J. Hay, W. R. Wadt, *J. Chem. Phys.* **1985**, *82*, 299–310.

Manuscript received: August 27, 2024
Revised manuscript received: October 08, 2024
Accepted manuscript online: October 27, 2024
Version of record online: ■■, ■■

6.2.3 Comparison of Low Temperature Methanol Aqueous Phase Reforming Catalysts - Definition of Standardized Reaction Conditions and Considerations toward Applications

Hendrik A. Kempf, Henrik Junge and Matthias Beller

ACS Catal **2024**, *14*, 18116-18123

DOI: 10.1021/acscatal.4c05489

Author contributions:

In this manuscript, I carried out all experimental work. The initial manuscript draft was prepared by myself. Subsequent editing and peer review was performed by all authors. My overall contribution to this work accounts to approximately 90%.

Signature of the student — Signature of the supervisor

(Hendrik Kempf) — **(Prof. Matthias Beller)**

ACS Catalysis

pubs.acs.org/acscatalysis
Perspective

Comparison of Low Temperature Methanol Aqueous Phase Reforming Catalysts—Definition of Standardized Reaction Conditions and Considerations toward Applications

Hendrik A. Kempf, Henrik Junge,* and Matthias Beller*

Cite This: *ACS Catal.* 2024, 14, 18116−18123
Read Online

ACCESS | Metrics & More | Article Recommendations | Supporting Information

ABSTRACT: A comparison of state-of-the-art catalysts for low temperature aqueous phase reforming (APR) of methanol is presented. To facilitate future applications, catalyst tests under two standardized sets of reaction conditions are proposed.

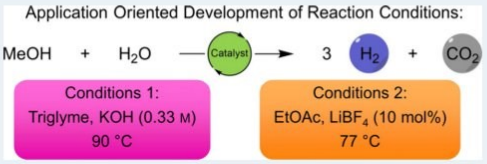

KEYWORDS: *Application, Green Chemistry, Homogeneous Catalysis, Methanol Dehydrogenation, Pincer Complexes*

INTRODUCTION

To realize carbon-neutral energy technologies in the near future, the use of renewable resources is expected to rise.[1−4] Wind and solar energy cannot be stored easily and have the disadvantage not providing a constant energy production.[5−7] To solve these problems, a variety of technologies for the interconversion between electric and chemical energy are currently investigated.[4,5,8−10] In most concepts, the generation of hydrogen via water electrolysis constitutes the first step.[5,11,12] It can easily be converted to electricity and mechanical energy.[4,6] However, the storage and transportation of gaseous and liquified hydrogen is difficult and inefficient.[5,7,12,13] These problems can be circumvented by the use of appropriate hydrogen carriers.[13,14] Hence, in the past two decades a variety of storage materials including methanol, formic acid, ammonia, ammonia borane, decalin, methylcyclohexane, perhydro-dibenzyltoluene and others have been proposed.[5,7,9,12,13,15] Among these, methanol is probably the most important due to its physical properties, availability, and high hydrogen content.

So far, the vast majority of hydrogen (>90%) is produced *via* classic steam reforming from natural gas and water in the presence of appropriate heterogeneous catalysts.[16−18] Apart from the fossil feedstocks, disadvantages of this process are high reaction temperatures and concomitant CO formation. Those drawbacks can be overcome by low temperature aqueous phase reforming (APR) of green methanol, which is available from biowaste or hydrogenation of carbon dioxide (summarized in Figure 1). First examples of APR were reported by Dumesic and co-workers in 2002.[19] More specifically, they dehydrogenated methanol and other biomass derived hydrocarbons at high temperature and pressure (230 °C, 29 bar) using a Pt@γ-Al_2O_3 catalyst reaching a TOF of 420 h^{-1}. Unfortunately, CO content (<300 ppm) was relatively high, requiring further cleaning of the produced gas, e.g., by water gas shift reaction.

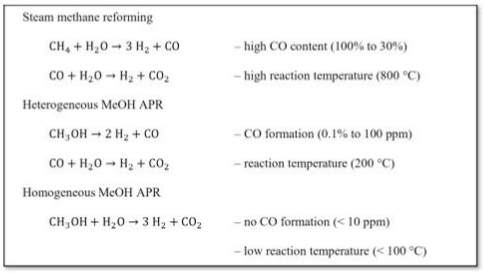

Figure 1. Overview of reforming methods for hydrogen production.

Another important step in methanol APR was reached in 2013. In this year, the groups of Beller[20] and Grützmacher[21] independently reported ruthenium catalyzed low temperature (<100 °C) methanol APR for the first time (Figure 2). Trincado, Grützmacher and co-workers used Ru-catalyst **2** and achieved a TOF of 54 h^{-1} using triethylamine as base. In this case, CO could not be detected; however, no detection limit was reported. Beller and co-workers performed the reaction in

Received: September 9, 2024
Revised: November 15, 2024
Accepted: November 15, 2024

https://doi.org/10.1021/acscatal.4c05489
ACS Catal. 2024, 14, 18116−18123

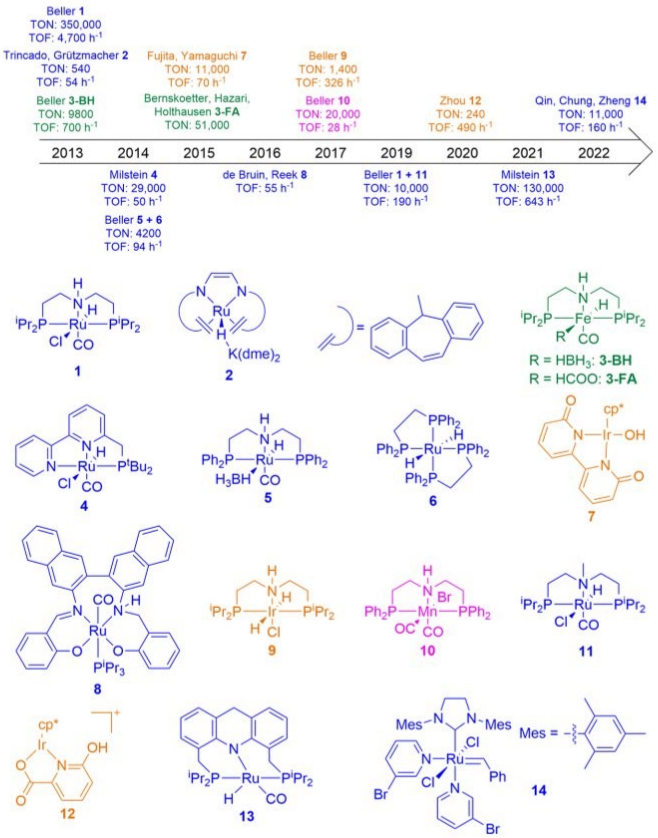

Figure 2. Ruthenium (blue), iron (green), manganese (pink) and iridium (orange) catalysts used in methanol APR. For details, see SI Table S1.

a basic aqueous solution (8 M KOH) utilizing complex **1**. This allowed the production of "pure" hydrogen gas with a turnover frequency (TOF) of 4700 h^{-1} and CO content of <10 ppm. Notably, both works were performed at ambient pressure and showed significantly improved activity of the catalyst compared to the early work by Dumesic and co-workers.[19] In the next year, Beller and co-workers expanded the use of PNP-pincer complexes toward additive free methanol APR utilizing a bicatalytic system.[22] The additive free nature of this catalytic transformation necessitated the use of a solvent. In this reaction, the so-called Ru-MACHO-BH catalyst (**5**) showed high activity in the dehydrogenation of methanol to formic acid and a second catalyst $[Ru(H)_2(dppe)_2]$ (**6**, dppe = 1,2−bis(diphenylphosphino)ethane) was highly active in the reformation of the in situ generated formic acid. With the resulting synergistic effect, a TOF of 94 h^{-1} was reached. The amount of CO was below 8 ppm. In 2019, Beller and co-workers combined both these approaches to methanol APR to generate an improved catalytic system.[23] They could reduce the base concentration by the introduction of a solvent and produced a 3:1 mixture of hydrogen and CO_2 with a TOF of 194 h^{-1}. The amount of CO stayed below 10 ppm. The applied catalyst system was immobilized in a supported liquid phase by Haumann and co-workers and used in methanol steam reformation at 150 °C.[24,25] The last entry on ruthenium PNP-pincer catalyzed methanol APR was performed by Milstein and co-workers. It constitutes of a Ru-acridine complex **13** in the presence of hexyl mercaptan as an additive.[26] Performing the reaction at 150 °C in an autoclave, a TOF of 643 h^{-1} is achieved (Figure 2). The amount of CO was below 20 ppm.

Another early work on methanol APR was conducted by Milstein and co-workers in 2014. They reported a Ru-PNN Pincer catalyst **4** for the base-mediated methanol APR (Figure 2).[27] The reaction was performed in an autoclave with a TOF of 50 h^{-1}. The reaction solution could be recycled three times without loss in activity and without detection of CO. However, no detection limit was reported. In 2016, de Bruin, Reek and co-workers synthesized Ru-salen complex **8** active in methanol APR (Figure 2).[28] They achieved a TOF of 55 h^{-1}. CO content was below an unspecified detection limit. Qin, Chung, Zheng and co-workers showed that Grubbs metathesis catalysts (**14**) are active in methanol APR, too (Figure 2).[29] They reached a TOF of 158 h^{-1} with a CO content of <10

https://doi.org/10.1021/acscatal.4c05489
ACS Catal. 2024, 14, 18116−18123

ppm. Finally, Qin, Zhu and Zheng synthesized a PNNP-ruthenium complex for methanol APR.[30] At 120 °C reaction temperature, they could achieve a TOF of 158 h^{-1}. Again, the amount of CO was very low (<10 ppm). It is worth noting that all the systems highlighted in this paragraph utilize high amounts of strong base (8 M KOH).

As shown in Figure 2, besides ruthenium complexes, methanol APR has been reported with iridium catalysts **7** by Fujita, Yamaguchi and co-workers already in 2015.[11] They reached a TON of 10,500 with NaOH as base. The amount of formed CO was not reported. In 2017, Beller and co-workers improved the TOF from 70 h^{-1} to 326 h^{-1} utilizing an iridium pincer catalyst (**9**, Figure 2).[31] Here, KOH as a base was used, but no data for the CO content were reported, too. In 2020, Zhou and co-workers published another iridium based system (**12**) for methanol APR, as shown in Figure 2.[14] They achieved a high TOF of 491 h^{-1} but comparably low TON of 235 utilizing Na_2CO_3 as the base. The amount of CO was below an unspecified detection limit.

Apart from all of these noble metal catalysts, other metal complexes based on iron and manganese have been reported for methanol reformation under mild conditions (Figure 2). The first work applying iron complexes was published in 2013.[32] High catalyst activity (TOF > 700 h^{-1}) and productivity (TON of 10,000) was achieved while CO content was insignificant (<10 ppm). Two years later, Bernskoetter, Hazari, Holthausen and co-workers improved the catalyst performance by substituting KOH with $LiBF_4$.[33] More specifically, they reached a high TON of 51,000 and the produced gas contained <0.1% CO. A screening of Lewis acids revealed, that small, oxophilic cations, like Li^+ and Na^+, and weakly or noncoordinating anions, like PF_6^-, BF_4^- and OTf^-, result in the highest activity. Overall, $LiBF_4$ proved to give the best results. The improved performance was explained by Lewis acid enhanced decarboxylation of the Fe formate complex.

In 2017, some of us reported the first methanol APR in the presence of manganese complexes (**10**, Figure 2). Similar catalyst TON (20,000) to iron complexes were achieved. Notably, the respective manganese pincer complex showed a remarkable stability of more than one month utilizing KOH as the base and triglyme as the solvent. The amount of generated CO was not reported.

To summarize, in most of the above-mentioned examples, reaction optimization mainly focused on reaching highest yields, catalyst turnover numbers (TON) and/or frequencies (TOF). Besides those parameters describing the catalyst performance, other important aspects must be taken into consideration for potential applications, e.g. combining hydrogen generation and its direct application in fuel cells. Essential aspects include hydrogen production rate and product purity (especially CO content). Cost for metal precursors, ligands, and additives as well as energy efficiency are additional concerns. As an example, for an application in polymer electrolyte fuel cells (PEMFC), the produced gas must contain <10 ppm of CO.[34] This necessitates a low reaction temperature (<100 °C) to prevent the formation of CO by water gas shift reaction. It also enables the opportunity to use reaction heat from other processes in a production plant as a heat source. Furthermore, high gas evolution rate and catalyst stability are vital for an application in PEMFC.

As shown in Figure 2 and SI Table S1, most reported systems operated under vastly different reaction conditions hindering an objective performance comparison of different catalysts. Here, we present an appropriate assessment of known catalysts in methanol APR under standardized conditions. These investigations provide insights into the catalytic activities and help decide which catalysts are worthy of being further investigated for stability tests, longer term reactions, and upscaling with respect to potential applications. Additionally, further ruthenium complexes not yet tested in methanol APR were employed.

RESULTS AND DISCUSSION

As evident from the literature examples described before, the choice of suitable reaction conditions, especially of additives, is of utmost importance (reaction conditions are summarized in detail in SI Table S1). Consequently, the presented literature examples were evaluated on two main criteria, to judge their potential for industrial applicability: 1) Catalysts should show good activities under the respective reaction conditions, and 2) should allow for the stable generation of significant amounts of hydrogen during a quickly reached working phase. Based on these criteria, the reaction conditions presented by Beller and co-workers in 2019,[23] and by Bernskoetter, Hazari, Holthausen and co-workers in 2015[33] were chosen due to the applicability potential as well as to cover the opposite kind of additives:

1. Basic additives (Beller and co-workers): MeOH (9 mL), H_2O (1 mL), triglyme (20 mL), KOH (10 mmol), catalyst (0.015 mol %, 8.5 μmol), T_{set} = 92.5 °C.[23]
2. Lewis acidic additives (Bernskoetter, Hazari, Holthausen and co-workers): MeOH (160 μL), H_2O (18 μL), EtOAc (10 mL), $LiBF_4$ (0.1 mmol), catalyst (0.01 mol %, 0.1 μmol), T_{set} = 80 °C.[33]

The Lewis acidic reaction conditions fulfill these criteria by reaching high activity and selectivity in combination with a stable gas evolution during the working phase (TON: 51,000). The system based on basic additives offers a highly stable working phase, which is reached within a short time frame and a high activity (TON: 10,000; TOF: 190 h^{-1}). To properly evaluate the unique characteristics of this reaction system, the interplay between base concentration, solvent and reaction temperature must be elucidated.

In general, maximum reaction temperature is limited by the boiling point of methanol when working without solvent.[23] However, this limit can be raised by increasing the amount of base used[20,23,28,29,32] or by introduction of a high boiling solvent.[23] For example, the internal reaction temperature could be increased from 68 °C (1 M KOH) to 88.5 °C (8 M KOH) by raising the amount of base. The same result was observed using triglyme as solvent at lower base concentrations (1 M KOH).[23]

The evaluation of these effects requires a closer look at methanol reformation. In presence of a strong base, usually KOH, methanol is converted to hydrogen and carbonate (eq 1). In this process, a strong base is converted to a weaker one, and consequently, the pH-value drops. This part of the reaction is called the initiation phase (Figure 3). It is characterized by a high reaction rate and the evolution of pure hydrogen gas. After full consumption of the strong base, the so-called working phase starts (Figure 3). Here, methanol and water are converted to hydrogen and carbon dioxide (eq 2). The pH-value is stable, and the reaction proceeds slower than during the initiation phase. For applications of these reaction conditions, it is beneficial to reach the working phase

https://doi.org/10.1021/acscatal.4c05489
ACS Catal. 2024, 14, 18116−18123

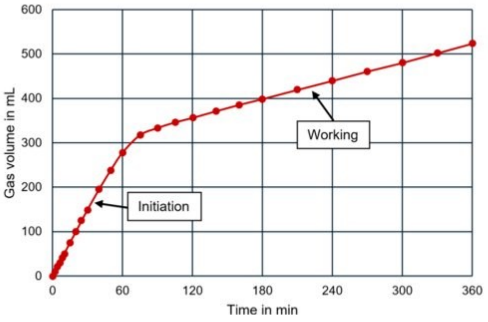

Figure 3. Ru-catalyzed methanol APR:[23] Different reaction phases.

fast. Therefore, to reach high reaction temperatures, a high boiling solvent in combination with low amounts of a base should be used.

$$CH_3OH + H_2O + KOH \rightarrow 3H_2 + KHCO_3 \quad (1)$$

$$CH_3OH + H_2O \rightarrow 3H_2 + CO_2 \quad (2)$$

Having established two sets of reaction conditions for methanol APR, their suitability as standardized systems was further evaluated. Focusing on basic additives first, for a proper comparison of catalysts, mainly their working phase and CO impurities are of interest. Additionally, a short initiation time is beneficial. Successful validation of our results with literature revealed a working phase TOF of 143 h^{-1} for **RuPN^{H}P^{i}Pr** (Table 1, entries 1 and 2) and 168 h^{-1} for **RuPN^{Me}P^{i}Pr**, which is comparable to the reported values (SI Table S1).[23] However, the CO content was slightly higher than originally reported (53 and 19 ppm, respectively). Notably, for most of the tested catalysts CO-contents between 10 and 90 ppm were observed (Table 1).

Next, the influence of different N substituents on the catalytic activity was investigated. The introduction of a vinylic N-substituent at the nitrogen atom of the catalyst backbone (**RuPN^{Alkene}P^{i}Pr**, a mixture of two complexes was employed, since the isolation of the pure compound is not possible[35]) resulted in good activity (Table 1, entry 3). A working phase TOF of 153 h^{-1} after an initiation time of 3.5 h could be reached, resulting in results similar to those for **RuPN^{Me}P^{i}Pr**. Significant improvements in activity and reproducibility compared to the base-free reaction conditions[35] were achieved with the proposed standardized reaction conditions. With a phenyl group at this position, almost all activity was lost during initiation phase, despite the catalyst being highly active in formic acid dehydrogenation (Table 1, entry 4).[36]

Classic **Ru-MACHO** showed activity very similar to that of **RuPN^{H}P^{i}Pr** in the working phase, but a longer initiation phase was observed (Table 1, entry 5). Next, the activity regarding different ligand backbones was investigated. A pyridyl group in the backbone resulted in a slightly lower activity of 122 h^{-1}

Table 1. Comparison of Different Ruthenium Catalysts in Methanol APR[a]

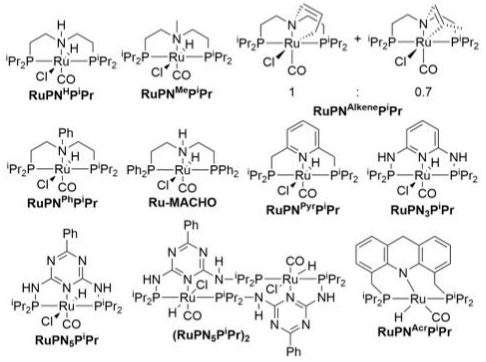

Entry	Catalyst	Initiation time in h	Initiation phase TOF in h^{-1}	Working phase TOF in h^{-1}	Gas evolution rate in mL/h	CO content in ppm
1	**RuPN^{H}P^{i}Pr**	1.8	917	144	42	57
2	**RuPN^{Me}P^{i}Pr**	3.0	547	168	48	24
3	**RuPN^{Alkene}P^{i}Pr**[b]	3.5	519	153	43	50
4	**RuPN^{Ph}P^{i}Pr**[b)]	4 d[c]	16	–	–	65
5	**Ru-MACHO**	2.7	597	153	44	58
6	**RuPN^{Pyr}P^{i}Pr**	5.0	339	122	33	<10
7	**RuPN$_3$P^{i}Pr**	18 h	84	0	0	563
8	**RuPN$_5$P^{i}Pr**[b]	8 d	9	2	0.43	86
9	**(RuPN$_5$P^{i}Pr)$_2$**[b]	31 d[c]	5	–	–	31
10	**RuPN^{Acr}P^{i}Pr**	30 d[c]	4	–	–	578

[a]Reaction conditions: MeOH (9.00 mL), H_2O (1.00 mL), triglyme (20.0 mL), KOH (10.0 mmol), catalyst (8.32 to 8.99 μmol), T_{set} = 92.5 °C. TOF was calculated as an average over the whole initiation or working phase. Gas evolution rate was calculated as an average over the whole working phase. Working phase started after 340 mL gas evolution. [b]For these complexes, methanol APR was not extensively demonstrated prior to this work. [c]Estimated initiation time.

https://doi.org/10.1021/acscatal.4c05489
ACS Catal. 2024, 14, 18116−18123

Table 2. Comparison of Different Metal PNP Pincer Complexes in Methanol APR[a]

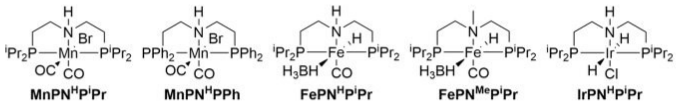

MnPN^{H}P^{i}Pr **MnPN^{H}PPh** **FePN^{H}P^{i}Pr** **FePN^{Me}P^{i}Pr** **IrPN^{H}P^{i}Pr**

Entry	Catalyst	Initiation time in h	Initiation phase TOF in h^{-1}	Working phase TOF in h^{-1}	Gas evolution rate in mL/h	CO content in ppm
1	**MnPN^{H}P^{i}Pr**	–	–	–	–	–
2	**MnPN^{H}PPh**[b]	–	–	–	–	–
3	**FePN^{H}P^{i}Pr**	8.7 h	183	44	12	48
4	**FePN^{Me}P^{i}Pr**[b]	17 h[c]	92	–	–	112
5	**IrPN^{H}P^{i}Pr**[d]	5.4 d	17	3	0.75	60

[a]Reaction conditions: MeOH (9.00 mL), H_2O (1.00 mL), triglyme (20.0 mL), KOH (10.0 mmol), catalyst (8.41 to 8.99 μmol), T_{set} = 92.5 °C, 6 h. TOF was calculated as an average over the whole initiation or working phase. Gas evolution rate was calculated as an average over the whole working phase. Working phase started after 340 mL gas evolution. [b]For these complexes, methanol APR was not investigated prior to this work. [c]Estimated initiation time. [d]Working phase started after 450 mL gas evolution.

Table 3. Effect of $LiBF_4$ on the Gas Evolution of Metal Pincer Complexes[a]

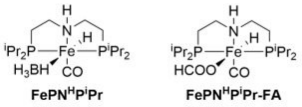

FePN^{H}P^{i}Pr **FePN^{H}P^{i}Pr-FA**

Entry	Catalyst	Catalyst amount in μmol	Solvent	Additives	Gas evolution in mL
1[33]	**FePN^{H}P^{i}Pr-FA**	0.10	EtOAc	10 mol % $LiBF_4$	98[b]
2	**FePN^{H}P^{i}Pr**	0.10	EtOAc	10 mol % $LiBF_4$	0
3	**FePN^{H}P^{i}Pr**	0.10	EtOAc	10 mol % $LiBF_4$ 0.1 mol % KOH	0
4	**FePN^{H}P^{i}Pr**	8.39 to 8.49	Triglyme	10 mol % $LiBF_4$	0
5	**FePN^{H}P^{i}Pr**	8.44 to 8.74	Triglyme	10 mol % $LiBF_4$ 18 mol % KOH	280
6	**FePN^{H}P^{i}Pr**	8.52 to 8.74	Triglyme	18 mol % KOH	304
7	**RuPN^{H}P^{i}Pr**	0.10	EtOAc	10 mol % $LiBF_4$	0
8	**RuPN^{H}P^{i}Pr**	8.49 to 8.66	Triglyme	10 mol % $LiBF_4$	0
9	**RuPN^{H}P^{i}Pr**	8.60 to 8.71	Triglyme	10 mol % $LiBF_4$ 18 mol % KOH	429
10	**RuPN^{H}P^{i}Pr**	8.85 to 8.90	Triglyme	18 mol % KOH	523
11	**IrPN^{H}P^{i}Pr**	0.10	EtOAc	10 mol % $LiBF_4$	0
12[c]	**IrPN^{H}P^{i}Pr**	4.25 to 4.47	Triglyme	10 mol % $LiBF_4$	0
13[c]	**IrPN^{H}P^{i}Pr**	4.26	Triglyme	10 mol % $LiBF_4$ 18 mol % KOH	43
14[c, 31]	**IrPN^{H}P^{i}Pr**	4.18	Triglyme	18 mol % KOH	82

[a]Reaction conditions with EtOAc as solvent: MeOH (160 μL), H_2O (18 μL), EtOAc (10.0 mL), $LiBF_4$ (10 mol %, 0.1 mmol), catalyst (0.01 mol %), T_{set} = 80 °C. The gas evolution after 18 h is recorded. Reaction conditions with triglyme as solvent: MeOH (9.00 mL), H_2O (1.00 mL), triglyme (20.0 mL), KOH (18 mol %, 10 mmol), $LiBF_4$ (10 mol %, 5.55 mmol), catalyst (8.39 to 8.90 μmol), T_{set} = 92.5 °C. The gas evolution after 6 h is recorded. Reactions without base were performed with the activated catalysts [Ru(PN^{H}P^{i}Pr)(CO)$(H)_2$] and [Ir(PN^{H}P^{i}Pr)$(H)_3$]. [b]The gas evolution after 52 h is recorded. [c]Reaction conditions: MeOH (9.00 mL), H_2O (1.00 mL), KOH (5.00 mmol), $LiBF_4$ (5.00 mmol), catalyst (4.18 to 4.47 μmol), T_{set} = 94 °C. The gas evolution after 3 h is recorded.

during the working phase and a longer initiation time of 5 h (Table 1, entry 6). For **RuPN$_3$P^{i}Pr**, a longer initiation time of 18 h was determined (Table 1, entry 7), and all activity was lost at the end of the initiation phase. Over the course of the reaction, the CO content increased from <10 ppm (6 h) to 563 ppm (7 d). This large amount of CO at the end of the reaction corresponds to the loss of one CO ligand from catalyst. Hence, in this case it is possible that the catalyst decomposes under loss of CO. Next, the recently introduced monomeric **RuPN$_5$P^{i}Pr** and dimeric **(RuPN$_5$P^{i}Pr)$_2$** catalysts[37] were examined in methanol APR, too (Table 1, entries 8 and 9). Similar to the recently reported formic acid dehydrogenation, initial activity of the monomeric complex was significantly higher than that of the dimeric one (SI Figure S3).[37] Both complexes showed deactivation during the initiation phase. Due to the estimated initiation time (31 d) of the dimeric complex, the working phase was not investigated. After an initiation time of 8 d, monomeric complex gave a working phase TOF of 2 h^{-1}. **RuPN^{Acr}P^{i}Pr** is known to perform methanol APR at 150 °C with high turnover frequencies (Figure 2, Table S1).[26] However, at lower temperature (90 °C), an initiation phase TOF of 4 h^{-1} was measured, resulting in an estimated initiation time of 30 d (Table 1, entry 10). Therefore, the working phase behavior of this complex was not

https://doi.org/10.1021/acscatal.4c05489
ACS Catal. 2024, 14, 18116−18123

investigated. In addition, a significant CO content (578 ppm) was measured.

Apart from ruthenium catalysts, other PNP pincer complexes with different metal centers were investigated. Despite previous successful works,[38] both applied manganese catalysts showed no activity under these more practical reaction conditions (Table 2, entries 1 and 2). In contrast, **FePN^{H}P^{i}Pr** is active with a TOF of 183 h^{-1} during the initiation phase (Table 2, entry 3). For this catalyst, this is a significant improvement in activity if values with similar base concentrations are compared (SI, Table S1). The standardized reaction conditions proposed here also allow the observation of a working phase for the first time for an iron catalyst in base mediated methanol APR (TOF of 44 h^{-1} and a gas evolution rate of 12 mL/h). As another iron-based pincer complex, *N*-methylated **FePN^{Me}P^{i}Pr** was investigated (Table 2, entry 4). Despite iron complexes usually following an outer sphere reaction mechanism,[33,39−43] this complex is known to be active in formic acid dehydrogenation.[44] More specifically, an initiation phase TOF of 92 h^{-1} was obtained for **FePN^{Me}P^{i}Pr**. This represents 50% of the activity of **FePN^{H}P^{i}Pr**. Compared to all previously tested molecularly defined complexes, the respective iridium complex **IrPN^{H}P^{i}Pr** showed an unusual behavior in methanol APR (SI Figure S5). Once the pH value of the reaction started to drop, a sharp increase in catalyst activity was observed. However, this "high activity phase" was not permanent, and the reaction rate slowly decreased. Since the working phase is characterized by a steady gas evolution, its start was defined at 450 mL of gas evolution. Therefore, a working phase TOF of 3 h^{-1} after an initiation phase of 5.4 d was observed (Table 2, entry 5). The sharp increase in activity can be explained by the high activity at low base concentrations.[31] Since 60 ppm of CO were detected in the produced gas, the formation of the inactive carbonyl complex is likely, as described by us previously.[31]

The second set of reaction conditions to evaluate potential catalysts more appropriately is based on works by Bernskoetter, Hazari, Holthausen, and co-workers.[33,45] Their screening, as summarized above, resulted in the following optimized reaction conditions:

MeOH (160 μL), H_2O (18 μL), EtOAc (10 mL), $LiBF_4$ (0.1 mmol), catalyst (0.01 mol %, 0.1 μmol), T_{set} = 80 °C.

Utilizing this reaction system Bernskoetter, Hazari, Holthausen and co-workers could reach a high TON of 51,000 for the iron complex **FePN^{H}P^{i}Pr-FA** (Table 3, entry 1).[33] When switching from this iron formate complex to the corresponding HBH_3-complex **FePN^{H}P^{i}Pr**, no gas evolution was observed after 18 h (Table 3, entry 2). Activation of the catalyst with a base prior to the reaction led to no improvement (Table 3, entry 3). By slowly altering the reaction conditions toward the basic set of reaction conditions discussed above, activity could only be observed after base was added (Table 3, entries 4−6). Similar results were obtained using ruthenium and iridium complexes (Table 3, entries 7−14). Only in reactions with a base could activity be observed for the catalysts. It is worth noting that there is a slight increase in activity when no $LiBF_4$ was used (280 to 304 mL for iron, 429 to 523 mL for ruthenium and 43 to 82 mL for iridium). The same trend was observed by Kirchner, Gonsalvi and co-workers in formic acid dehydrogenation.[46] The catalyst lost all activity when the base was replaced with $LiBF_4$. These results indicate a detrimental effect of $LiBF_4$ on the catalytic activity for most catalytic systems, resulting in a very limited applicability of $LiBF_4$ as an additive in standardized systems.

CONCLUSION AND ECONOMIC CONSIDERATIONS

Low temperature aqueous phase reforming (APR) of green methanol, which should be available on a larger scale from biowaste or hydrogenation of carbon dioxide in the future, offers a highly attractive possibility as part of hydrogen storage technologies. Crucial for the application of such processes will be the development of the appropriate catalysts. To identify the optimal system, an objective evaluation of such materials under the same conditions is a prerequisite. Therefore, we propose here the use of two different standardized reaction conditions to investigate the initial potential of the new catalysts.

Author: In addition, we would like to emphasize that significant improvements in performance are still needed for practical scale application (>10 ton-scale MeOH). This fact is illustrated by the following calculation: The current price for hydrogen gas is around $2/kg. Typically, in catalytic reactions, the price of catalyst should be below 5% of the products price. This corresponds to a target catalyst price of $2.0\cdot10^{-4}$ $\$\cdot mol_{H_2}^{-1}$. Based on this information, the stability (TON) of the catalyst in dependence on its cost is calculated (Figure 4).

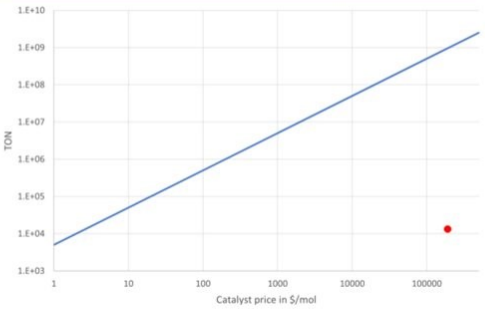

Figure 4. Catalyst stability (TON) in dependence of its cost for methanol APR (blue). The red dot marks cost and TON for the commercially available so far best catalyst **RuPN^{H}P^{i}Pr** under basic reaction conditions. A catalyst costing $200/mol would need to achieve a TON of at least 10^6 to be profitable (i.e., contribute less than 5% to the product cost).

More specifically, examining one of the best catalysts **RuPN^{H}P^{i}Pr** (priced at $405/g or $190,000/mol) more closely, an overall TON of 10^9 must be reached for real world applications. Considering the present catalyst activity, this would correspond to a reaction time of around 750 years! Therefore, it is evident that the presently known catalyst performance must be enhanced by at least 3 orders of magnitude. Such improvements are typically not possible by simple optimization of process conditions and minor catalyst variations. In fact, completely new developments from ground up are needed, which should be aware of the realistic requirements for catalyst applications. Moreover, we would like to point out that catalyst costs should be seen in a holistic way. For the catalyst above, the costs of metal and ligand are nearly the same. Hence, simply switching from Ru-PNP to Fe-PNP complexes does not solve this dilemma. We encourage all

https://doi.org/10.1021/acscatal.4c05489
ACS Catal. 2024, 14, 18116−18123

researchers interested in this field to specifically look for the combination of abundant metals and cheap ligands.

■ ASSOCIATED CONTENT

Supporting Information

The Supporting Information is available free of charge at https://pubs.acs.org/doi/10.1021/acscatal.4c05489.

General methods, experimental details, and literature overview (PDF)

■ AUTHOR INFORMATION

Corresponding Authors

Henrik Junge − *Leibniz-Institut für Katalyse e.V., 18059 Rostock, Germany;* orcid.org/0000-0002-7603-1984; Email: henrik.junge@catalysis.de

Matthias Beller − *Leibniz-Institut für Katalyse e.V., 18059 Rostock, Germany;* orcid.org/0000-0001-5709-0965; Email: matthias.beller@catalysis.de

Author

Hendrik A. Kempf − *Leibniz-Institut für Katalyse e.V., 18059 Rostock, Germany;* orcid.org/0009-0002-8780-4361

Complete contact information is available at: https://pubs.acs.org/10.1021/acscatal.4c05489

Author Contributions

H. K. carried out all experiments. All authors discussed the results and prepared the manuscript.

Notes

The authors declare no competing financial interest.

■ ACKNOWLEDGMENTS

This work was funded by the German Federal Ministry for Economic Affairs and Climate Action within the project "MEGA" (FKZ: 03EN5006A). We thank Anja Kammer for analytical support and valuable discussions.

■ REFERENCES

(1) *Bp Energy Outlook 2022*; bp p.l.c., 2022.

(2) *Bp Statistical Review of World Energy 2021*; bp p.l.c., 2021.

(3) *World Energy Outlook 2021*; IEA, 2021.

(4) Hester, R. E.; Harrison, R. M. *Energy Storage Options and Their Environmental Impact*; Royal Society of Chemistry, 2018.

(5) Mellmann, D.; Sponholz, P.; Junge, H.; Beller, M. Formic Acid as a Hydrogen Storage Material - Development of Homogeneous Catalysts for Selective Hydrogen Release. *Chem. Soc. Rev.* **2016**, *45* (14), 3954−3988.

(6) Moriarty, P.; Honnery, D. A Hydrogen Standard for Future Energy Accounting? *Int. J. Hydrog. Energy* **2010**, *35* (22), 12374−12380.

(7) Zheng, J.; Zhou, H.; Wang, C.-G.; Ye, E.; Xu, J. W.; Loh, X. J.; Li, Z. Current Research Progress and Perspectives on Liquid Hydrogen Rich Molecules in Sustainable Hydrogen Storage. *Energy Stor. Mater.* **2021**, *35*, 695−722.

(8) Dagle, R. A.; Holladay, J. D. Methanol Steam Reforming for Hydrogen Production. *Chem. Rev.* **2007**, *107* (10), 3992−4021.

(9) Kumar, A.; Daw, P.; Milstein, D. Homogeneous Catalysis for Sustainable Energy: Hydrogen and Methanol Economies, Fuels from Biomass, and Related Topics. *Chem. Rev.* **2022**, *122* (1), 385−441.

(10) Koohi-Fayegh, S.; Rosen, M. A. A Review of Energy Storage Types, Applications and Recent Developments. *J. Energy Storage* **2020**, *27*, 101047.

(11) Fujita, K.; Kawahara, R.; Aikawa, T.; Yamaguchi, R. Hydrogen Production from a Methanol-Water Solution Catalyzed by an Anionic Iridium Complex Bearing a Functional Bipyridonate Ligand under Weakly Basic Conditions. *Angew. Chem., Int. Ed.* **2015**, *54* (31), 9057−9060.

(12) Abdalla, A. M.; Hossain, S.; Nisfindy, O. B.; Azad, A. T.; Dawood, M.; Azad, A. K. Hydrogen Production, Storage, Transportation and Key Challenges with Applications: A Review. *Energy Convers. Manag.* **2018**, *165*, 602−627.

(13) Sreedhar, I.; Kamani, K. M.; Kamani, B. M.; Reddy, B. M.; Venugopal, A. A Bird's Eye View on Process and Engineering Aspects of Hydrogen Storage. *Renew. Sust. Energy Rev.* **2018**, *91*, 838−860.

(14) Bai, C.; Wang, H.; Ning, F.; Fu, J.; Wei, J.; Lu, G.; Shen, Y.; Zhou, X. Second Sphere Ligand Promoted Organoiridium Catalysts for Methanol Dehydrogenation under Mild Conditions. *ChemCatChem.* **2020**, *12* (16), 4024−4028.

(15) Chen, X.; Yang, X. Mechanistic Insights and Computational Design of Transition-Metal Catalysts for Hydrogenation and Dehydrogenation Reactions. *Chem. Rec.* **2016**, *16* (5), 2364−2378.

(16) Ranjekar, A. M.; Yadav, G. D. Steam Reforming of Methanol for Hydrogen Production: A Critical Analysis of Catalysis, Processes, and Scope. *Ind. Eng. Chem. Res.* **2021**, *60* (1), 89−113.

(17) Chen, L.; Qi, Z.; Zhang, S.; Su, J.; Somorjai, G. A. Catalytic Hydrogen Production from Methane: A Review on Recent Progress and Prospect. *Catalysts* **2020**, *10* (8), 858−876.

(18) Megía, P. J.; Vizcaíno, A. J.; Calles, J. A.; Carrero, A. Hydrogen Production Technologies: From Fossil Fuels toward Renewable Sources. A Mini Review. *Energy Fuels* **2021**, *35* (20), 16403−16415.

(19) Cortright, R. D.; Davda, R. R.; Dumesic, J. A. Hydrogen from Catalytic Reforming of Biomass-Derived Hydrocarbons in Liquid Water. *Nature* **2002**, *418* (6901), 964−967.

(20) Nielsen, M.; Alberico, E.; Baumann, W.; Drexler, H. J.; Junge, H.; Gladiali, S.; Beller, M. Low-Temperature Aqueous-Phase Methanol Dehydrogenation to Hydrogen and Carbon Dioxide. *Nature* **2013**, *495* (7439), 85−89.

(21) Rodriguez-Lugo, R. E.; Trincado, M.; Vogt, M.; Tewes, F.; Santiso-Quinones, G.; Grützmacher, H. A Homogeneous Transition Metal Complex for Clean Hydrogen Production from Methanol-Water Mixtures. *Nat. Chem.* **2013**, *5* (4), 342−347.

(22) Monney, A.; Barsch, E.; Sponholz, P.; Junge, H.; Ludwig, R.; Beller, M. Base-Free Hydrogen Generation from Methanol Using a Bi-Catalytic System. *Chem. Commun.* **2014**, *50* (6), 707−709.

(23) Agapova, A.; Junge, H.; Beller, M. Developing Bicatalytic Cascade Reactions: Ruthenium-Catalyzed Hydrogen Generation from Methanol. *Chem.—Eur. J.* **2019**, *25* (40), 9345−9349.

(24) Schwarz, C. H.; Agapova, A.; Junge, H.; Haumann, M. Immobilization of a Selective Ru-Pincer Complex for Low Temperature Methanol Reforming−Material and Process Improvements. *Catal. Today* **2020**, *342*, 178−186.

(25) Schwarz, C. H.; Kraus, D.; Alberico, E.; Junge, H.; Haumann, M. Immobilized Ru-Pincer Complexes for Continuous Gas-Phase Low-Temperature Methanol Reforming-Improving the Activity by a Second Ru-Complex and Variation of Hydroxide Additives. *Eur. J. Inorg. Chem.* **2021**, *2021* (2021), 1745−1751.

(26) Luo, J.; Kar, S.; Rauch, M.; Montag, M.; Ben-David, Y.; Milstein, D. Efficient Base-Free Aqueous Reforming of Methanol Homogeneously Catalyzed by Ruthenium Exhibiting a Remarkable Acceleration by Added Catalytic Thiol. *J. Am. Chem. Soc.* **2021**, *143* (41), 17284−17291.

(27) Hu, P.; Diskin-Posner, Y.; Ben-David, Y.; Milstein, D. Reusable Homogeneous Catalytic System for Hydrogen Production from Methanol and Water. *ACS Catal.* **2014**, *4* (8), 2649−2652.

(28) van de Watering, F. F.; Lutz, M.; Dzik, W. I.; de Bruin, B.; Reek, J. N. Reactivity of a Ruthenium-Carbonyl Complex in the Methanol Dehydrogenation Reaction. *ChemCatChem.* **2016**, *8* (17), 2752−2756.

(29) Wang, Q.; Lan, J.; Liang, R.; Xia, Y.; Qin, L.; Chung, L. W.; Zheng, Z. New Tricks for an Old Dog: Grubbs Catalysts Enable Efficient Hydrogen Production from Aqueous-Phase Methanol Reforming. *ACS Catal.* **2022**, *12* (4), 2212−2222.

(30) Chen, Z.; Xia, Y.; Ma, C.; Wang, Q.; Qin, L.; Zhu, X.; Zheng, Z. Hydrogen Production Via the Aqueous-Phase Reforming of Methanol Catalyzed by Ru(II) Complexes of PNNP Ligands. *Inorg. Chem. Front.* **2023**, *10* (3), 756−767.
(31) Prichatz, C.; Alberico, E.; Baumann, W.; Junge, H.; Beller, M. Iridium-PNP Pincer Complexes for Methanol Dehydrogenation at Low Base Concentration. *ChemCatChem.* **2017**, *9* (11), 1891−1896.
(32) Alberico, E.; Sponholz, P.; Cordes, C.; Nielsen, M.; Drexler, H. J.; Baumann, W.; Junge, H.; Beller, M. Selective Hydrogen Production from Methanol with a Defined Iron Pincer Catalyst under Mild Conditions. *Angew. Chem., Int. Ed.* **2013**, *52* (52), 14162−14166.
(33) Bielinski, E. A.; Förster, M.; Zhang, Y.; Bernskoetter, W. H.; Hazari, N.; Holthausen, M. C. Base-Free Methanol Dehydrogenation Using a Pincer-Supported Iron Compound and Lewis Acid Co-Catalyst. *ACS Catal.* **2015**, *5* (4), 2404−2415.
(34) Lopes, P. P.; Freitas, K. S.; Ticianelli, E. A. CO Tolerance of PEMFC Anodes: Mechanisms and Electrode Designs. *Electrocatal* **2010**, *1* (4), 200−212.
(35) Kempf, H. A.; López Robledo, G.; Spannenberg, A.; Junge, K.; Jiao, H.; Junge, H.; Beller, M. Synthesis of Ru-PNPC Pincer Complexes and Applications in Catalytic Hydrogenation and Dehydrogenation Reactions. *ChemCatChem.* **2024**, No. e202401481.
(36) Curley, J. B.; Hert, C.; Bernskoetter, W. H.; Hazari, N.; Mercado, B. Q. Control of Catalyst Isomers Using an *N*-Phenyl-Substituted $Rn(CH_2CH_2P^iPr_2)_2$ Pincer Ligand in CO_2 Hydrogenation and Formic Acid Dehydrogenation. *Inorg. Chem.* **2022**, *61* (1), 643−656.
(37) Kempf, H. A.; Both, N. F.; Stein, C. A. M.; Spannenberg, A.; Junge, K.; Junge, H.; Beller, M. Synthesis of Guanamine-Based Ruthenium Pincer Complexes and Their Application in Catalytic (De)Hydrogenation Reactions. *Organometallics* **2024**, *43*, 2450.
(38) Anderez-Fernandez, M.; Vogt, L. K.; Fischer, S.; Zhou, W.; Jiao, H.; Garbe, M.; Elangovan, S.; Junge, K.; Junge, H.; Ludwig, R.; Beller, M. A Stable Manganese Pincer Catalyst for the Selective Dehydrogenation of Methanol. *Angew. Chem., Int. Ed.* **2017**, *129* (2), 574−577.
(39) Bellows, S. M.; Chakraborty, S.; Gary, J. B.; Jones, W. D.; Cundari, T. R. An Uncanny Dehydrogenation Mechanism: Polar Bond Control over Stepwise or Concerted Transition States. *Inorg. Chem.* **2017**, *56* (10), 5519−5524.
(40) Budweg, S.; Wei, Z.; Jiao, H.; Junge, K.; Beller, M. Iron-PNP-Pincer-Catalyzed Transfer Dehydrogenation of Secondary Alcohols. *ChemSusChem* **2019**, *12* (13), 2988−2993.
(41) Qu, S.; Dai, H.; Dang, Y.; Song, C.; Wang, Z.-X.; Guan, H. Computational Mechanistic Study of Fe-Catalyzed Hydrogenation of Esters to Alcohols: Improving Catalysis by Accelerating Precatalyst Activation with a Lewis Base. *ACS Catal.* **2014**, *4* (12), 4377−4388.
(42) Elangovan, S.; Wendt, B.; Topf, C.; Bachmann, S.; Scalone, M.; Spannenberg, A.; Jiao, H.; Baumann, W.; Junge, K.; Beller, M. Improved Second Generation Iron Pincer Complexes for Effective Ester Hydrogenation. *Adv. Synth. Catal.* **2016**, *358* (5), 820−825.
(43) Chakraborty, S.; Lagaditis, P. O.; Förster, M.; Bielinski, E. A.; Hazari, N.; Holthausen, M. C.; Jones, W. D.; Schneider, S. Well-Defined Iron Catalysts for the Acceptorless Reversible Dehydrogenation-Hydrogenation of Alcohols and Ketones. *ACS Catal.* **2014**, *4* (11), 3994−4003.
(44) Curley, J. B.; Smith, N. E.; Bernskoetter, W. H.; Hazari, N.; Mercado, B. Q. Catalytic Formic Acid Dehydrogenation and CO_2 Hydrogenation Using Iron PNRP Pincer Complexes with Isonitrile Ligands. *Organometallics* **2018**, *37* (21), 3846−3853.
(45) Bielinski, E. A.; Lagaditis, P. O.; Zhang, Y.; Mercado, B. Q.; Wurtele, C.; Bernskoetter, W. H.; Hazari, N.; Schneider, S. Lewis Acid-Assisted Formic Acid Dehydrogenation Using a Pincer-Supported Iron Catalyst. *J. Am. Chem. Soc.* **2014**, *136* (29), 10234−10237.
(46) Mellone, I.; Gorgas, N.; Bertini, F.; Peruzzini, M.; Kirchner, K.; Gonsalvi, L. Selective Formic Acid Dehydrogenation Catalyzed by Fe-PNP Pincer Complexes Based on the 2,6-Diaminopyridine Scaffold. *Organometallics* **2016**, *35* (19), 3344−3349.

https://doi.org/10.1021/acscatal.4c05489
ACS Catal. 2024, 14, 18116−18123

6.3 Full publication list

Kempf, H. A.; Both, N. F.; Stein, C. A. M.; Spannenberg, A.; Junge, K.; Junge, H.; Beller, M. Synthesis of Guanamine-Based Ruthenium Pincer Complexes and Their Application in Catalytic (De)Hydrogenation Reactions. *Organometallics* **2024**, *43* (20), 2450-2457.

Kempf, H. A.; López Robledo, G.; Spannenberg, A.; Junge, K.; Jiao, H.; Junge, H.; Beller, M. Synthesis of Ru-Pnpc Pincer Complexes and Applications in Catalytic Hydrogenation and Dehydrogenation Reactions. *ChemCatChem* **2024**, e202401481.

Kempf, H. A.; Junge, H.; Beller, M. Comparison of Low Temperature Methanol Aqueous Phase Reforming Catalysts─Definition of Standardized Reaction Conditions and Considerations toward Applications. *ACS Catal.* **2024**, *14*, 18116-18123.

6.4 Presented Posters

H. Kempf, H. Junge, M. Beller, 3rd ComBioCat Symposium 2022, Rostock, 8th - 9th June 2022, Development of the ruthenium catalyzed methanol reformation.

Hendrik Kempf, Henrik Junge, Matthias Beller, 56. Jahrestreffen Deutscher Katalytiker, Weimar, 15-17th March 2023, Standardization of Reaction Conditions for the Aqueous Phase Methanol Reformation.

H. A. Kempf, N. F. Both, C. A. M. Stein, A. Spannenberg, K. Junge, H. Junge, M. Beller, ISHC 2024, Triest, 21-26th July 2024, Synthesis of Guanamine-Based Ruthenium Pincer Complexes and Their Application in Catalytic (De)hydrogenation Reactions.

6.5 Curriculum Vitae

Personal data:

Name	Hendrik Kempf
Date of birth	26.11.1996
Place of birth	Aschaffenburg, Germany
Address	Ulmenstraße 3, 18057 Rostock
E-Mail	hendrik.kempf@catalysis.de
ORCID	0009-0002-8780-4361

Education:

2003-2007:	Grundschule Schule am Weinberg Michelbach
2007-2015:	Spessartgymnasium Alzenau
2015-2018:	Bachelor of Science in chemistry at the University of Bayreuth. Bachelor thesis in the group of Prof. Dr. Andreas Greiner about PLimC Blockcopolymers
2018-2021:	Master of Science in natural products & drug chemistry at the University of Bayreuth. Master thesis with Prof. Dr. Rhett Kempe about the rearrangement and hydrogenation of cyanoimines.
Since 2021:	Doctoral researcher at the Leibniz-Institut für Katalyse e. V. with Prof. Dr. Matthias Beller.

Internships:

July 2012:	Internship at Singulus Technologies AG
April 2013:	Internship at Evonik Industries AG in the department Inorganic Materials
March 2017:	Internship at Allessa GmBH in the department of Elemental Analysis

Further Skills and Achievements:

Further training	2024 Qualification course “Leadership and Communication skills”
Extracurriculars	2009-2015 Organization and hosting of summergames
	2014-2016 Member of the Parish council of the Kuratie St. Philippus & Jakobus
	2018-2020 Organization of the university choir Bayreuth
	2022-2024 Volunteer long night of science (LNDW), Likat Rostock
Languages	German (native), English (fluent), Latin (basics)
IT	MS Office (Word, Excel, PowerPoint, Outlook), Citavi, EndNote, ChemDraw, MestReNova, TopSpin, Scifinder, Reaxys, ChemStation

6.6 Selbstständigkeitserklärung

Doktorandinnen/Doktoranden-Erklärung gemäß § 4 Absatz 1 Buchstaben g und h der Promotionsordnung der Mathematisch-Naturwissenschaftlichen Fakultät der Universität Rostock

Name Hendrik Andreas Kempf
(Name, Vorname)

Anschrift Ulmenstraße 3, 18057 Rostock
(Straße, PLZ, Wohnort)

Ich beabsichtige, eine Dissertation zum Thema

New Ruthenium Pincer Catalysts for (De)hydrogenation Reactions

an der Mathematisch-Naturwissenschaftlichen Fakultät der Universität Rostock anzufertigen. Dabei werde ich von Frau/Herrn
Prof. Dr. Matthias Beller
betreut.

Ich gebe folgende Erklärung ab:
1. Die Gelegenheit zum vorliegenden Promotionsvorhaben ist mir nicht kommerziell vermittelt worden. Insbesondere habe ich keine Organisation eingeschaltet, die gegen Entgelt Betreuerinnen/Betreuer für die Anfertigung von Dissertationen sucht oder die mir obliegenden Pflichten hinsichtlich der Prüfungsleistungen für mich ganz oder teilweise erledigt.
2. Ich versichere hiermit an Eides statt, dass ich die vorliegende Arbeit selbstständig angefertigt und ohne fremde Hilfe verfasst habe. Dazu habe ich keine außer den von mir angegebenen Hilfsmitteln und Quellen verwendet und die den benutzten Werken inhaltlich und wörtlich entnommenen Stellen habe ich als solche kenntlich gemacht.

....., den ....
(Ort) (Unterschrift)